



Birzeit University

Faculty of Engineering and Technology

Joint Master Program in Electrical Engineering (JMEE)

# **Controlling a Sensorless PMSM Fed from VSI Using Hybrid Position Estimation Technique**

Prepared by:  
Odai Bassam Abbadi

Supervised by:  
Dr. Muhammad Abu Khaizaran

This Master Thesis is submitted in partial fulfillment of the requirements for the  
Master Degree in Electrical Engineering

BIRZEIT  
December 2021

**Controlling a Sensorless PMSM Fed from VSI Using Hybrid  
Position Estimation Technique**

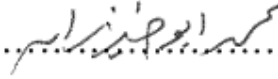
التحكم عديم المجسات في المحرك التزامني ذي المغناطيس الدائم من خلال تقنية تقدير الوضعية  
الهجينة

Submitted by:

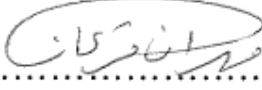
**Odai Abbadi**

**Approved by the Examining Committee**

Dr. Muhammad Abu-Khaizaran

.....  


Dr. Mahran Quraan

.....  


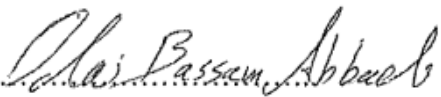
Dr. Hakam Shehadeh

.....  


BIRZEIT, PALESTINE  
January 2022

## DECLARATION

I declare that this thesis entitled “Controlling a Sensorless PMSM Fed from VSI Using Hybrid Position Estimation Technique” is the result of my own research except as cited in the references. It is being submitted to the Master’s Degree in Electrical Engineering from the Faculty of Engineering and Technology at Birzeit University, Palestine. The thesis has not been accepted for any degree and is not concurrently submitted in candidature of any other degree.

Signature: 

Name: Odai Abbadi

# *Abstract*

Due to the increase in electric vehicle (EV) production and the gearless traction machines applications, the permanent magnet synchronous motor (PMSM) has a wide range of use because of its high torque, fast response, and high-power density, which make it a hot topic in research and studies. In order to control a PMSM, the rotor position and speed are needed to be determined accurately. The sensorless control eliminates the use of the encoder sensor, resolver, or any position detection hardware equipment, by using estimators and observers as rotor position determinators, reducing the traction cost, volume, and maintenance requirements. Two types of estimators have been studied in this research, Improved Sliding Mode Observer with chattering elimination technique and speed-related estimation, which observe the rotor position accurately during the medium and high-speed range, and High-Frequency Injection with accurate standstill and low-speed estimator.

In this research, the inner rotor permanent magnet synchronous motor (IRPMSM) is studied, as an application in EV and traction machines, fed from voltage source inverter (VSI) controlled by a sensorless vector controller to eliminate the position sensor increasing the system's reliability, performance, and decreasing the motor size and cost. These goals achieved by designing a hybrid estimation algorithm which uses two parallel stages; one for the standstill and low-speed condition and the other for medium and high speed, combined in one system to estimate the speed and position during all speed ranges with minimum estimation error, lower power loss and lower injection noise.

# المستخلص

نظرًا لزيادة إنتاج المركبات الكهربائية وتطبيقات آلات الجر بدون تروس ، يتمتع المحرك المتزامن بالمغناطيس الدائم بمجموعة واسعة من الاستخدام بسبب عزم الدوران العالي، والاستجابة السريعة، وكثافة الطاقة العالية، مما يجعله موضوع هام في البحوث والدراسات. من أجل السيطرة على المحرك المقترح، هناك حاجة إلى معرفة زوايه دوار المحرك وسرعته وتحديدها بدقة. يعمل جهاز التحكم بدون مستشعر على التخلص من استخدام مستشعر سرعه المحرك أو أي جهاز من أجهزة قياس السرعه والزوايه ، وذلك باستخدام أدوات التقدير والتقريب والحساب لتقدير زوايه دوار المحرك وسرعته، مما يقلل من تكاليف المحرك والحجم والصيانة. تمت دراسة نوعين من المقدرات والحاسبات في هذا البحث، مراقب وضع انزلاق محسن متغير مع السرعه مع تقنية التخلص من التشويش، والذي يراقب زوايه دوار المحرك بدقة خلال السرعات المتوسطة والعاليه، والحقق عالي التردد دقيق المراقبه اثناء الركود والسرعات المنخفضه. في هذا البحث، تمت دراسة المحرك المتزامن بالمغناطيس الدائم، كتطبيق في آلات المركبات الكهربائيه ومحركات الجر، والتي يتم تغذيتها من عاكس مصدر الجهد متغير الجهد والتردد والذي يتم التحكم فيه بواسطة جهاز تحكم متجهي بدون استشعار للتخلص من استخدام مستشعر زوايه المحرك مما يزيد من موثوقية النظام وأدائه وتقليل حجم المحرك والتكلفة، بطريقة ممنهجه للتخلص من التشويش الصادر من متحكم مصدر الجهد والتردد , الامر والذي بدوره يقلل من تكلفه النظام، باستخدام خوارزمية تقدير هجين تستخدم مرحلتين متوازيتين؛ إحداهما اثناء الركود والثبات, واثنا حالة السرعه المنخفضة والأخرى للسرعه المتوسطة والعاليه، مجتمعة في نظام واحد لتقدير السرعه والزوايه خلال جميع نطاقات السرعه بأقل خطأ في التقدير و أقل ضياع للطاقه وتقليل الضوضاء الناجمه عن طريقه الضخ عاليه التردد.

# Contents

<b>Acronyms and Abbreviations .....</b>	<b>viii</b>
<b>List of Symbols .....</b>	<b>ix</b>
<b>List of Figures.....</b>	<b>xi</b>
<b>Chapter 1 Introduction.....</b>	<b>1</b>
1.1 Overview .....	1
1.2 Problem Statement.....	2
1.3 Methodology .....	2
1.4 Research Goals .....	4
1.5 Organization of the Report .....	4
<b>Chapter 2 Literature Review .....</b>	<b>5</b>
2.1 Control Methods.....	5
2.1.1 Scalar Control .....	5
2.1.2 Vector Control.....	6
2.2 Observers and Estimators .....	8
2.2.1 Extended Kalman Filter .....	8
2.2.2 Phase-Locked Loop.....	9
2.2.3 Sliding Mode Observer (SMO).....	9
2.3 Signal Injection and Saliency Tracking Estimators.....	12
2.3.1 Saliency Property in PMSM .....	12
2.3.2 Voltage Pulse Estimator.....	14
2.3.3 High-Frequency Injection Estimator.....	15
2.3.4 The Polarity Determination.....	17
2.4 Literature Summery.....	18
<b>Chapter 3 Proposed Hybrid System.....</b>	<b>19</b>
3.1 Mathematical Model of PMSM.....	19
3.2 Sliding Mode Observer.....	21

3.2.1	SMO for Outer Rotor Non-Salient Pole PMSM .....	21
3.2.2	SMO for Inner Rotor Salient Pole PMSM.....	22
3.3	High-Frequency Injection .....	28
3.4	Direct Extraction Method.....	30
3.5	The Proposed Hybrid System.....	31
<b>Chapter 4 Simulation and Results .....</b>		<b>37</b>
4.1	Sliding Mode Observer .....	38
4.1.1	Conventional Sliding Mode Observer .....	41
4.1.2	Improved Relay Sliding Mode Observer .....	43
4.1.3	SMO Conclusion and Contributions.....	50
4.2	Direct Extraction Method.....	51
4.3	High-Frequency Injection .....	54
4.3.1	Blocks Description.....	54
4.3.2	Estimator Design and Simulation .....	56
4.3.3	All-Speed Ranges Simulation.....	59
4.3.4	Polarity Detection and Zero-Speed Simulation .....	60
4.3.5	Injection Voltage Magnitude and Frequency Effect .....	63
4.3.6	Loading Effect .....	64
4.3.7	HFI Conclusion and Contributions .....	66
4.4	Hybrid System.....	67
<b>Chapter 5 Conclusions and Future Work.....</b>		<b>71</b>
5.1	Conclusions .....	71
5.2	Future Work .....	73
<b>References .....</b>		<b>75</b>

# Acronyms and Abbreviations

AC	Alternating Current
DC	Direct Current
DTC	Direct Torque Control
EMF	Pulse Width Modulation
EV	Electric Vehicle
FOC	Field-Oriented Control
HFI	High Frequency Injection
IRPMSM	Inner Rotor Permanent Magnet Synchronous Motor
MPC	Model Predictive Control
PLL	Phase-Locked Loop
PM	Permanent Magnet
PMSM	Permanent Magnet Synchronous Motor
PWM	Pulse Width Modulation
SMC	Sliding Mode Control
SMO	Sliding Mode Observer
SMPMSM	Surface Mounted Permanent Magnet Synchronous Motor



# List of Symbols

$\theta_r$	Rotor Position
$\varphi_\alpha$	Alpha Component of PM Flux Linkage
$\varphi_\beta$	Beta Component of PM Flux Linkage
$\varphi_r$	PM Flux Linkage
$d$	Motor Shaft Diameter
$e_\alpha$	Alpha Component of Back EMF
$e_\beta$	Beta Component of Back EMF
$e_s$	Motor Back EMF $[e_\alpha \ e_\beta]^T$
$\hat{e}_\alpha$	Estimated Alpha Component of Back EMF
$\hat{e}_\beta$	Estimated Beta Component of Back EMF
$G$	Improved SMO Gain
$i_\alpha$	Alpha Component of Stator Current
$i_\beta$	Beta Component of Stator Current
$i_{\alpha i}$	Alpha Component of Injected Stator Current
$i_{\beta i}$	Beta Component of Injected Stator Current
$I_r$	Motor Rated Current
$i_s$	Stator Current $[i_\alpha \ i_\beta]^T$
$\hat{i}_\alpha$	Estimated Alpha Component of Stator Current
$\hat{i}_\beta$	Estimated Beta Component of Stator Current
$\hat{i}_s$	Estimated Stator Current $[\hat{i}_\alpha \ \hat{i}_\beta]^T$
$\bar{i}_s$	Stator Current Estimation Error

$J$	Motor Inertia
$K$	Conventional SMO Gain
$L$	Motor Winding Inductance
$L_d$	Direct Component of Motor Winding Inductance
$L_q$	Quadrature Component of Motor Winding Inductance
$n$	Motor Rated Speed
$P$	Motor Poles Number
$R$	Stator Resistance
$RLY$	Improved SMO Sigmoid Relay
$T_{ind}$	Motor Induced Torque
$T_l$	Motor Applied Load Torque
$v_\alpha$	Alpha Component of Stator Voltage
$v_\beta$	Beta Component of Stator Voltage
$v_{\alpha i}$	Alpha Component of Injected Stator Voltage
$v_{\beta i}$	Beta Component of Injected Stator Voltage
$v_i$	Injected Stator Voltage $[v_{\alpha i} \quad v_{\beta i}]^T$
$v_s$	Stator Voltage $[v_\alpha \quad v_\beta]^T$
$\omega_f$	Fundamental Frequency
$\omega_i$	Injected Frequency
$\omega_r$	Rotor Speed
$Z$	Sliding Switch Output $[z_\alpha \quad z_\beta]^T$
$z_\alpha$	Alpha Component of Sliding Switch Output
$z_\beta$	Beta Component of Sliding Switch Output

# List of Figures

Fig. 1-1: The Proposed Methodology .....	3
Fig. 2-1: The Diagram of PMSM Control Methods.....	6
Fig. 2-2: The Diagram of the Conventional SMO .....	10
Fig. 2-3: The diagram of SMO Stator Current's Estimator Block .....	10
Fig. 2-4: The Speed Related Sigmoid Function [25] .....	12
Fig. 2-5: The PMSM Types According to the PM's Arrangements [27].....	13
Fig. 2-6: High-Frequency Injection Estimation Process Stages.....	16
Fig. 2-7: (a): Salient Motor Inductance During Normal Rotation of Motor, (b): Salient Motor Inductance During Rotation of Motor with Polarity Check Signal Injection [41].....	17
Fig. 3-1: The per Phase Equivalent Circuit of PMSM .....	19
Fig. 3-2: PMSM Modelling in All Stator Reference Frames .....	20
Fig. 3-3: High-Frequency Injection Filtration Stages .....	28
Fig. 3-4: The General Block Diagram of the Hybrid Observer .....	32
Fig. 3-5: The Hybrid Switching System Flow Chart .....	34
Fig. 4-1: A Prototype Motor Nameplate .....	37
Fig. 4-2: Simulink Model of the Proposed SMO System .....	38
Fig. 4-3: Field Oriented Controller Block.....	39
Fig. 4-4: Motor-Inverter pair Model Block.....	40
Fig. 4-5: Observer Block.....	40
Fig. 4-6: The Designed $\alpha$ -Observer of the Conventional SMO .....	41
Fig. 4-7: The Estimated and Measured Speed of the Controlled PMSM.....	41
Fig. 4-8: The Delay and Offset of the SMO Estimated Speed.....	42

Fig. 4-9: The Estimated and the Measured Position Using Conventional SMO .....	42
Fig. 4-10: The Designed $\alpha$ -Observer of the Improved SMO .....	43
Fig. 4-11: Improved SMO (a) The Estimated and the Measured Position .....	44
Fig. 4-12. (a): Reference Speed in (rpm). (b): The Estimated and the Measured Electrical Position. (c): The Estimation Error in the PM Electrical Position.....	45
Fig. 4-13. For Low-Speed Simulation: (a): The Applied Load Torque (b): The Uncompensated Estimation Error in the Electrical Position. (c): The Compensated Estimation Error in the Electrical Position.....	46
Fig. 4-14. For High-Speed Simulation: (a): The Applied Load Torque b): The Uncompensated Estimation Error in the Electrical Position. (c): The Compensated Estimation Error in the Electrical Position.....	47
Fig. 4-15: The Effect of Increasing Speed and Load Torque on the Rotational Currents, Electrical Position Error, and Induced Torque Error .....	48
Fig. 4-16: The General Simulation of the Proposed SMO Under Full Load in Both Directions and Both of Low and High Speed in Both Directions .....	49
Fig. 4-17. (a): The SMO Estimated Mechanical Speed for Variable Reference Speed and Reference Torque (b): The Rotational Components of the Controlled Voltage.....	50
Fig. 4-18. (a): The Controller Reference Speed (b): The Stator Electrical Reference Frame Currents (c): The Stator Stationery Reference Frame Currents (d): The Estimated Position Using the Direct Extracted Method .....	51
Fig. 4-19. (a): The Controller Reference Speed (b): The Tested Load Torque (c): The Stator Stationery Reference Frame Currents (d): The Estimated and the Real Position Using the Direct Extracted Method.....	52

Fig. 4-20: The Initial Values of the Estimated and the Real Position While Standing at Different Positions .....	53
Fig. 4-21: Simulink Model of the Simulated HFI System .....	54
Fig. 4-22: Space Vector Pulse Width Modulation (SVPWM) Block .....	55
Fig. 4-23: The HFI Estimation Stages Blocks .....	56
Fig. 4-24: The Stationary Drawn Currents During Injection .....	57
Fig. 4-25: The Four Stages of Position Sinusoidal Information Extraction.....	58
Fig. 4-26: The First Synchronous Filter Frequency Effect .....	58
Fig. 4-27. (a): The HFI Estimated Position During Deferent Ranges of Speed, (b): The HFI Estimated Electrical Position Error from Low to High Speed.....	59
Fig. 4-28: The Estimation Delay Shown in the Estimated Position and Error .....	60
Fig. 4-29: The Uncompensated Polarity Estimated Position When the Permanent Magnets Located: (a) At the First Polarity Cycle at Starting, (b): At the Second Polarity Cycle at Starting.....	62
Fig. 4-30: Polarity Compensated SMO Estimated Position for Different Polarity Locations	62
Fig. 4-31: Injection Voltage Amplitude Effect on Torque, Speed and Estimated Position ....	64
Fig. 4-32: The Load Effect on the Estimated Position During Standstill .....	65
Fig. 4-33: The General Simulation of the Proposed HFI Estimator under Full load in both Directions and at Low and High Speeds in both Directions. ....	66
Fig. 4-34: Full Speed Hybrid Estimated Mechanical Speed and Electrical Position.....	68
Fig. 4-35: General Simulation of Electrical Position and Mechanical Speed Hybrid Estimation During all Operation Regions of the Studied Motor.....	70



# Chapter 1

## Introduction

---

### 1.1 Overview

Recently, the PMSM had the lion's share in the trend market of traction machine applications and electric vehicles, because of its advantages, over other Alternating Current motors, such as high-power density and lower losses. It uses permanent magnets instead of the rotor winding on the surface of the rotor, which increases the motor power density, decreases the effect of temperature and size [1]. On the other hand, the usage of the Permanent Magnet (PM) makes the control of the motor more complex, because the excitation current depends on the permanent magnets and its angular position related to the stator winding. As a result, the position of the permanent magnet needs to be known to make a complete control on the motor in the absence of the rotor winding, using an encoder as a position sensor connected to the shaft of the motor. The PM position could be determined and the control is achieved by controlling the speed via transforming the  $(a \ b \ c)$  stator current into two orthogonal signal frames to control the torque and the flux of the motor [2].

Using the absolute encoder has many disadvantages on the system; it increases the cost and the size of the motor [3]. The encoder wiring is affected by the noise and the electromagnetic signals, which affect the reliability of the system.

The sensorless control eliminates the existence of the encoder and decreases the cost of the system. The position can be estimated, by using an estimator to calculate the estimated position depending on the measured data of the stator currents and voltages, increasing the reliability of the system and reducing the motor parameter variation effect on the controller. On the other hand, constructing the observer increases the complexity of the control system. Many types of observers have been developed and tested on the PMSM such as Kalman filter and Sliding Mode Observer (SMO). A hybrid controller is proposed as a position and speed estimator.

## **1.2 Problem Statement**

Controlling the PMSM needs an accurate control algorithm to be used and the determination of the rotor position is necessary to complete the vector control algorithm. The determination of the rotor position using external position sensors affects the system cost, volume, control reliability and the sensors maintenance need. On the other hand, the position estimators face many challenges behind its advantages; such as noise, complexity, and poor estimation at some ranges of speed.

## **1.3 Methodology**

The Methodology used in this research starts with a literature review, which contains reviewing and comparison of different types of position and speed estimators. A comparison should be made for the advantages of all the studied estimators, and the literature need to be summarized before selecting the candidate estimators. High speed estimator and low speed estimator which will be selected from the studied estimators should be studied and designed to contribute the estimation accuracy. Then the Controller should be developed and designed to achieve the speed, torque, and flux control of the prototype Permanent Magnet Synchronous Motor (PMSM) using the Field Oriented Control (FOC) mechanism. The system estimators need to be studied, mathematically modeled, and simulated separately using the prototype motor and the proposed controller regarding to the region of operation, and studying all the motor's load-speed conditions as an application of electric vehicle. A hybrid system is suggested to be designed containing the advantages of the selected estimators to achieve a full speed range estimation. Finally, the validation of the proposed system should be done by simulating the proposed system on the prototype motor to validate the research goals and hypotheses in all its conditions. While the following Fig. 1-1 shows a flow chart of the proposed methodology.



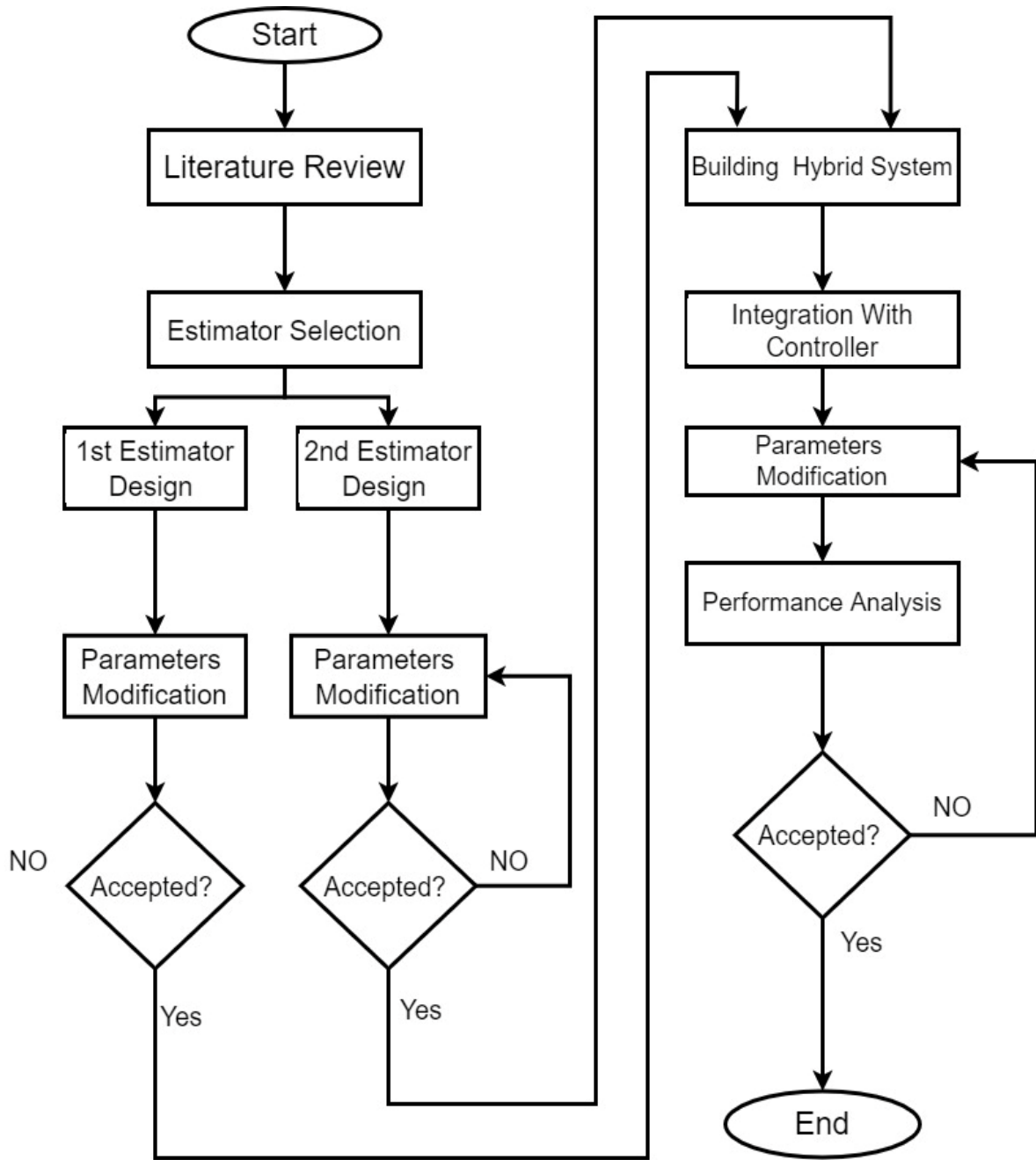


Fig. 1-1: The Proposed Methodology

## 1.4 Research Goals

The objectives of the research are as follow:

- To build the structure of the proposed hybrid observer and represent the mathematical implementation of the observation process and control algorithm
- To achieve an accurate estimation of rotor position and speed during the speed range and standstill with lower cost and execution process
- To achieve the minimum effect on the torque ripple, by implementing and enhancing the proposed control scheme
- To examine the proposed system using Matlab/Simulink using a real PMSM model during all motoring load conditions and all speed ranges

## 1.5 Organization of the Report

The report is organized into five chapters and the rest of this report is organized as follows:

- Chapter 2 presents a review of Control Techniques used in controlling the flux and torque of alternating current motors. The chapter also presents a review of different observer types used in sensorless control techniques.
- Chapter 3 introduces the construction, the mathematical implementation, and the basic principle of operation of the studied motor and controller. It also describes the construction and the principle of operation of the proposed estimation technique.
- Chapter 4 presents the simulation results of the proposed estimation techniques combined with the controller.
- The last chapter concludes the work presented in the research and proposes future work.

# Chapter 2

## Literature Review

---

Recently, the Permanent Magnet Synchronous Motor (PMSM) has a wide range of use in many applications, such as Electric Vehicles (EV) and traction machines, because of its small size, high power density, and high efficiency, which make it a good choice in the trend market. On the other hand, the control of PMSM faces many challenges, which make it more complex than other types of motors. Therefore, the control of the motor has a wide range of studies. This chapter reviews the main types of controlling the PMSM, also reviews the types of position measurement sensors and the observers' types depending on the estimation accuracy, reliability, and complexity.

### 2.1 Control Methods

Controlling the speed of a PMSM according to the applied winding input voltage can be classified into two types; scalar and vector control. They control the input frequency depending on the speed commands. While in order to avoid the field weakening and providing the maximum required torque, the voltage should be also controlled.

#### 2.1.1 Scalar Control

In this method, the voltage and the frequency of the stator of the motor have a constant ratio to achieve working at the rated load in a simple procedure and a wide range of speed control. In synchronous motors, an open-loop controller could be simply used to drive the motor at the dedicated torque and speed using the controlled voltage and frequency. The scalar control algorithm has a good steady-state result compared to the conventional controlled algorithms, but it has a poor transient result and slow response time during acceleration [4].

## 2.1.2 Vector Control

The AC motor has a dependency between the torque and the flux, which need to be controlled separately, and to perform an independent control for both torque and flux, dedicated measuring sensors measure the motor parameters such as stator resistance and winding inductance, also stator components such as voltages and currents. Control techniques of PMSM are classified according to the block diagram of Fig. 2-1, where the Field-Oriented Control (FOC) and Direct Torque Control (DTC) have been studied in the following subsections [5].

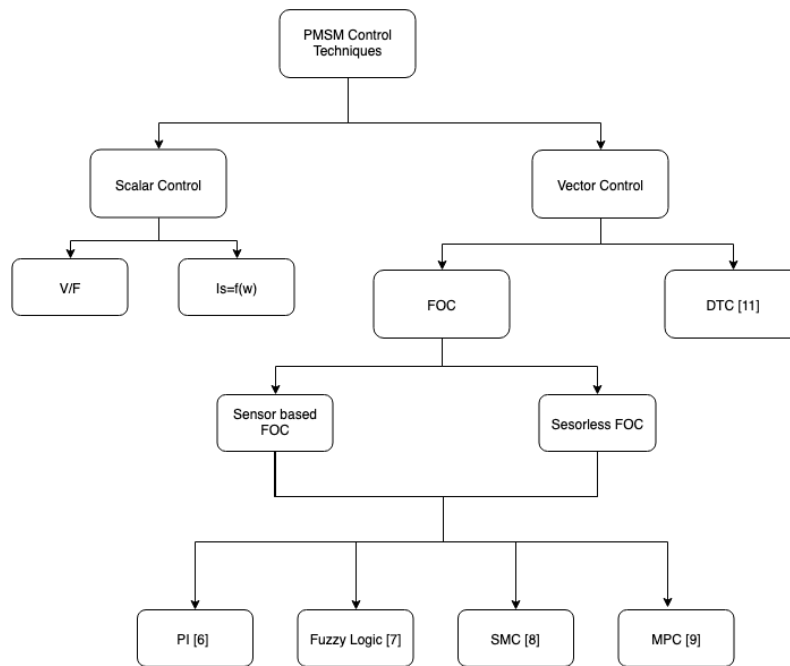


Fig. 2-1: The Diagram of PMSM Control Methods

### 2.1.2.1 Field Oriented Control

The most common method in vector control of the PMSM depends on transforming the stator current from the stator reference frame into the  $\alpha$ - $\beta$  stationary reference frame, while the rotor position is needed to complete the transforming from the stationary reference frame into the rotating d-q reference frame. In order to control the speed, flux, and torque, the control should be made by measuring the feedback data from the d-q components of the currents, which are proportional to the dedicated references. A regulator is used to process the error signal of the reference and feedback signals such as Proportional Integral (PI) [6], Fuzzy [7], Sliding Mode

Controller (SMC) [8], or Model Predict Control (MPC) [9], is used. It gives control on both torque and flux at the same time at all speed ranges even at low speed with different transient and dynamic behavior and steady-state accuracy depending on the application and the regulator used [10].

#### **2.1.2.1.1 Sensor-Based FOC**

The vector control Field Oriented Control (FOC) of PMSM depends on the determination of the rotor position to complete the transformation from the stationary  $\alpha$ - $\beta$  reference frame into the d-q rotating reference frame. The determination of the position could be achieved by using measuring devices such as optical sensors, tachometer, or resolvers. On the other hand, the measuring of the rotor position suffers from the error generated by the noise of the environment and the variation of machine parameters that affect the control system. Also, the cost, the size, and the maintenance requirements limit the usage of the speed and position sensor.

An optical encoder has been introduced and improved to measure and process the sinusoidal form of the rotor position and speed to reduce the measured error in the final stage of transformation and to be used directly without processing.

#### **2.1.2.1.2 Sensorless FOC**

In the sensorless FOC, instead of measuring the position data and affecting the reliability of the system, a position estimator could be used in determining the rotor position, back EMF, and flux of the motor in order to complete the control process. This method eliminates the position sensor and their maintenance requirements, reduces the size and cost of the system, increases reliability, and enhances the speed tracking capability, and reduces the ripple in the output speed and torque [2].

In order to determine the position, an observer, estimator, or test injection calculators could be used and processed, with different precision and accuracy depending on the used application. The following section describes different types of sensorless estimators used in controlling the FOC of PMSM.

### **2.1.2.2 Direct Torque Control**

Direct Torque Control (DTC) is used to control the torque and the speed of alternating current machines by measuring the stator currents and voltages using current and voltage sensors. The flux linkage could be found from the voltage measured, while the torque is calculated from the measured voltages and currents, to establish the control procedure in the stator reference frame, which cancels the need of the rotor position in controlling the flux and the torque. A simple on/off controller could be used to determine the controller reference values in order to achieve the system requirements. The DTC method suffers from ripples of the motor's torque, currents, and flux linkage during steady-state operation especially at the low speeds [11].

## **2.2 Observers and Estimators**

The observer is needed to estimate the online value of the rotor position and speed according to complete the vector control process and determine the direction of the permanent magnet for flux calculations. The observers differ in their complexity, response time, and their accuracy, as shown in the following subsections, which describe different types of position observers.

### **2.2.1 Extended Kalman Filter**

It's a non-linear state variable estimator, which uses the noise signal to optimize the estimation of the stator flux linkage and the rotor position [12]. The estimator does not need the initial rotor position to complete the estimation, as it works with optimization problems; it studies the measured and the estimated state variables and the calculated states from the motor model in a complex matrix and large executions, which need a long time to be evaluated. The major drawback of this method is the tuning of the covariance matrices [13], which makes the estimator more complex and not suitable for low-budget applications, and also fails to be accurate at low speeds [14].

## **2.2.2 Phase-Locked Loop**

This method relies on estimating the rotor position and speed from the information of the estimated back EMF; such an estimator might be with another one. It reduces the chattering effect and accurately determines the position information using a PID controller with a low error [15]. The estimation method suffers from the tuning problem and the controller's parameter identification during different speed ranges and directions. A compensation mechanism is needed also to overcome the offset in the position estimation [16].

## **2.2.3 Sliding Mode Observer (SMO)**

The sliding mode observer is a non-linear estimator that has been widely used in sensorless traction machine vector control flux and speed estimations. The observer is used to force the error in the estimated stator current and back EMF signal to decay with the zero linear sliding surfaces of the error signal, by switching the control signal, forcing the system to slide around the sliding reduced-order surface using two different control signals according to the direction of the measured signal and errors [17]. Many different types of sliding mode observers have been studied and written in the following subsections.

### **2.2.3.3 Conventional Sliding Mode Observer (SMO)**

The Conventional SMO uses the measured currents and voltages error states to slide around the zero sliding surface, using two different linear control signals switched using a signum relay switch as in Fig. 2-2, which causes the nonlinearity of the system. The structure and the performance of the SMO are accurate and robust due to parameter variations such as stator resistance, inductance, and torque constant [18]. The main drawback of the conventional SMO is the switching function in the continuous-time domain between the two sides of the sliding surfaces, which will cause chattering problems in the observer presented as high-frequency components in the estimated back electromotive force (EMF). The chattering problem needs to be filtered, and consequently, the filtering will cause phase delay in the system introducing an error in the estimation, while a compensation mechanism is needed to overcome this error in the rotor position [19].

Fig. 2-2 shows the general block diagram of the conventional SMO connected to the PMSM controller, while the SMO stator current estimator contains the algorithm for calculating the stator current depending on the stator voltage and sliding current, as shown in Fig. 2-3.

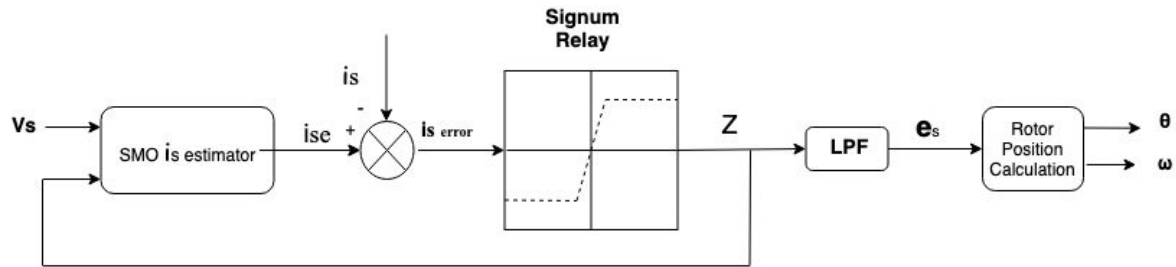


Fig. 2-2: The Diagram of the Conventional SMO

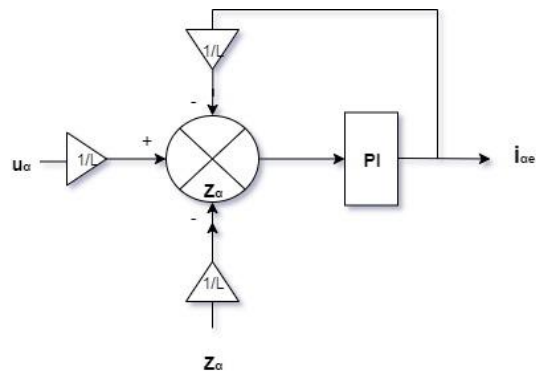


Fig. 2-3: The diagram of SMO Stator Current's Estimator Block

The error obtained in the stator current estimation can be used to drive the sliding signum switch into its sliding mode, which generates the switched  $Z$ . On the other hand, the current estimation depends on the  $Z$  signal in estimating the stator current. Sliding the currents through the signum relay forces the error to slides around zero approaching the value of the motor back electromotive force. Sliding around zero current error makes the filtered switch's sliding output to be equal to the motor estimated electromotive force (EMF). Equation (2.1) describes the relationship between the signum relay output and the estimated back EMF [20].

$$\hat{e}_\alpha = \frac{\omega_c}{s + \omega_c} Z_\alpha \quad (2.1)$$



Where  $\hat{e}_\alpha$  represents the  $\alpha$  component of the estimated back EMF,  $\omega_c$  represents the low pass filter cutoff frequency, and  $Z_\alpha$  represents the  $\alpha$  component of the signum relay output. The position calculator block is used to calculate the rotor position and speed from the estimated back EMF, which feeds the controller by the appropriate data to control the flux and the torque depending on the dedicated speed [21].

The estimated current ( $i_s$ ), the winding voltage ( $v_s$ ), and the relay outputs ( $Z$ ) consist of two components in the stationary frame ( $\alpha, \beta$ ), while the current estimator block consists of two estimators to estimate both of the current components.

#### **2.2.3.4 Second-Order Sliding Mode Observer**

The higher-order sliding mode observer consists of an additional differentiator to overcome the chattering problem caused by the switching relay, the sliding differentiator is added to the conventional sliding mode observer to eliminate the chattering effect, thus to omit the usage of the low pass filter [20].

#### **2.2.3.5 Sliding Mode Observer with Improved Relay**

The switched relay in the conventional SMO causes chattering which, appears as a high-frequency noise in the estimation of back EMF value. The chattering is caused because of the fast switching during the sliding between the sides of the sliding surface, while a low pass filter needs to be used to overcome this problem. On the other hand, the switching relay could be improved by curving the switching using different types of switching relays. In [22], a sigmoid function has been proposed as a switching relay for the SMO instead of the conventional signum switch. It reduces the chattering effect, speeds up operation, and simplifies the executions [23]. Using a curved sigmoid function as a sliding switching mechanism, cancels the needs for the low pass filter in estimating the electromotive force, which improves the estimating process without filtering time delay effect, which cancels the need for the position estimation compensation process.

The sigmoid function is classified as one of the activation functions, which limits the output to a range between 0 and 1, with a curvy slope and (S) shape. Sigmoid function has been used

in machine learning and artificial intelligence applications, to overcome the infinite repeated switching mechanism to avoid controller failure caused by hard switching [24].

A speed-related sigmoid function has been improved in [25] to omit the chattering problem at the full speed range. It controls the feedback gain of the observer as in eq. (2.1) to overcome the level of speed on the observer output, eliminating the harmonics at higher speeds by increasing the thickness of the sigmoid function and increasing the response speed at lower speeds by decreasing the sigmoid function thickness [25]. Fig. 2-4 shows the effect of the speed on the thickness of the sigmoid function relay.

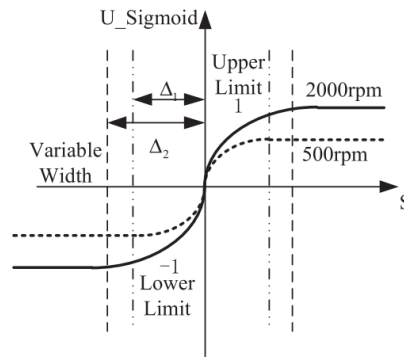


Fig. 2-4: The Speed Related Sigmoid Function [25]

## 2.3 Signal Injection and Saliency Tracking Estimators

The starting and standstill rotor position estimation couldn't be found using the back EMF estimation. An alternate method is introduced to determine the zero and low-speed position of the rotor using the saliency property of the motor by injecting additional voltage to the stator winding, which does not affect the operation of the motor. This method tracks the saliency of the motor to determine the position by measuring the stator currents and decomposing their components to extract the rotor position information. Different types of estimators are listed in the following subsections depending on the type of the injected signal.

### 2.3.1 Saliency Property in PMSM

The PMSM type can be defined and classified depending on the rotor coupling method used in the traction application. It also depends on the rotor geometry, and the location of the

Permanent Magnets (PM's) on the rotor. While the PM location defines the saliency type of the motor such as salient and non-salient PMSM or Inner Rotor Permanent Magnet Synchronous Motor (IRPMSM) and Surface Mounted Permanent Magnet Synchronous Motor (SMPMSM).

Fig. 2-5 shows the location of the permanent magnets depending on the motor rotor type. The SMPMSM has the permanent magnets located on the surface of the motor, and this type of PMSM rotor usually has the rotor surrounding the motor stator with a large sheave diameter, and it is used for gearless direct coupling hoists traction machines and for direct coupling, wheel connected electric vehicles. While the IRPMSM has its permanent magnets located built-in inside the motor rotor iron, and this type of PMSM saves the work space, reduces the motor volume, and increasing the motor power density, making it widely used in the commercial market [26].

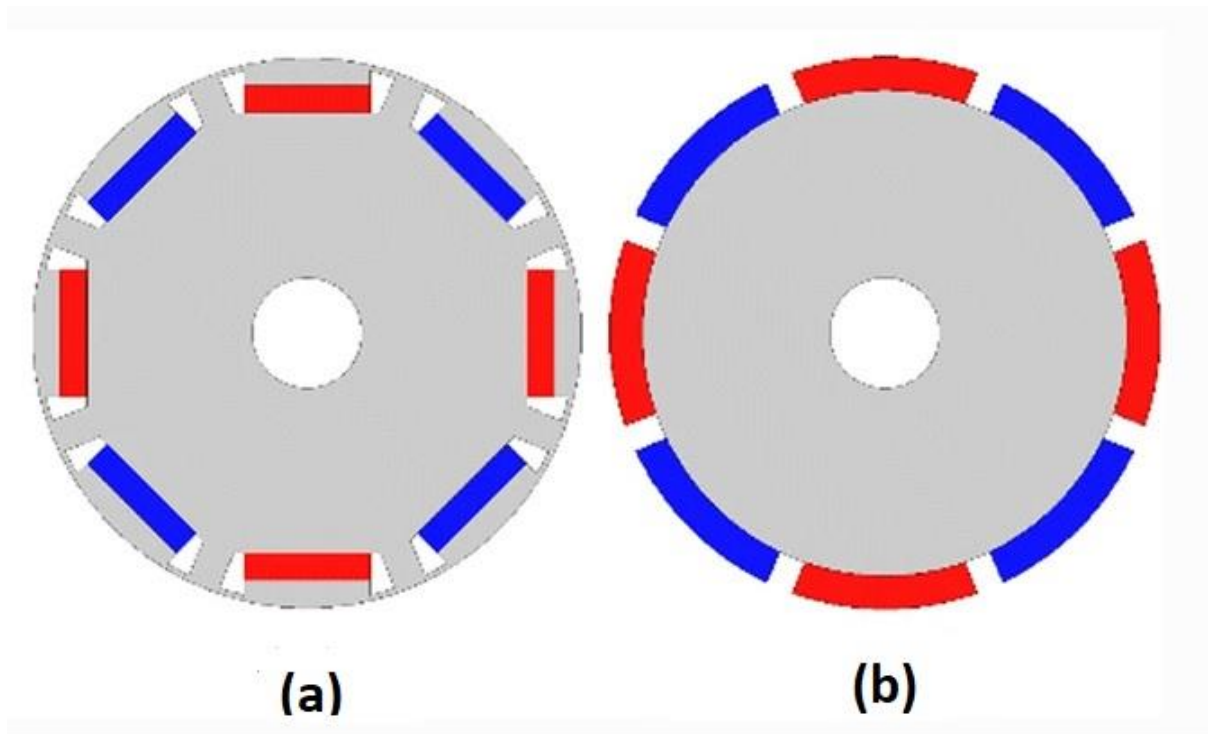


Fig. 2-5: The PMSM Types According to the PM's Arrangements [27]

According to the permanence of the PM's, the effective air gap in the IRPMSM in the rotational reference frame d-axis is much larger than that in the quadrature q-axis, which makes

the difference in the rotational reference frame inductance components more significant and varies depending on the location of the PM's, making the d-axis inductance in the IRPMSM is lower than the q-axis inductance. On the other hand, the SMPMSM rotational reference frame inductance components are the same along with the rotation of the motor and the permanent magnet due to the equality of the direct and the quadrature airgaps [28]. The difference between the quadrature and the direct components defines the rotor geometry saliency property of the PMSM, which makes the ability to track the PM's location due to the relation between both of the inductance components and the direction of the magnets. On the other hand, the SMPMSMs have no geometry saliency in their inductance components, but a saturation saliency, which could be induced when the flux saturating the iron core making a difference in the inductance rotational components [28]– [30].

There are many methods to track the rotor position by measuring the saliency in the motor drawn currents, and these types could be classified according to the signals injected to the stator windings to high and low signal injection method, sinusoidal and pulsating voltage injection methods [31], [32]. While the high-frequency injection and the voltage pulsating injection estimators have been introduced in the following subsections.

### **2.3.2 Voltage Pulse Estimator**

The voltage pulse estimator, based on injecting a dedicated voltage pulse magnitude and width applied to the motor windings does not depend on the saliency of the motor, which makes it applicable for both types of PMSM rotors; surface-mounted and interior rotor. However, it depends on the stator iron saturation due to the stator current results from the stator injected pulse [33]. The estimation process depends on measuring the d-axis current drawn from the stator windings during the voltage test vector injection at standstill, without any effect from the variation of the motor parameters. The method succeeds in estimating the rotor starting position of both types of motor rotors without the need for motor saliency. On the other hand, it works only during zero speed operation with a degree of estimation error, also it cannot be used during motor rotation [30].

### 2.3.3 High-Frequency Injection Estimator

To overcome the problem of determining the rotor position at a standstill and low speeds, a high-frequency signal could be injected into the rotating  $\alpha$ - $\beta$  components of the voltage with a frequency much higher than the fundamental frequency to track the rotor position information according to the geometry saliency of the PMSM, while the injected voltage produces a high-frequency inductance variant rotating currents, which is drawn by the motor stator windings, which need to be processed and demodulated to extract the rotor position in cascaded steps depending on the injection selected reference frame [34] [35]. The injected signal could be represented as shown in eq. (2.2) [34]:

$$V_i = \begin{bmatrix} V_{\alpha i} \\ V_{\beta i} \end{bmatrix} = |V| \begin{bmatrix} -\sin(\omega_i t) \\ \cos(\omega_i t) \end{bmatrix} \quad (2.2)$$

where  $V_{\alpha i}, V_{\beta i}$  are the  $\alpha, \beta$  components of the high-frequency injected voltage, while  $\omega_i$  represents the frequency at which the injected voltage has been modulated.

While using the current sensors, the measured stator current in the rotating  $\alpha$ - $\beta$  frame contains multiple components with harmonics as in eq. (2.3) [36]:

$$\begin{bmatrix} i_{\alpha i} \\ i_{\beta i} \end{bmatrix} = \begin{bmatrix} I_1 \cos(\omega_i t) + I_2 \cos(2\theta_r - \omega_i t) \\ I_1 \sin(\omega_i t) + I_2 \sin(2\theta_r - \omega_i t) \end{bmatrix} \quad (2.3)$$

where  $i_{\alpha i}, i_{\beta i}$  are the  $\alpha, \beta$  components of the high-frequency stator's drawn currents, and  $\omega_i, \omega_f$ , and  $\theta_r$  represents the frequency at which the injected voltage has been modulated, the fundamental frequency of the motor, and the rotor position, respectively. The measured stator current contains the position information, which is located in the negative sequence component. It also contains the fundamental and positive sequence components. An accurate procedure needs to be evaluated to extract the position information from the measured current, by applying the measured value into a bandpass filter to remove the fundamental component, then it is applied to a separator to extract the negative component originating the positive sequence into DC component in a process called coordination rotation [37]. The DC component could be removed by using a low pass filter followed by an inverse coordination rotation to return the frame into the synchronous frame. Fig. 5-2 shows the main steps of the injection process.

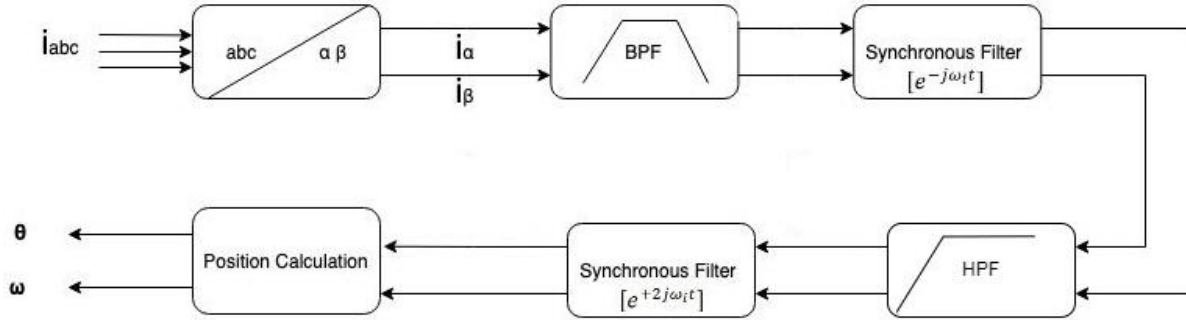


Fig. 2-6: High-Frequency Injection Estimation Process Stages

The injection process solved the problem of finding the rotor position at a standstill and low speeds during the absence of the electromotive force. It uses the saliency property of the difference between the quadrature and direct inductance of the Inner Rotor Permanent Magnet Synchronous Motor (IRPMSM) stator [38]. On the other hand, the process uses the variable inductance of the operated motor, which makes it affected by the variant of the motor parameters during the motor rotation and condition, which needs to be online tuned during the motor operation to enhance the demodulation process in all conditions, as illustrated in [37].

The Surface Mounted Permanent Magnet Synchronous Motor (SMPMSM) rotor position also could be estimated under the high-frequency injection method, as illustrated in [38] [39], where a dual iron saturation technique is used to produce a saturation saliency making differences between the rotational components of the stator inductance to estimate the starting and standstill PM position, which determines the rotor position during standstill possible for all types of the PMSM.

On the other hand, this method uses the injected power to estimate the position, which increases the power consumption, vibration in the produced torque and produces an audible noise due to the high-frequency components in the input voltage.

### 2.3.4 The Polarity Determination

The previous conventional methods of frequency injection could determine the position and direction of rotation in the low-speed region and standstill. On the other hand, it estimates the starting position in one-half of the rotation cycle without identifying the polarity of the PMs. For completing the control process, the position needs to be determined in all planes and directions [40].

Two standstill pulse voltages could be used to identify whether the PM flux linkage and the stator flux linkage are at the same rotation cycle polarity or not. While by measuring the stator currents for both testing pulses conditions, the polarity could be defined. If the direct current measured during the second pulse test is larger than that during the first test, compensation is needed to add 180 electrical degrees to the rotor position. On the other hand, this method should be operated before the starting of the motor, and independently from the estimation process and the controller, which increases the complexity of the estimation system [41].

Fig. 2-7 shows the effect of injecting a bi-directional voltage pulse on the rotational reference frame inductance, which makes the rotor current direct component during the negative pulse larger than its magnitude during negative pulse when the north pole is located in the first cycle of the PM rotation. On the other hand, the second cycle of the PM rotation is obtained when the direct current during the positive pulse injection is less than its magnitude during the negative pulse injection.

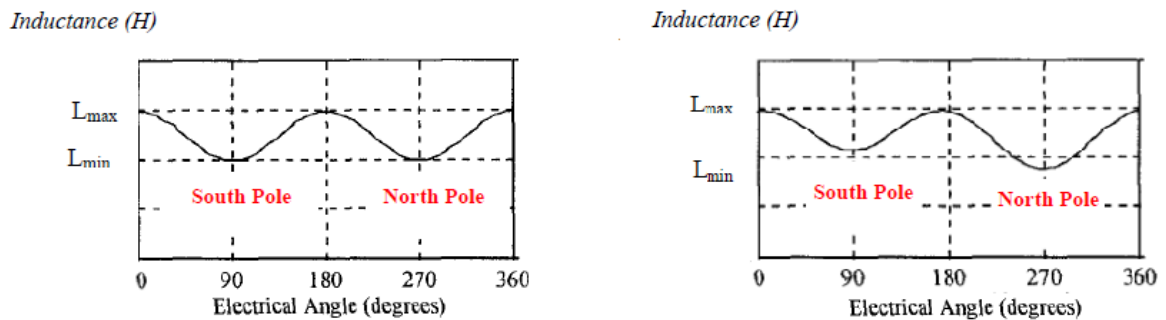


Fig. 2-7: (a): Salient Motor Inductance During Normal Rotation of Motor, (b): Salient Motor Inductance During Rotation of Motor with Polarity Check Signal Injection [41]

## 2.4 Literature Summery

According to the previous study, each estimator has its advantages among the other estimators in their accuracy, complexity, region of operation, response time, and the external environment effect. While in order to candidate the preferred estimator, the following comparison in Table 2-1 has been made regrading to the previous specifications. While EKF, PLL, SMO, IMP.SMO, VP, HFI represents Extended Kalmen Filter, Phase Locked Loop, Sliding Mode Observer, Improved Sliding Mode Observer, Voltage Pulse, and High Frequency Injection respectively.

Table 2-1:  
Estimator Comparison

	Accuracy	Regions Of Operation	Response Time	External Effect	Complexity
EKF	. Time delay	. High Speed	. Slow Response	. No Effect	. Complex . Needs Tune
PLL	. Time delay	. High Speed	. Fast Response	. Parameter	. Complex . Needs Tune
SMO	. Chattering . Time Delay	. High Speed	. Slow Response	. No Effect	. Simple
IMP. SMO	. Accurate . Low Error	. Low Speed . High Speed	. Slow Response	. No Effect	. Simple
VP	. Low Error	. Zero Speed . Low Speed . Unipolar	. Fast Response	. Noise . Power Loss . Parameter	. Complex
HFI	. Time Delay	. Zero Speed . Low Speed . High Speed . Unipolar	. Fast Response	. Noise . Power Loss . Parameter	. Simple . Complex Polarity



# Chapter 3

## Proposed Hybrid System

---

This chapter introduces the construction and the basic principle of operation of the PMSM. It also presents the Vector Control approach on the motor and studying the motor components in multi-reference frames. Finally, it presents the model of the traction motor and the mathematical model of the proposed hybrid estimation process.

### 3.1 Mathematical Model of PMSM

In order to model the sensorless control of PMSM, a stationary reference frame must be introduced and studied because of the fact that, the independence of the stationary reference frame from the rotor position information, while the position and angular speed could be executed from this frame.

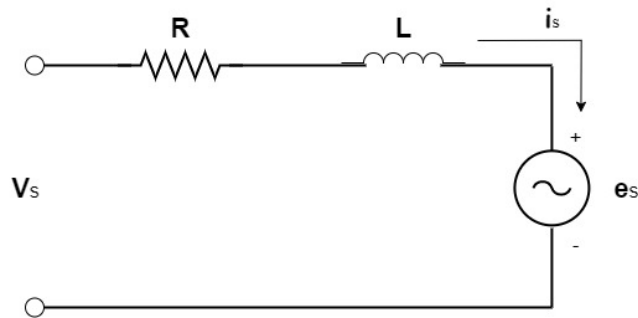


Fig. 3-1: The per Phase Equivalent Circuit of PMSM

Fig. 3-1 shows the stationary reference frame ( $\alpha, \beta$ ) equivalent circuit of Permanent Magnet Synchronous Motor (PMSM), while the state-space representation of the equivalent circuit has been derived as illustrated by eq. (3.1):

$$\frac{d}{dt} i_s = -\frac{R}{L} i_s - \frac{1}{L} e_s + \frac{1}{L} v_s \quad (3.1)$$

where  $i_s$  represents the  $(\alpha, \beta)$  stator currents components,  $e_s$  represents the  $(\alpha, \beta)$  back EMF voltage's components,  $v_s$  represents the  $(\alpha, \beta)$  stator winding input voltage components, in the stationary reference frame, where the back EMF can be represented as:

$$\begin{bmatrix} e_\alpha \\ e_\beta \end{bmatrix} = \begin{bmatrix} -K\omega_r \sin \theta \\ K\omega_r \cos \theta \end{bmatrix} \quad (3.2)$$

where  $\omega_r$  is the rotor speed and  $\theta$  represent the rotor magnetic position.

Expanding eq. (3.1) yields:

$$\frac{d}{dt} \begin{bmatrix} i_\alpha \\ i_\beta \end{bmatrix} = \begin{bmatrix} -\frac{R}{L} & 0 \\ 0 & -\frac{R}{L} \end{bmatrix} \begin{bmatrix} i_\alpha \\ i_\beta \end{bmatrix} - \frac{1}{L} \begin{bmatrix} e_\alpha \\ e_\beta \end{bmatrix} + \frac{1}{L} \begin{bmatrix} v_\alpha \\ v_\beta \end{bmatrix} \quad (3.3)$$

From Newton's second law, the torque and inertia relation are described by the eq. (3.4):

$$J \frac{d\omega_r}{dt} = T_{ind} - T_l \quad (3.4)$$

where  $J$  is the rotor's inertia,  $T_l$  represents the load torque, while  $T_{ind}$  represents the induced motor torque, and could be represented in the stationary reference frame by eq. (3.5) [44]:

$$T_{ind} = \frac{3}{2} P [\varphi_\alpha i_\beta - \varphi_\beta i_\alpha] \quad (3.5)$$

where  $\varphi_{\alpha,\beta}$  are the instant flux linkage of the motor in the stationary reference frame, and  $P$  represents the pole-pairs number.

Fig. 3-2 shows the 2-poles PMSM model in the stationery, rotating, and the stator winding reference frames. The stator currents stationery reference frame can be determined regardless to knowing the rotor electrical position, which offers two orthogonal components of the stator currents to be used in the estimation of the motor EMF stationery components.

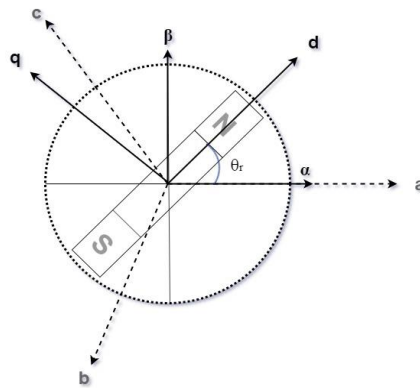


Fig. 3-2: PMSM Modelling in All Stator Reference Frames

## 3.2 Sliding Mode Observer

To study the sliding mode observer, the state space system has to be defined by considering the following system in eq. (3.6):

$$\dot{X} = AX + BU \quad (3.6)$$

and by using the input vector U which is defined as eq. (3.7):

$$U = \begin{cases} u_-, & s(x) < 0 \\ u_+, & s(x) \geq 0 \end{cases} \quad (3.7)$$

Defining the hyperplane,  $S(x) = [\hat{i}_s - i_s]$ , which defines the switching plane of the observer, where  $S(x) = 0$  represents the surface plane, which separates the two systems of controlling depending on the sign of the plane  $S(x)$  and  $\dot{S}(x)$ , while the system will operate in the sliding mode when  $\dot{S}(x) = S(x) = 0$ .

### 3.2.1 SMO for Outer Rotor Non-Salient Pole PMSM

The general torque-flux equation of the PMSM is shown in eq. (3.8), while the non-salient Pole PMSM torque equation has been presented by eq. (3.9) [44].

$$T_e = \frac{P}{2} [\varphi_d i_q - \varphi_q i_d] \quad (3.8)$$

$$T_e = \frac{P}{2} [\varphi_m i_q] \quad (3.9)$$

On the other hand, to obtain the sliding mode observer equation, the current observer condition has to be recognized, by considering the estimated current and the measured stator current. Recalling eq. (3.1), the current observer could be expressed by:

$$\frac{d}{dt} \hat{i}_s = -\frac{R}{L} \hat{i}_s + \frac{1}{L} v_s - \frac{1}{L} \text{RLY}[\hat{i}_s - i_s] \quad (3.10)$$

Where  $\hat{i}_s$  represents the ( $\alpha$ ,  $\beta$ ) components of the estimated stator currents, while RLY stands for the switching relay of the sliding mode observer. By subtracting eq. (3.1) from eq. (3.10) and by considering  $\bar{i}_s = [\hat{i}_s - i_s]$ , eq. (3.11) can be obtained:

$$\frac{d}{dt} \bar{i}_s = -\frac{R}{L} \bar{i}_s + \frac{1}{L} v_s - \frac{1}{L} \text{RLY}[\bar{i}_s] \quad (3.11)$$

Considering the back EMF voltage of the motor as a disturbance, and slides around the zero-sliding surface, the stable sliding stator current error observer's output represents the estimated back EMF of the motor. The estimated rotor position has been obtained by using eq. (3.12):

$$\theta_e = -\tan^{-1} \left[ \frac{\hat{e}_\beta}{\hat{e}_\alpha} \right] \quad (3.12)$$

The estimated rotor speed could be obtained using eq. (3.13):

$$\omega_r = \frac{P}{2} \frac{d\theta_e}{dt} \quad (3.13)$$

By considering the switching relay, RLY, the system needs to be free of chattering problem, an improved sigmoid function could be considered which has a soft switching mechanism with speed-related boundaries. Equation (3.14) describes the switching relay function [25].

$$\text{RLY} = G \left( \left[ \frac{2}{1 + e^{-ax}} \right] - 1 \right) \quad (3.14)$$

where  $a$  defines the shape of the switching function slope and  $G$  describes the switching gain, while in order to define the boundaries of the gain  $G$ , speed relation gain could be used to change the observer response time depending on the switching times during the speed angular cycle and using a constant switching frequency, eliminating the chattering problem and ensuring the robustness of the motor control system during low and high speeds.

### 3.2.2 SMO for Inner Rotor Salient Pole PMSM

According to the saliency property, the orthogonal components of the stator currents differ in their magnitude and phase. They are alternating by rotating the motor which changes the permanent magnet position, which makes the flux linkage not constant in the motor. While this

property could be used to separate the orthogonal states of the observed currents, which increases the observer parameters degree of freedom reducing the estimation error, even at low speeds, and controlling the accuracy of the estimated state variables in all motor situations, such as field weakening operation, Overspeed operation, overload operation, and constant power region operation. While the following eq. (3.15) shows the d-q representation of the presented salient pole motor's torque equation [45].

$$T_e = \frac{P}{2} [\varphi_m i_q + (L_d - L_q) i_d i_q] \quad (3.15)$$

### 3.2.2.1 IRPMSM SMO State Space Representation

While the  $\alpha, \beta$  representation of the salient pole PMSM voltage is represented by eq. (3.16), which finds the mutual relation between the direct and the quadrature components of the stator inductance:

$$\begin{aligned} \begin{bmatrix} v_\alpha \\ v_\beta \end{bmatrix} &= \begin{bmatrix} R_s + \rho L_d & \omega(L_d - L_q) \\ \omega(L_q - L_d) & R_s + \rho L_d \end{bmatrix} \begin{bmatrix} i_\alpha \\ i_\beta \end{bmatrix} \\ &+ [\omega \varphi_m + (L_d - L_q)(\omega i_d - \rho i_q)] \begin{bmatrix} -\sin(\theta) \\ \cos(\theta) \end{bmatrix} \end{aligned} \quad (3.16)$$

where  $\rho$  represents the differential operator and  $\theta$  represents the PM electrical position. The first term of the previous equation describes the induced voltage in the stator windings in terms of the stationary reference frame currents and the rotation reference frame stators inductance. While the second term describes the extended electromotive force, which has been induced according to the rotation of the motor that rotates by the rotation of the d, q alternating inductances.

Equation (3.16) could be simplified as eq. (3.17).

$$\begin{bmatrix} v_\alpha \\ v_\beta \end{bmatrix} = \begin{bmatrix} R_s + \rho L_d & \omega(L_d - L_q) \\ \omega(L_q - L_d) & R_s + \rho L_d \end{bmatrix} \begin{bmatrix} i_\alpha \\ i_\beta \end{bmatrix} + \begin{bmatrix} e_\alpha \\ e_\beta \end{bmatrix} \quad (3.17)$$

From eq. (3.14), the rotor position appears in the extended back EMF term, while the other term is free of the rotor position information and the rotational reference frame current

components, and to determine the rotor electrical position, the electromotive force term needs to be estimated. From the previous equation, the stationery current model of the motor could be obtained as eq. (3.18):

$$\begin{bmatrix} \frac{di_\alpha}{dt} \\ \frac{di_\beta}{dt} \end{bmatrix} = \begin{bmatrix} \frac{-R_s}{L_d} & \frac{-\omega(L_d - L_q)}{L_d} \\ \frac{\omega(L_d - L_q)}{L_q} & \frac{-R_s}{L_q} \end{bmatrix} \begin{bmatrix} i_\alpha \\ i_\beta \end{bmatrix} + \begin{bmatrix} \frac{1}{L_d} & 0 \\ 0 & \frac{1}{L_q} \end{bmatrix} \begin{bmatrix} V_\alpha \\ V_\beta \end{bmatrix} - \begin{bmatrix} \frac{1}{L_d} & 0 \\ 0 & \frac{1}{L_q} \end{bmatrix} \begin{bmatrix} e_\alpha \\ e_\beta \end{bmatrix} \quad (3.18)$$

From eq. (3.18), the SMO model of the IRPMSM could be derived, following the same procedure of derivation in the conventional one such as that of eq. (3.10), and the model is shown in the following equation (3.19). Where  $V_{\alpha s}$ ,  $V_{\beta s}$ , and  $G$  represent the controlled  $\alpha$ ,  $\beta$  voltages in the FOC block, and the switch relay gain respectively.

$$\begin{bmatrix} \frac{d\hat{i}_\alpha}{dt} \\ \frac{d\hat{i}_\beta}{dt} \end{bmatrix} = \begin{bmatrix} \frac{-R_s}{L_d} & \frac{-\hat{\omega}(L_d - L_q)}{L_d} \\ \frac{\hat{\omega}(L_d - L_q)}{L_q} & \frac{-R_s}{L_q} \end{bmatrix} \begin{bmatrix} \hat{i}_\alpha \\ \hat{i}_\beta \end{bmatrix} + \begin{bmatrix} \frac{1}{L_d} & 0 \\ 0 & \frac{1}{L_q} \end{bmatrix} \begin{bmatrix} V_{\alpha s} \\ V_{\beta s} \end{bmatrix} + [G] \begin{bmatrix} RLY(\hat{i}_\alpha - i_\alpha) \\ RLY(\hat{i}_\beta - i_\beta) \end{bmatrix} \quad (3.19)$$

By subtracting eq. (3.18) from eq. (3.19), the error model equation could be obtained and derived as eq. (3.20), for the sliding surface derivation and stability check.

$$\frac{d(\bar{i}_{\alpha,\beta})}{dt} = \begin{bmatrix} \frac{-R_s}{L_d} & 0 \\ 0 & \frac{-R_s}{L_q} \end{bmatrix} \bar{i}_{\alpha,\beta} + (L_d - L_q) \begin{bmatrix} 0 & -\frac{1}{L_d} \\ \frac{1}{L_q} & 0 \end{bmatrix} \begin{bmatrix} \omega i_\alpha - \hat{\omega} \hat{i}_\alpha \\ \omega i_\beta - \hat{\omega} \hat{i}_\beta \end{bmatrix} - \begin{bmatrix} \frac{1}{L_d} & 0 \\ 0 & \frac{1}{L_q} \end{bmatrix} e_{\alpha,\beta} - [G] \begin{bmatrix} RLY(\hat{i}_\alpha - i_\alpha) \\ RLY(\hat{i}_\beta - i_\beta) \end{bmatrix} \quad (3.20)$$

When  $\hat{\omega} = \omega$  on the sliding surface, then:

$$(L_d - L_q) \begin{bmatrix} \frac{1}{L_d} & 0 \\ 0 & \frac{1}{L_q} \end{bmatrix} \begin{bmatrix} \hat{\omega} \hat{i}_\beta - \omega i_\beta \\ \hat{\omega} \hat{i}_\alpha - \omega i_\alpha \end{bmatrix} = \hat{\omega} (L_d - L_q) \begin{bmatrix} \frac{1}{L_d} & 0 \\ 0 & \frac{1}{L_q} \end{bmatrix} I^{-1} \bar{i}_{\alpha,\beta} \quad (3.21)$$

where  $\bar{i}_{\alpha,\beta} = [\hat{i}_\alpha - i_\alpha \quad \hat{i}_\beta - i_\beta]^T$ , and  $e_{\alpha,\beta} = \left[ \frac{\omega \varphi_m + (L_d - L_q)(\omega id - Pi_q)}{L_d} \right] [\sin \theta \quad -\cos \theta]^T$ .

Defining the hyperplane,  $S(x) = [i_\alpha - \hat{i}_\alpha \quad i_\beta - \hat{i}_\beta]^T$ , which defines the switching plane of the observer, where  $S(x) = 0$  represents the surface plane when the estimation error is zero, which separates the two systems of controlling depending on the sign of the plane  $S(x)$  and

$\dot{S}(x)$ , such as in the previous subsection, while the system will operate in the sliding mode when  $\dot{S}(x) = S(x) = 0$ .

Therefore, the previous model equation, eq. (3.20), could be simplified and represented as eq. (3.22):

$$\begin{aligned} \dot{S}(x) = & -R_s \begin{bmatrix} \frac{1}{L_d} & 0 \\ 0 & \frac{1}{L_q} \end{bmatrix} S(x) + \hat{\omega}(L_d - L_q) \begin{bmatrix} \frac{1}{L_d} & 0 \\ 0 & \frac{1}{L_q} \end{bmatrix} I^{-1} S(x) - \begin{bmatrix} \frac{1}{L_d} & 0 \\ 0 & \frac{1}{L_q} \end{bmatrix} e_{\alpha,\beta} \\ & - [G] \begin{bmatrix} RLY(\hat{i}_\alpha - i_\alpha) \\ RLY(\hat{i}_\beta - i_\beta) \end{bmatrix} \end{aligned} \quad (3.22)$$

And by operating the system in the sliding mode, by choosing  $\dot{S}(x) = S(x) = 0$ , and while  $e_{\alpha,\beta}$  are bounded, and choosing  $G > \max\{|e_\alpha| \quad |e_\beta|\}$ , the estimation could be obtained and represented as eq. (3.23):

$$e_{\alpha,\beta} = [G] [-RLY(\hat{i}_\alpha - i_\alpha) \quad RLY(\hat{i}_\beta - i_\beta)]^T \quad (3.23)$$

### 3.2.2.2 Stability Analysis

According to Lyapunov Theorem, the stable system could be designed when the estimation system does not affect by system parameters as shown in the previous section, and by finding the stable sliding mode condition. The following eq. (3.24) defines the Lyapunov function:

$$V = \frac{1}{2} S^T S \quad (3.24)$$

And this theorem ensures the stability when  $V > 0$ , and  $\dot{V} < 0$  have been satisfied. And by substituting  $S(x) = [i_\alpha - \hat{i}_\alpha \quad i_\beta - \hat{i}_\beta]^T$  form in eq. (3.24), eq. (3.25) is obtained, which satisfies the first condition, where it will reach zero when the system aligns at the sliding surface with zero error, which ensures that V will be greater than zero.

$$V = \frac{1}{2} [(\hat{i}_\alpha - i_\alpha)^2 + (\hat{i}_\beta - i_\beta)^2] \geq 0 \quad (3.25)$$

Recalling eq. (3.24), and by taking the first derivative, the relation in eq. (3.26) is obtained:

$$\dot{V} = S^T \dot{S} = S_\alpha \dot{S}_\alpha + S_\beta \dot{S}_\beta \quad (3.26)$$

Separating the equation terms yields:

$$\begin{cases} S_\alpha \dot{S}_\alpha = \frac{-R_s}{L_d} S_\alpha^2 + \frac{\hat{\omega}(L_d - L_q)}{L_d} S_\alpha S_\beta - \frac{1}{L_d} S_\alpha e_\alpha - [G] RLY(S_\alpha) S_\alpha \\ S_\beta \dot{S}_\beta = \frac{-R_s}{L_q} S_\beta^2 + \frac{\hat{\omega}(L_d - L_q)}{L_q} S_\alpha S_\beta - \frac{1}{L_q} S_\beta e_\beta - [G] RLY(S_\beta) S_\beta \end{cases} \quad (3.27)$$

Knowing that  $L_d < L_q$  according to the saliency property and  $S_\beta$  could have a negative sign and by knowing that:  $\frac{-R_s}{L_d} S_\alpha^2 < 0$ , and  $\frac{-R_s}{L_q} S_\beta^2 < 0$ , then the system will be stable if:

$$\frac{\hat{\omega}(L_d - L_q)}{L_d} S_\alpha S_\beta < 0, \text{ and } -\frac{1}{L_d} S_\alpha e_\alpha < 0$$

This could be achieved if eq. (3.28) satisfied, making the stationary components of the proposed observer to have nonequal gains.

$$\begin{cases} G_\alpha > \max \left\{ \frac{\hat{\omega}(L_d - L_q)}{L_d} S_\beta - \frac{1}{L_d} e_\alpha \right\} \\ G_\beta > \max \left\{ \frac{\hat{\omega}(L_d - L_q)}{L_q} S_\alpha - \frac{1}{L_q} e_\beta \right\} \end{cases} \quad (3.28)$$

### 3.2.2.3 Position and Speed Calculation

According to the SMO theorem and the estimating of the stationery components of the electromotive force in eq. (3.22) and eq. (3.23), and according to the PMSM electromotive force speed relation, the stationary components of the Back Electromotive Force are linearly proportional to the rotating speed as was shown in eq. (3.2), which contains the speed magnitude and the position of the rotating permanent magnet as in eq. (3.29):

$$\begin{aligned} \omega_r &= K \sqrt{e_\alpha^2 + e_\beta^2} \\ \theta &= -\tan^{-1} \frac{e_\beta}{e_\alpha} \end{aligned} \quad (3.29)$$

The rotor electrical position estimator estimates the rotor position according to the estimated Back Electromotive Force using the inverse tangent function of the EMF stationary



components fraction and additional conditional functions to convert the tangent function from half-cycle range into full-cycle range. On the other hand, these additional conditional functions are added a half-cycle to the estimated position during the reverse rotation of the motor in the conventional SMO, which makes an estimation offset error by  $\pi$  rads. The conventional SMO speed estimator also couldn't find the direction of rotation and gives a positive output according to the back EMF components magnitude.

To detect the direction of rotor speed rotation, an additional condition needs to be adopted to the speed estimator, which depends on the estimated rotor electrical position slope. The first derivative of the electrical position presents the rotor speed and is theoretically used as the speed estimator, but as a real estimator, the chattering existence, even if it has been minimized, and the estimation noise even if it has been filtered, leads to the nonlinearity of the position signal, while the discrete first derivative will not precisely estimate the rotor speed in both directions when choosing a large step time sampling. On the other hand, if the sampling time of the estimated position has been minimized, the derivative will fail to estimates the rotor speed due to the noise signal adopted to the position signal making it non-linear. Therefore, the derivative of the estimated speed with a large sampling time could be used as a direction conditioner to the presented speed estimator to detect the direction of the rotor rotation according to the position slope, while the acceleration direction could be obtained from finding the second derivative of the position signal.

Recalling eq. (3.13), and where the system works under the SMO operation region, the following identities in eq. (3.30) could be obtained:

$$\left( \begin{array}{l} \text{Forward Rotation if } \frac{d\theta_e}{dt} > 0 \\ \text{Reverse Rotation if } \frac{d\theta_e}{dt} < 0 \\ \text{Zero Speed if } \frac{d\theta_e}{dt} = 0 \\ \text{Positive acceleration if } \frac{d_2\theta_e}{dt^2} > 0 \\ \text{Positive acceleration if } \frac{d_2\theta_e}{dt^2} < 0 \\ \text{Constant Speed if } \frac{d_2\theta_e}{dt^2} = 0 \end{array} \right) \quad (3.30)$$

### 3.3 High-Frequency Injection

The standstill condition of rotor position estimation could not be achieved using the sliding mode observer. The stator windings during standstill draw DC currents, which makes the EMF estimation unstable. The position determination could not be implemented using the previous stator currents and back EMF estimators. Therefore, the DC currents drawn by the motor need to be used to determine the rotor position implementing the saliency property.

Injecting a high-frequency low voltage into the stator windings during standstill and during the motor rotation, does not affect the normal controlled rotation of the motor. On the other hand, it produces high frequency drawn currents beside the fundamental component of the stator drawn currents during the motor holding and rotating. These high-frequency currents can be extracted and processed to extract the rotor's initial and rotating electrical position.

Fig. 3-3 shows the filtration stages of the measured injection stator current. The injected currents to the stator winding during standstill and low speed will draw high-frequency stationary frame currents as in eq. (3.31) [36]:

$$\begin{bmatrix} i_{\alpha i} \\ i_{\beta i} \end{bmatrix} = \begin{bmatrix} I_0 \cos(\omega_f t) + I_1 \cos(\omega_i t) + I_2 \cos(2\theta_r - \omega_i t) \\ I_0 \sin(\omega_f t) + I_1 \sin(\omega_i t) + I_2 \sin(2\theta_r - \omega_i t) \end{bmatrix} \quad (3.31)$$

where  $\omega_f$ ,  $\omega_i$  and  $\theta_r$  are the fundamental angular frequency, the injected angular frequency, and the rotor permanent magnets position, respectively.

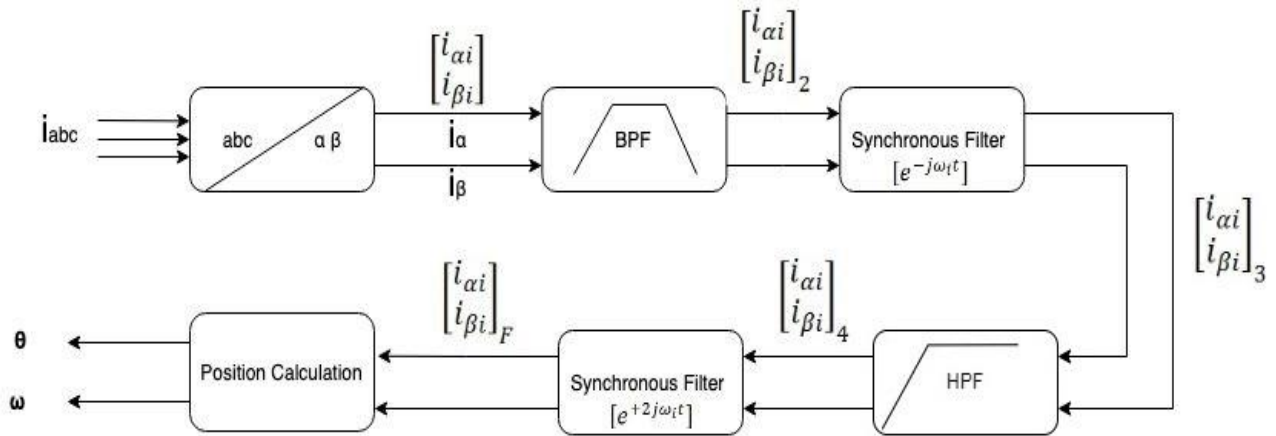


Fig. 3-3: High-Frequency Injection Filtration Stages

As in the case of low-speeds, currents modulated with the high-frequency estimator, contain position information in the negative sequence current component. The fundamental component could be removed using a bandpass filter producing the second level in the estimation as in eq. (3.32):

$$\begin{bmatrix} i_{\alpha i} \\ i_{\beta i} \end{bmatrix}_2 = \begin{bmatrix} I_1 \cos(\omega_i t) + I_2 \cos(2\theta_r - \omega_i t) \\ I_1 \sin(\omega_i t) + I_2 \sin(2\theta_r - \omega_i t) \end{bmatrix} \quad (3.32)$$

The following coordination rotation is needed to separate the positive sequence from eq. (3.16) and break it down to DC current. The negative sequence frequency has become twice the injection frequency obtaining the third level as in eq. (3.33):

$$\begin{bmatrix} i_{\alpha i} \\ i_{\beta i} \end{bmatrix}_3 = [e^{-j\omega_i t}] \begin{bmatrix} i_{\alpha i} \\ i_{\beta i} \end{bmatrix}_2 = \begin{bmatrix} I_{DC} + I_2 \cos(2\theta_r - 2\omega_i t) \\ I_{DC} + I_2 \sin(2\theta_r - 2\omega_i t) \end{bmatrix} \quad (3.33)$$

The DC component has been removed using a high pass filter, obtaining the fourth level as in eq. (3.34):

$$\begin{bmatrix} i_{\alpha i} \\ i_{\beta i} \end{bmatrix}_4 = \begin{bmatrix} I_2 \cos(2\theta_r - 2\omega_i t) \\ I_2 \sin(2\theta_r - 2\omega_i t) \end{bmatrix} \quad (3.34)$$

Moreover, the final level of the filtering mechanism consists of the inverse of coordination rotation to return the currents signal into the synchronous frame as in eq. (3.35):

$$\begin{bmatrix} i_{\alpha i} \\ i_{\beta i} \end{bmatrix}_F = [e^{+2j\omega_i t}] \begin{bmatrix} i_{\alpha i} \\ i_{\beta i} \end{bmatrix}_4 = \begin{bmatrix} I_2 \cos(2\theta_r) \\ I_2 \sin(2\theta_r) \end{bmatrix} \quad (3.35)$$

The rotor position uses the stationery components of the final level currents directly to complete the estimation as:

$$2\theta_r = \tan^{-1} \left[ \frac{i_{\beta i F}}{i_{\alpha i F}} \right] \quad (3.36)$$

where  $\theta_r$  could be easily determined from  $2\theta_r$  to provide the controller requirements.

### 3.4 Direct Extraction Method

The PMSM stator draws three symmetrical current components, which are shifted by 120 electrical degrees from each other. They rotate symmetrically with a rotating frequency that describes the motor's electrical speed. According to Mohan et al. in [44], the three-phase components of the drawn currents are written down in eqs. (3.37a) through (3.37c). Eq. (3.37d) shows the relationship between  $\theta_{i_s}$  and  $\theta_m$  [44], where  $I_s$  and  $\theta_{i_s}$  represent the magnitude and the angle of the stator phaser vector current, respectively, while  $\theta_m$  and  $\omega_m$  represent the mechanical position and the mechanical speed of the rotor, respectively.

$$i_a(t) = \frac{2}{3} I_s \cos(\theta_{i_s}(t)) \quad (3.37a)$$

$$i_b(t) = \frac{2}{3} I_s \cos\left(\theta_{i_s}(t) - \frac{2\pi}{3}\right) \quad (3.38)$$

$$i_c(t) = \frac{2}{3} I_s \cos\left(\theta_{i_s}(t) - \frac{4\pi}{3}\right) \quad (3.39)$$

$$\theta_{i_s}(t) = \frac{P}{2} [\theta_m(t)] \mp \frac{\pi}{2} = \frac{P}{2} [\theta_m(0) + \omega_m t] \mp \frac{\pi}{2} \quad (3.37d)$$

Transforming the previous three-phase components using Clark transforms into the stationary two components yields two orthogonal 90 degrees separated components of the stator drawn currents. The stationary components rotate with the motor's electrical frequency, as illustrated by eqs. (3.38a) through (3.38b):

$$i_\alpha(t) = \sqrt{2} I_s \cos\left(\theta_{i_s}(t)\right) \quad (3.38a)$$

$$i_\beta(t) = \sqrt{2} I_s \sin\left(\theta_{i_s}(t)\right) \quad (3.38b)$$

These current components contain the electrical position of the rotor  $\theta_e(t)$ , and it could be extracted easily using the tangent inverse of the components, as in eq. (3.39).

$$\theta_e(t) = \theta_{i_s}(t) \mp \frac{\pi}{2} = \tan^{-1} \left[ \frac{i_\beta(t)}{i_\alpha(t)} \right] \mp \frac{\pi}{2} \quad (3.39)$$

The magnitude of the measured stator currents represents the stable motor's applied torque during the steady-state response. Therefore, to extract the rotor's position, a significant current should be drawn from the stator, which requires a significant torque to be applied from the motor. The extracted position is the time-related frequency driven from the VSI. It presents the rotor's mechanical speed and position during the steady-state response of the motor, while it fails to find the rotor position during the transient response of the rotor speed and torque. At time zero, when operating the motor at holding zero speed, and by using zero initial condition for the Clark transformation, the initial extracted position from the holding DC currents represents the rotor's real initial position, even if the applied torque was zero. The extracted initial position of the unloaded motor can be used to determine the polarity of the estimated position in the HFI process.

### 3.5 The Proposed Hybrid System

The control mechanism needs to determine the rotor position during all speed ranges, including standstill. The improved sliding mode observer can observe precisely the rotor position within the high-speed ranges but fails at zero and very low speeds. However, it could estimate the position at low speeds with an acceptable estimation error. The injection process succeeds in determining rotor position during starting and low speeds precisely but can estimate the rotor position during high speeds with an acceptable estimation error. Avoiding the injection effect on the system losses and noise, and according to the failure of the SMO during zero speed, the hybrid process has been presented.

The hybrid process consists of both estimators, each one operates during its working speed range, using a robust switch to complete the observation result. Fig. 3-4 shows the general block diagram of the hybrid observation system and the switching mechanism. The hybrid system consists of a High-Frequency Injection (HFI) block, a polarity block, a Sliding Mode Observer (SMO) block, a switch block, and a speed estimator block. The hybrid estimator uses

the measured  $(\alpha, \beta)$  components of the stator currents and voltages to estimate the position and speed. The HFI block extracts the position information from the measured stationary components of the stator currents as was shown in Fig. 2-5, the filtration mechanism provides  $2\theta_r$ , while  $\theta_r$  needs to be extracted and the position polarity needs to be determined as in the polarity block.

The HFI estimation system extracts the rotor position from measuring the stator drawn currents of the high-frequency injection during standstill (DC-Injection). However, it extracts the position information in half the electrical cycle of rotation according to eq. (3.36), and the system should determine the polarity of the permanent magnet to pre-determine which cycle the estimated electrical position is located in before the high-frequency injection starts for a standstill electrical position estimation.

Two types of polarity determinators need to be analyzed and used within the system; the first one uses the stationary components of the stator drawn currents to detect the rotor initial position and the standstill electrical position. While the second one is to use a testing bi-directional voltage pulse, and the method compares the direct component of the stator winding currents during both of the two orthogonal voltage pulses.

The first method determines the starting position with polarity in all conditions, and determines the standstill position during loaded motor conditions, while the pulse method detects only the polarity.

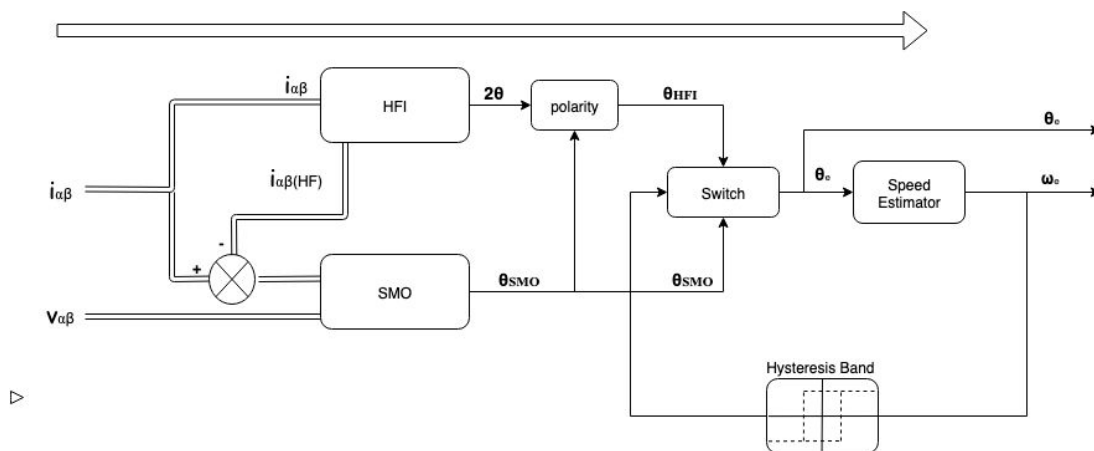


Fig. 3-4: The General Block Diagram of the Hybrid Observer

The polarity detection procedure needs to be applied to the system after any power failure, and speed or current related faults detection. While another method is used to minimize the usage of the HFI process using the previous data obtained and stored in the hybrid observer-high-frequency system after stopping. Such a hybrid polarity determination reduces the noise from the pulse testing mechanism and speeds up the system.

The SMO block contains the proposed Sliding Mode Observer estimator, which was shown in Fig. 2-2. The sliding estimation process uses the stationary components of the stator currents and subtracts the filtered high-frequency injected currents to complete the observation mechanism. This separation removes the mutual effect between both estimators during the synchronized estimation mechanism at a standstill and low speeds.

The switching mechanism between the observer and the estimator has been operated in the switch block. It is done depending on the accuracy's weight of the estimator's result, using a hysteresis band to avoid the polarity error during switching between the estimators.

The system operates the SMO all the time of operation and uses its estimated position in the SMO switch domain for medium and high speeds. While at low speeds, the observer estimates the position to calculate the error weight to improve the switching process. On the other hand, the system drive's the HFI estimator and injects the dedicated high-frequency signal during its switch domain of standstill and low speeds. Besides it stops the injection process during the SMO switch domain, to reduce the injection effect on the induced torque, the audible noise, and the winding power loss, while its error accuracy weight has been calculated during its switch domain and compared to the SMO error weight.

Fig. 3-5 shows the switching mechanism and polarity detection flowchart, which has been used to switch between the position estimators depending on the minimum estimation error and minimum power loss during all speed ranges under all load conditions, and the polarity compensation procedure. Such that,  $P_{obs}$ ,  $P_d$ ,  $P_i$ ,  $P_c$ ,  $P_{com}$ ,  $P_{hfi}$ , and  $P$ , represent the observer position, the direct stator position, the injection extracted position, the polarity comparator position, the injection compensated position, the HFI estimator position for zero and low speed, and the Hybrid result feedback Position, respectively, knowing that the edges of the controlled current are  $q_3 > q_2 > q_1 > q_0$ , and  $d_1 > d_0$  in the Schmitt trigger relays.

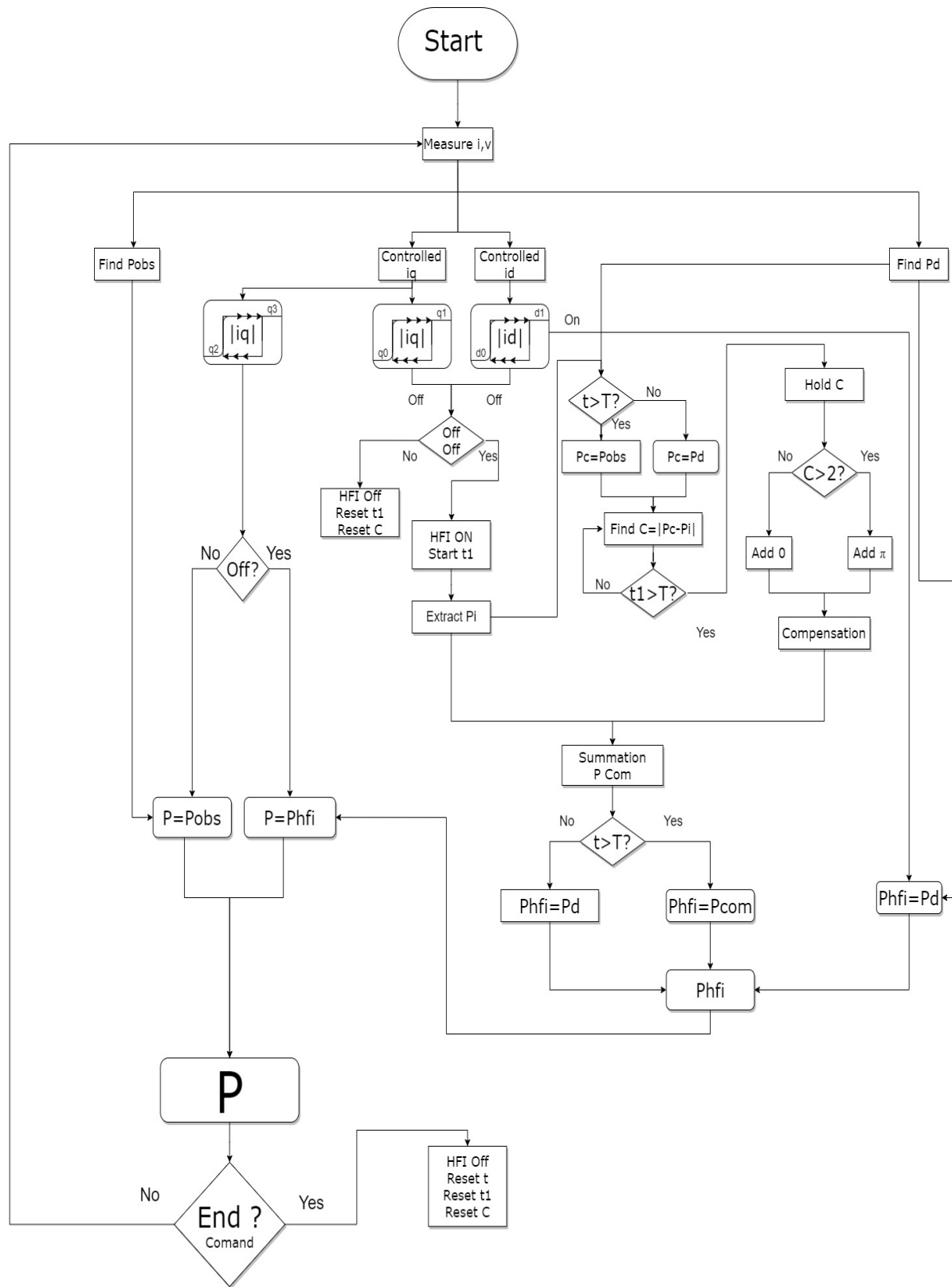


Fig. 3-5: The Hybrid Switching System Flow Chart



Fig. 3-6 shows the field oriented control of the permanent magnet synchronous motor, using the proposed hybrid observer, which controls the voltage source inverter using space vector pulse width modulation technique, feeding the motor by the dedicated controlled stator voltages depending on the references.

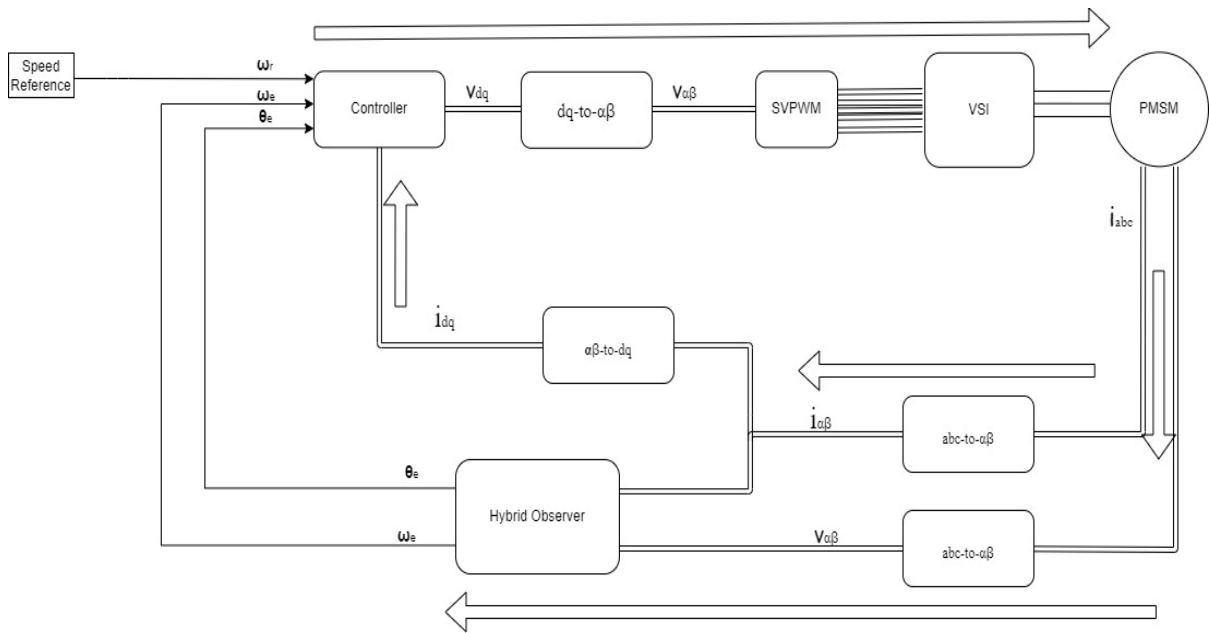


Fig. 3-6: The Proposed Hybrid Observer Connected to the Control System

The controller block in Fig. 3-6 regulates the speed error between the reference and estimated speed, it also regulates the direct and quadrature components of the stator currents error between the reference and the measured values. The field-orientation mechanism implies separate control for the torque and the flux. The (abc-to- $\alpha\beta$ ) block transforms the measured voltages and currents from the abc reference frame into stationary references frame, without the need for the rotor position, to provide the observer by the ( $\alpha$ ,  $\beta$ ) currents and voltages to complete the estimation. The ( $\alpha\beta$ -to-dq) block transforms the stationary reference frame of the measured stator currents into a rotating reference frame, which is used to complete the field orientation process, by using the estimated position data from the observer.

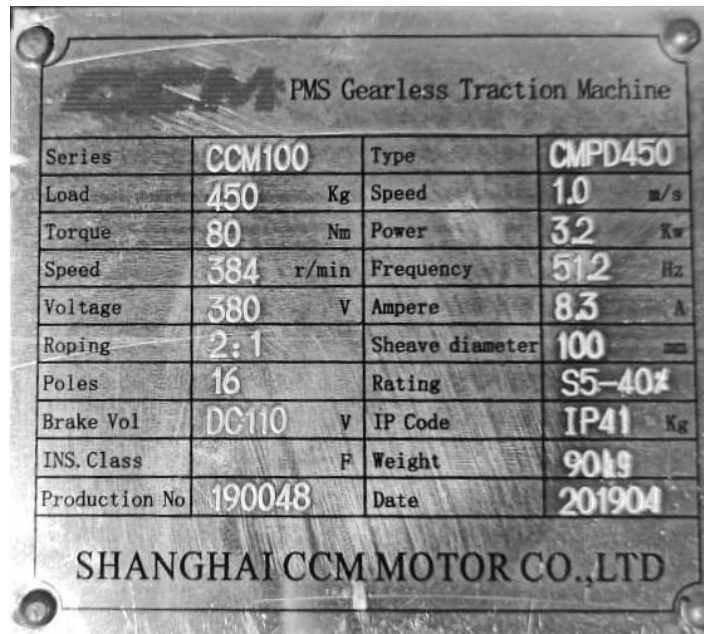
The controlled (d, q) components of the controller output are transformed into ( $\alpha$ ,  $\beta$ ) components, using a rotating to stationary reference frame transformation, which drives the gate signal in the SVPWM block.



# Chapter 4

## Simulation and Results

The system has been designed to accomplish the control system of a real prototype salient pole Inner Rotor Permanent Magnet Synchronous Motor (IRPMSM), whose nameplate is depicted in Fig. 4-1.



PMS Gearless Traction Machine			
Series	CCM100	Type	CMPD450
Load	450 Kg	Speed	1.0 m/s
Torque	80 Nm	Power	3.2 Kw
Speed	384 r/min	Frequency	51.2 Hz
Voltage	380 V	Ampere	8.3 A
Roping	2:1	Sheave diameter	100 mm
Poles	16	Rating	S5-40%
Brake Vol	DC110 V	IP Code	IP41 Kg
INS. Class	F	Weight	90kg
Production No	190048	Date	201904

SHANGHAI CCM MOTOR CO., LTD

Fig. 4-1: A Prototype Motor Nameplate

The prototype motor has been used as a direct coupling traction machine, the prototype winding parameters have been calculated using Mitsubishi drive unit's tuning program, by applying voltage pulse injection estimation mode. Table 4-1 shows the nameplate and the calculated parameters of the motor under study.

Table 4-1:  
Motor Parameters

Symbol	Quantity	Value (Unit)
$I_r$	Rated Current	8.3 A
$V_r$	Rated Voltage	380 V
$P$	Poles Number	16
$n$	Rated Speed	384 rpm
$d$	Sheave Diameter	100 mm
$L_d$	Inductance d-component	0.0023 H
$L_q$	Inductance q-component	0.0033 H
$\varphi_r$	Rotor Magnetic Flux Linkage	0.435 web
$R_s$	Stator phase Resistance	0.018 ohm

## 4.1 Sliding Mode Observer

The system has been controlled using Field-Oriented Control (FOC) with the current controller, by using the rotating frame transform, which determines the rotor position and speed using conventional Sliding Mode Observer (SMO), and improved relay SMO. The simulation was conducted in Matlab/Simulink environment. Fig. 4-2 shows the Simulink model of the proposed systems.

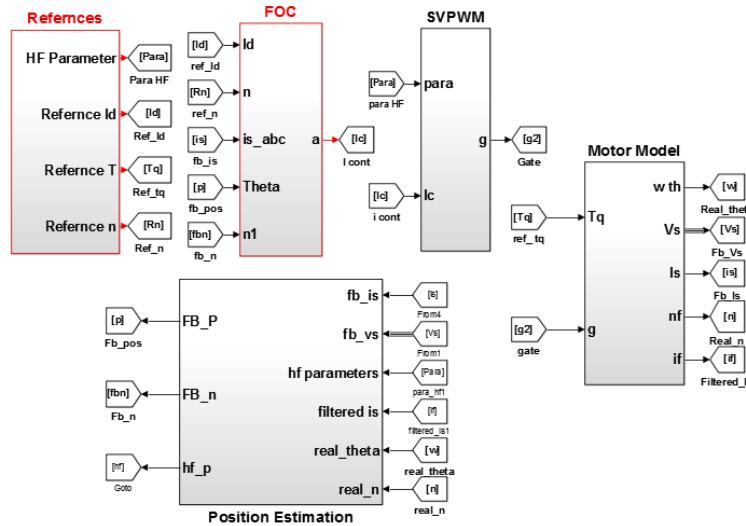


Fig. 4-2: Simulink Model of the Proposed SMO System

The reference block in Fig. 4-2 contains the references of speed, torque, and the direct component of the reference current. The reference speed expresses the speed order in rads per second, the reference torque contains the motor applied torque in Newton's meter, while the direct component of the reference current has been set to zero forcing the controller to produce the maximum motor torque per Ampere.

The controller block contains the Field Oriented Control, Park and Clark transformation, speed and currents regulators, and the current controller, while Fig. 4-3 shows the design of the controller block.

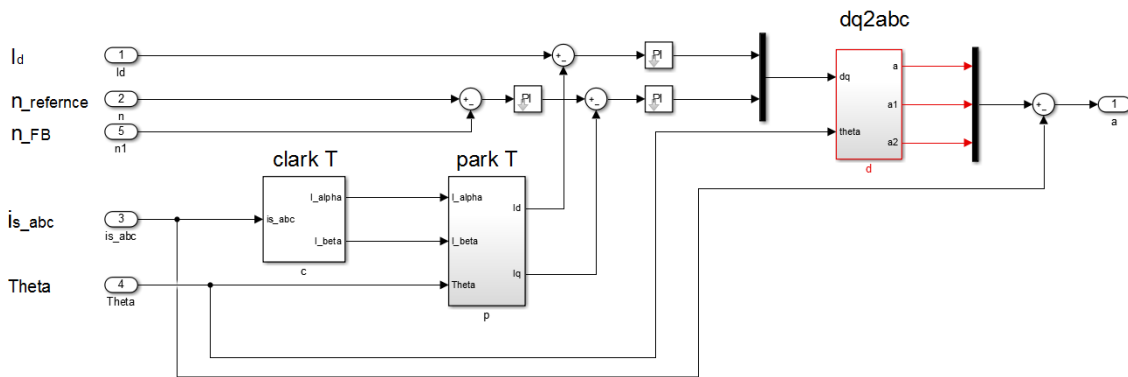


Fig. 4-3: Field Oriented Controller Block

The Space Vector Pulse Width Modulation (SVPWM) block transforms the controlled currents of the controller block into  $(\alpha, \beta)$  stationary reference frame, to establish the inverter gate signal, by using Matlab's library SVPWM block with 8kHz carrier frequency.

Fig. 4-4 shows the motor model block, which contains a two-level Voltage Source Inverter (VSI) derived by the gate signal, feeding the Matlab's Permanent Magnet Synchronous Motor (PMSM) library block. The motor model block contains the appropriate measuring devices. The observer block uses the measured voltages and currents from the motor model to estimate the rotor's position and speed.

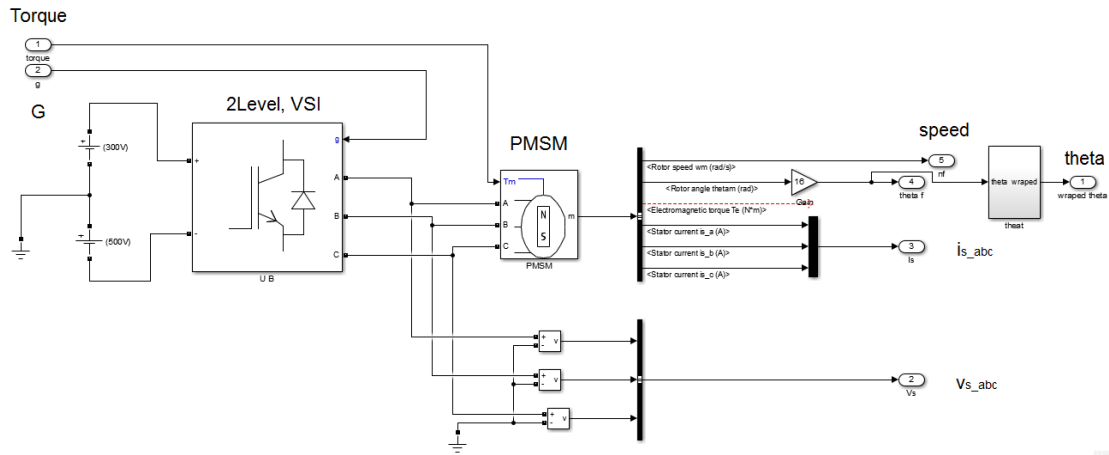


Fig. 4-4: Motor-Inverter pair Model Block

Fig. 4-5 shows the position and speed estimation model, two cascaded processes have been introduced; Back Electromotive Force estimation, and speed-position calculation. The speed calculation has been performed according to eq. (3.11), while the position calculation is performed according to eq. (3.10). The  $(\alpha, \beta)$  back EMF's estimation has been observed separately, each one in a block. It has been described and designed according to the proposed observers as in the following sections.

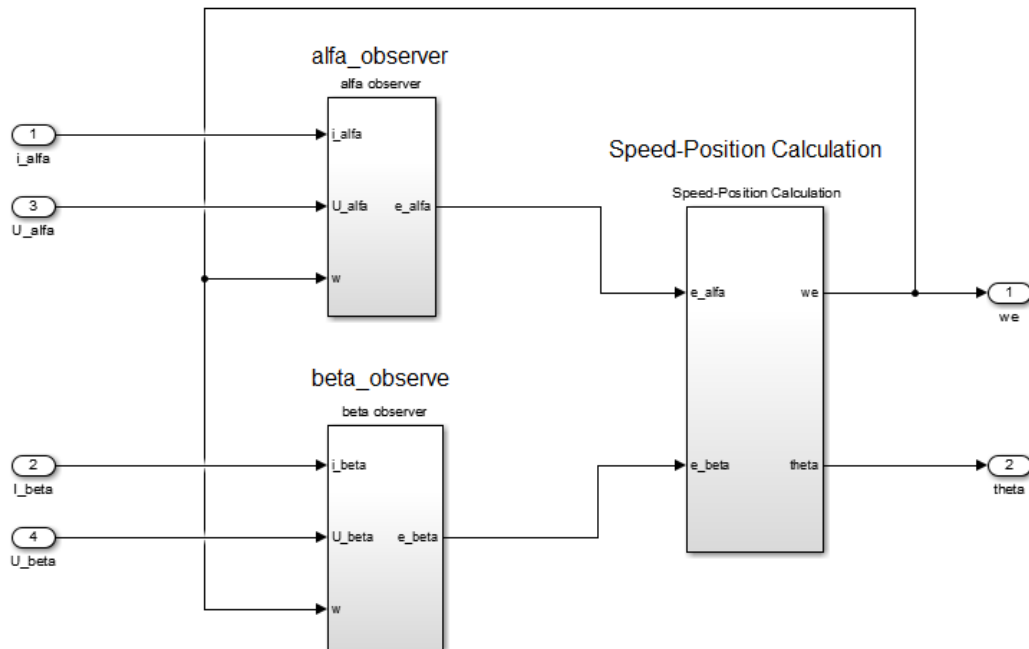


Fig. 4-5: Observer Block

### 4.1.1 Conventional Sliding Mode Observer

The conventional observer with signum function relay has been used to determine the rotor's position and speed. Field Oriented Control (FOC) has been used, it uses the measured stator currents and voltages from currents and voltages sensors. The controller has been applied to a prototype motor of the previous nameplate. While the conventional  $\alpha$ -observer is designed as in Fig. 4-6, the observer gain and filter have been designed to stabilize the observer and reduce the estimation error.

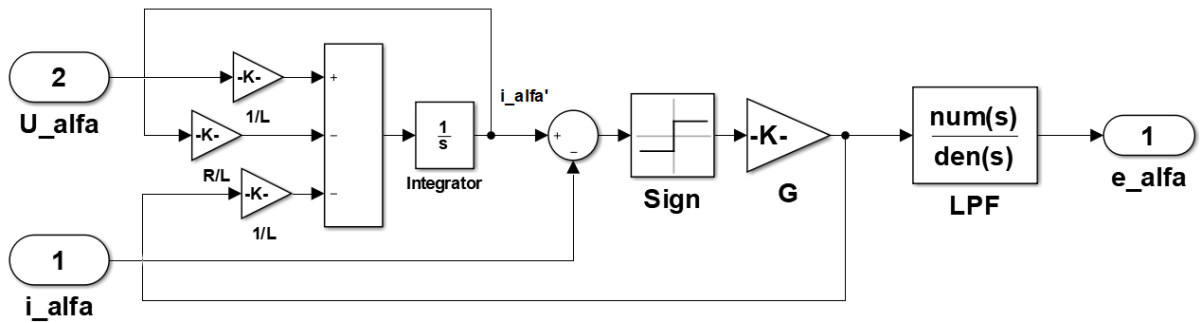


Fig. 4-6: The Designed  $\alpha$ -Observer of the Conventional SMO

Fig. 4-7 shows the estimated and measured speed of the motor. The aforementioned figure shows the estimated speed in a stepped reference speed, which shows the tracking accuracy of the observer. There is an error in determining the speed at low frequency and starting. It's clear from the figure that the low pass filter delayed the estimated position by a certain time related to the filter bandwidth, the wider the bandwidth is the smaller delay and larger ripple will be and vice versa.

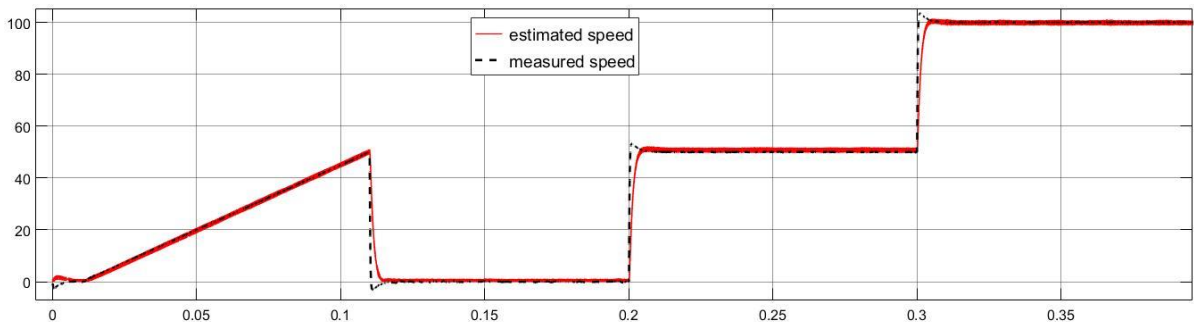


Fig. 4-7: The Estimated and Measured Speed of the Controlled PMSM

While Fig. 4-8 shows a delay and overshoot in the observed speed estimation, the delay is caused by filtering mechanism and chattering removing process, which delays the estimated back EMF filtered signal, affecting the estimated speed causing speed offset. While the overshoot in the estimated speed caused by the transient effect of the observer. The previous effect is clear in the position estimation as in Fig. 4-9, which shows the estimated and the measured position data. In order to track the rotor speed and position, compensation is needed to overcome this delay with a reduced ripple smooth estimation. The transient effect needs to be controlled by controlling the stator currents estimation error before using the sliding switch.

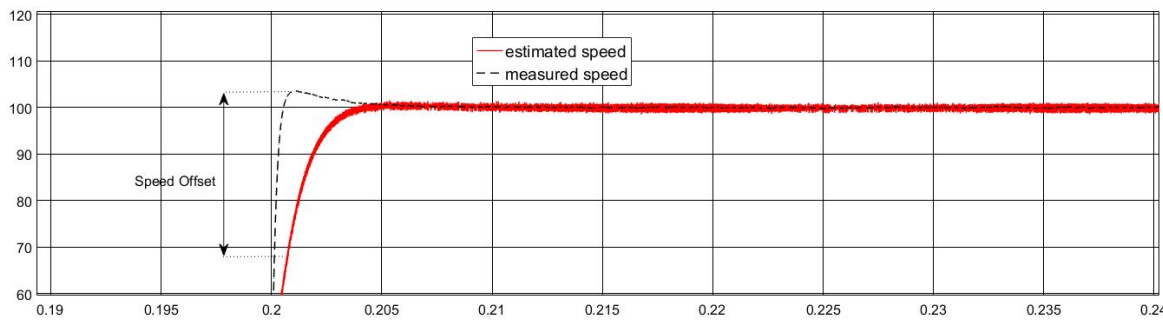


Fig. 4-8: The Delay and Offset of the SMO Estimated Speed

Fig. 4-9 shows the position estimation and the data measured using the shaft connected resolver, during standstill, low speed, and high speed. The Sliding Mode Observer (SMO) fails to estimate the rotor position during standstill. Noise signal, and the null calculations in the back EMF estimation cannot be accomplished. The failure of the estimation at standstill and low speeds appears in the unstable estimation period in the position estimation figure between 0.11s to 0.2s

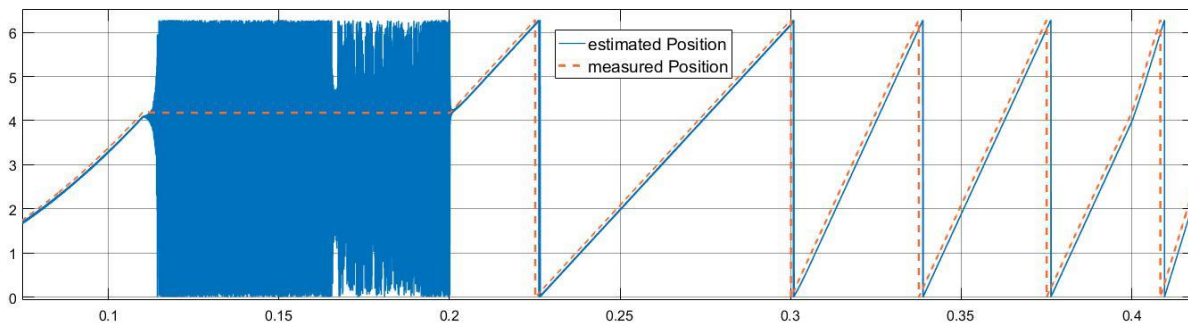


Fig. 4-9: The Estimated and the Measured Position Using Conventional SMO



### 4.1.2 Improved Relay Sliding Mode Observer

The improved observer with speed-related feedback and bandwidth sigmoid function relay has been used to determine the rotor position and speed, the sigmoid soft switching mechanism reduces the chattering effect which reduces the delay effect by eliminating the filters need. While the overshoot has been contributed and controlled by using a PI stator current error controller which can enhance the estimation error and the oscillations in the estimated position data. The estimation has been made by measuring the stator currents and voltages using currents and voltages sensors, which were applied to the motor with the previous nameplate.

The improved  $\alpha$ -observer has been designed, as depicted in Fig. 4-10. The observer gain and speed-related feedback have been designed to stabilize the observer and reduce the estimation error according to the operating speed. The sigmoid function eliminates the filtering needs, calculates the Back Electromotive Force, and omits the chattering problem, without causing any filtering delay, which eliminates the need for compensation. While the speed feedback is used to control the sigmoid bandwidth and is factorized by the other stationary current component  $i_\beta$ , which forces the error in the estimated stationary components of the back EMF to approaches zero, reducing the estimation delay and the torque effect, as will be presented in the next sub-sections.

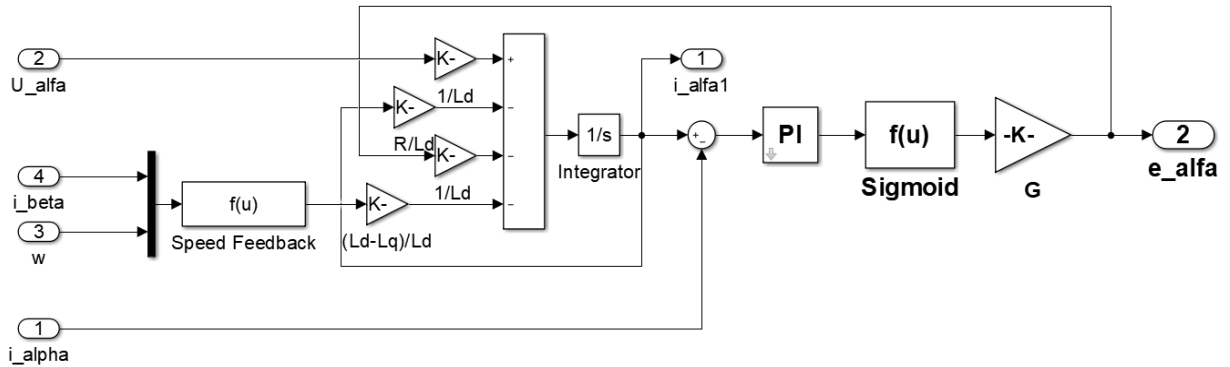


Fig. 4-10: The Designed  $\alpha$ -Observer of the Improved SMO

#### 4.1.2.1 Position and Speed Estimation

Fig. 4-11 shows the position and speed estimation, and the data measured using the Matlab built-in resolver, during standstill, low speeds, and high speeds. Like the conventional observer, the improved Sliding Mode Observer (SMO) fails to estimate the rotor position

during standstill. The ripple has been reduced during low speed by decreasing the relay bandwidth and gain. The error is reduced during the high speed by increasing the bandwidth, due to using the speed-related feedback.

Fig. 4-11 shows that, the improved Sliding Mode Observer eliminates the need for filters, and reduces the chattering. The speed estimation error decreased also compared to the conventional one, while both of them fail to estimate the position during standstill. The control system fails to estimate and detect the rotor’s position of the permanent magnets at standstill or starting.

Fig. 4-11. (a) shows that the estimation of the rotor electrical position of the permanent magnets fails at standstill, where the Back Electromotive Force (EMF) is not induced in the motor. On the other hand, the position has been estimated during the rotation of the motor, even at low speeds, which has been studied and simulated in Fig. 4-12.

Fig. 4-11. (b) shows that the SMO estimates the rotor speed at all speed ranges, even at zero and low speeds, because of its relation with the back EMF, which will record a zero induced EMF during the zero speed.

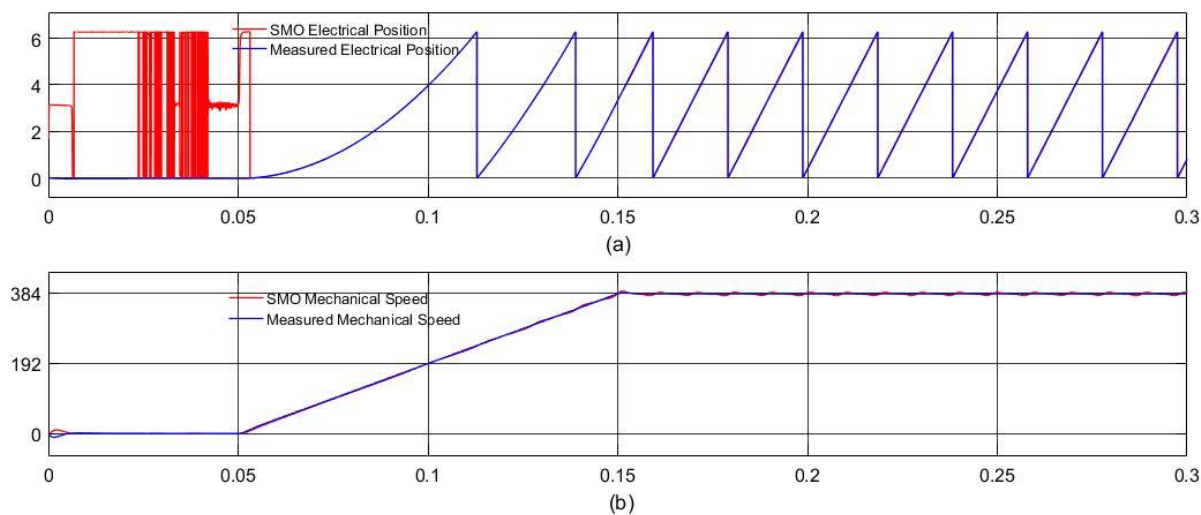


Fig. 4-11: Improved SMO (a) The Estimated and the Measured Position  
(b) The Estimated and the Measured Rotor Mechanical Speed

Fig. 4-12 shows the error between the estimated and the measured position in low-speed simulation, by selecting the starting angle of rotor permanent magnets north pole  $\frac{\pi}{2}$  leading the

d-axis of the nearest stator electrical pole. The simulation has been made with variable stepped reference speed, which consists of starting at a very low speed of 1 rpm, smooth accelerated reference speed from 1 to 5 mechanical rpm by 5 steps in 5 seconds.

At standstill, the VSI supplies the motor windings by a DC voltage, the currents drawn by the motor windings are also DC, which saturate the motor windings, and this saturation fails the estimation process of back EMF, making the estimator unstable during standstill as was shown in Fig. 4-11 (a). And by increasing the speed, the motors drawn currents rotates sinusoidally according to the rotating magnetic field, which induces a significant back EMF, which could be estimated using the dedicated observer decreasing the estimation error by increasing the motor speed, as shown in Fig. 4-13.

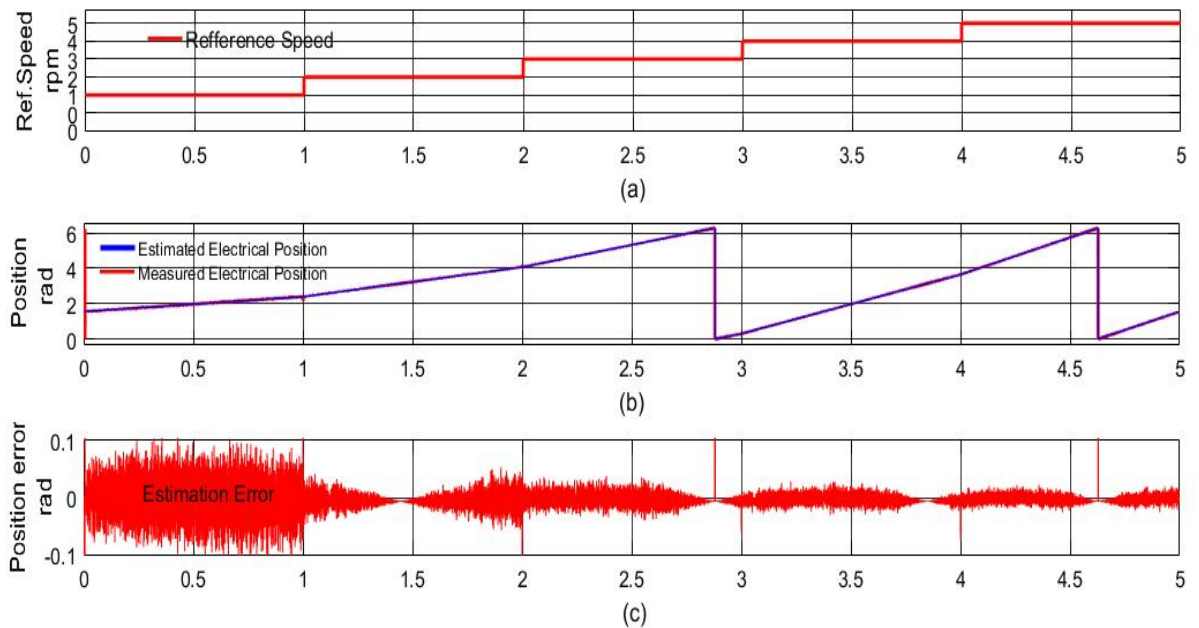


Fig. 4-12. (a): Reference Speed in (rpm). (b): The Estimated and the Measured Electrical Position. (c): The Estimation Error in the PM Electrical Position

#### 4.1.2.2 Load Effect on the Estimation Process

As studied previously, the SMO observes the rotor's electrical position by processing the measured stationary components of the stator currents, which are presented as the observer input. According to the observer design, the observer output and its states are affected by many factors, mainly changing the input behaviour, which in the case leads to study the load effect on the observer system.

Fig. 4-13 shows the simulation results of the estimated electrical position during a changing load torque; from the unloaded condition until reaching the fully loaded state, and overload condition during rotating the motor in low-speed region. The simulation shows that increasing the load torque during low-speed operation increases the position estimation error. Fig. 4-13 (b) shows that when adding the proposed speed-load self-compensator, the load effect on the estimation has been removed, while increasing the load and while loading with constant load.

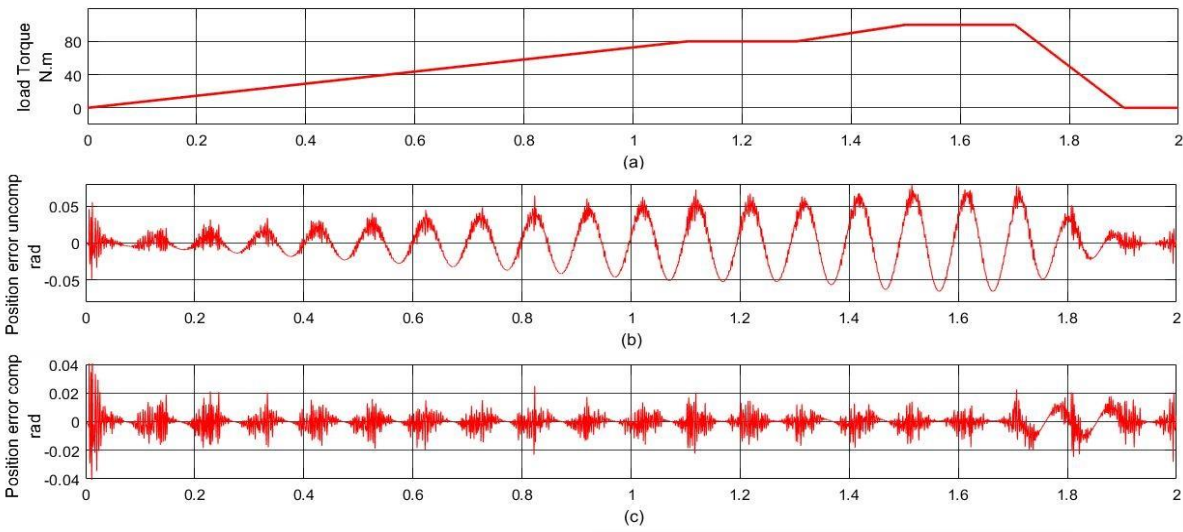


Fig. 4-13. For Low-Speed Simulation: (a): The Applied Load Torque (b): The Uncompensated Estimation Error in the Electrical Position. (c): The Compensated Estimation Error in the Electrical Position

Fig. 4-14 studies the load effect on the position estimation during the rotation of the motor at the rated speed, by changing the motor applied load torque as what has been studied previously in the previous figure.

Increasing the load torque affects the SMO speed feedback compensation process for the salient pole PMSM, which in this case decreases by operating the motor at a slower speed, making the SMO estimation process to be affected by the consumed power of the operation. To decrease the power effect on the estimation process, extra sinusoidal compensation is designed to synchronize between the motor load current and the estimated speed to control the feedback consumed power. On the other hand, the estimated and controlled quadrature current represents the load and its direction, which needs to be modified to compensate for the rotor position load effect, and it needs to be controlled separately without affecting the speed compensator. The simulation shows how the speed-load self-compensator removes the estimation load effect during operating the motor during high speed.

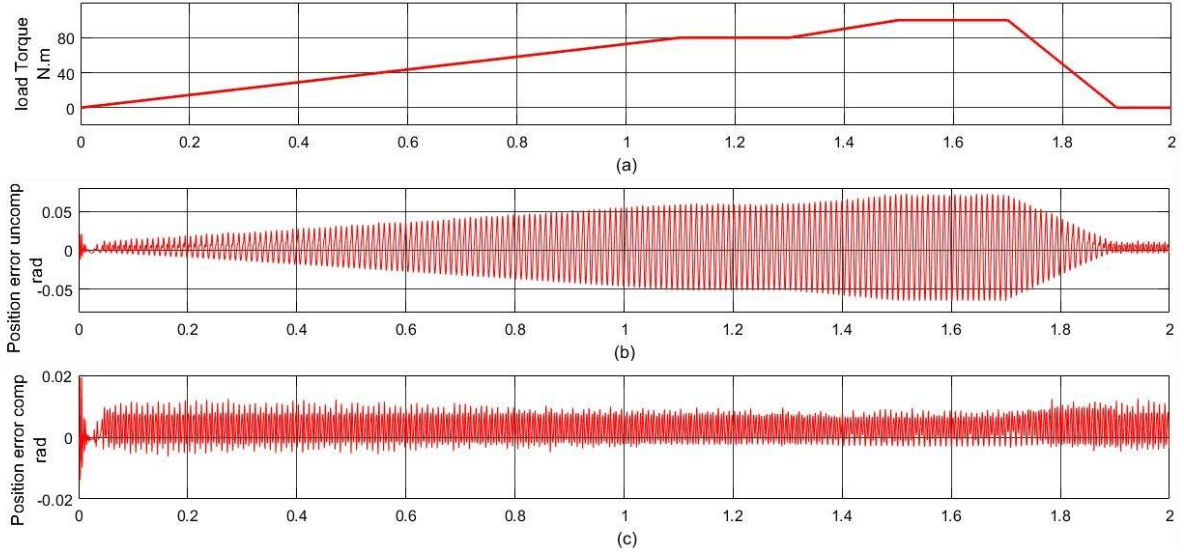


Fig. 4-14. For High-Speed Simulation: (a): The Applied Load Torque b): The Uncompensated Estimation Error in the Electrical Position. (c): The Compensated Estimation Error in the Electrical Position

Fig. 4-15 shows the relationship between the induced torque and the estimated  $i_q$ . It shows also the power compensated SMO estimation simulation during increasing the operating speed from standstill to full speed in 1.8 seconds and continuing the simulation at the rated speed, during low load, half load, and full rated load. The power compensator holds the estimation error at the minimum value and decreases the speed and torque vibrations.

It has been shown from Fig. 4-15 that, the improved compensated SMO estimates the rotor electrical PM position with estimation error near ( $\pm 0.001 \text{ rad}$ ) at medium speed, and increased by increasing the speed into full speed to estimation error near ( $\pm 0.005 \text{ rad}$ ), which could be represented mechanically between ( $\pm 0.000125 \text{ rad}$ ), and ( $\pm 0.000625 \text{ rad}$ ) at full speed, or in mechanical degree in between ( $\pm 0.012^\circ$ ), and ( $\pm 0.06^\circ$ ) at full speed.

The improved compensated SMO estimation process is not affected by changing the load torque from zero to full load, because of using the quadrature rotational current feedback as a torque effect compensator to calibrate the compensated electrical position during any torque variations, even at reversed torque and during braking. Fig. 4-15: (a), (b), and (c) show the effect of changing the load torque on the components of the rotational current.

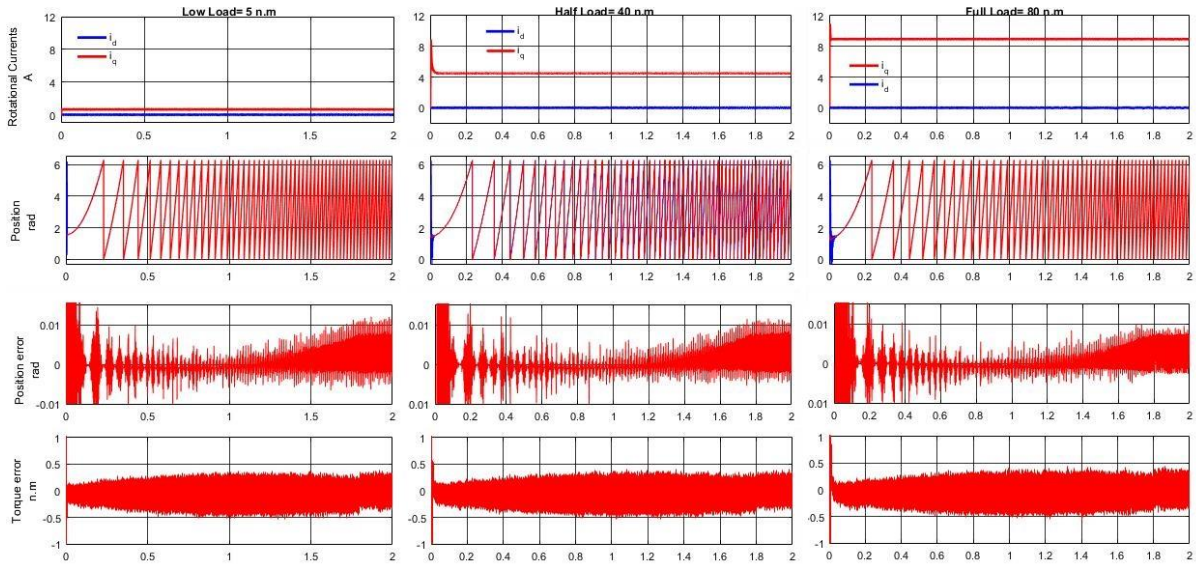


Fig. 4-15: The Effect of Increasing Speed and Load Torque on the Rotational Currents, Electrical Position Error, and Induced Torque Error

Fig. 4-16 studies the SMO estimated position reversal, which estimates the rotor position in all speed-torque directions, during motoring and braking operations, by applying twice the load torque. The first one is forward and the second is reversed, and by selecting two speed references, the first one is shown in Fig. 4-16. (a), starts from a standstill at zero speed and increases to 38 rpm, and the second one is shown in Fig. 4-16. (b), which increases to full speed in both directions, from forward to reverse and vice-versa during two cases of applied full load torque, to study the estimation capability in all motoring-breaking operation regions in four cases of load torque and four cases of rotor speed.

The following general simulation studied all the cases of the motoring-breaking operation of the presented motor under the improved SMO estimation process. It shows that the maximum error obtained in the position estimation is less than 0.005 rad in electrical PM position estimation in all cases even at high speeds at full load and less than 0.001 rad at low speeds which is presented in the error subfigures in Fig. 4-16. (g) for low-speed electrical position estimation error and in Fig. 4-16. (h) for full-speed electrical position estimation error. While Fig. 4-16. (c) and (d) show the mechanical speed estimation under all the conditions of the reference speed and torque in all motor operation regions.

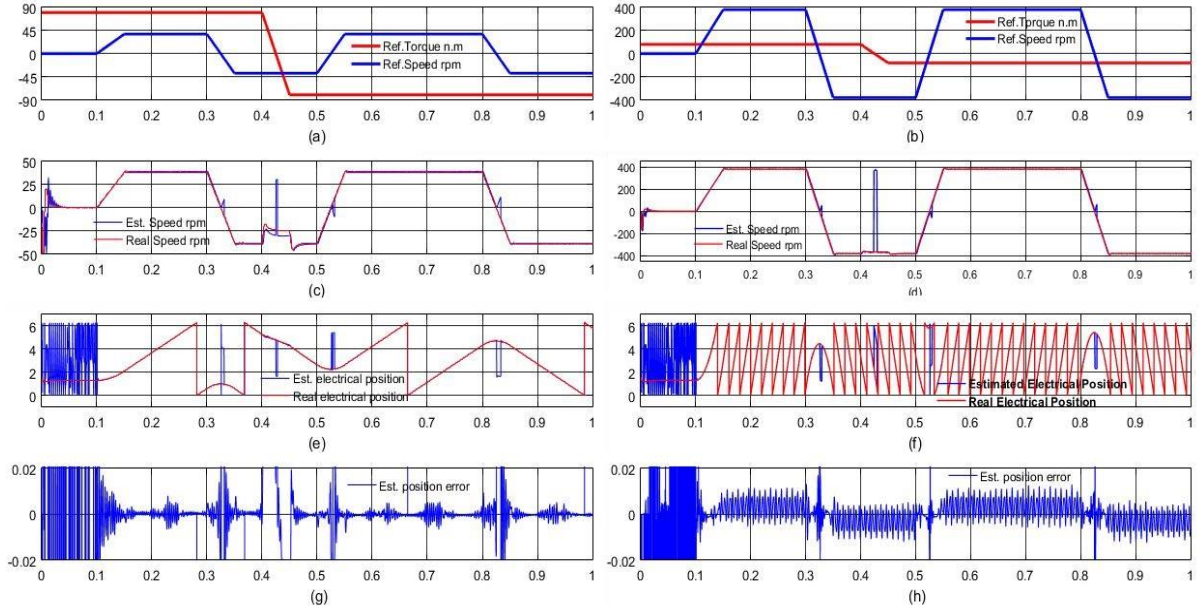


Fig. 4-16: The General Simulation of the Proposed SMO Under Full Load in Both Directions and Both of Low and High Speed in Both Directions

It has been shown also from the previous Fig. 4-16. (e) and (f) that the estimated electrical position has an offset of  $(\pi)$  during the point the changeover of the motor speed between both directions at the point close to zero, due to the estimation huge noise near the zero-speed comparing to the effective estimated back EMF. While this offset period could be minimized and neglected by decreasing the time of changing the direction of the speed using a larger acceleration during approaching the speed near zero.

The estimation error in the mechanical speed is near  $1 \text{ rpm}$  during low and medium speed and about  $\pm 2 \text{ rpm}$  during full speed. The direction of rotation is extracted from the controlled components of  $V_d$  and  $V_q$ , which is shown in Fig. 4-17 during high-speed simulation.

To solve the failure or the offset of the estimated position during standstill and at the points of changing the direction of rotation, an extra two estimators has been presented in the following sections. They estimate the rotor position during this situation regardless of speed-related states such as the Back EMF. One of the estimators uses a simple direct calculation on the measured components of the stator currents and determine the rotor position with some restrictions, while the other injects some extra voltages to the stator winding to extract the rotor position in the regions of operation where the SMO fails.

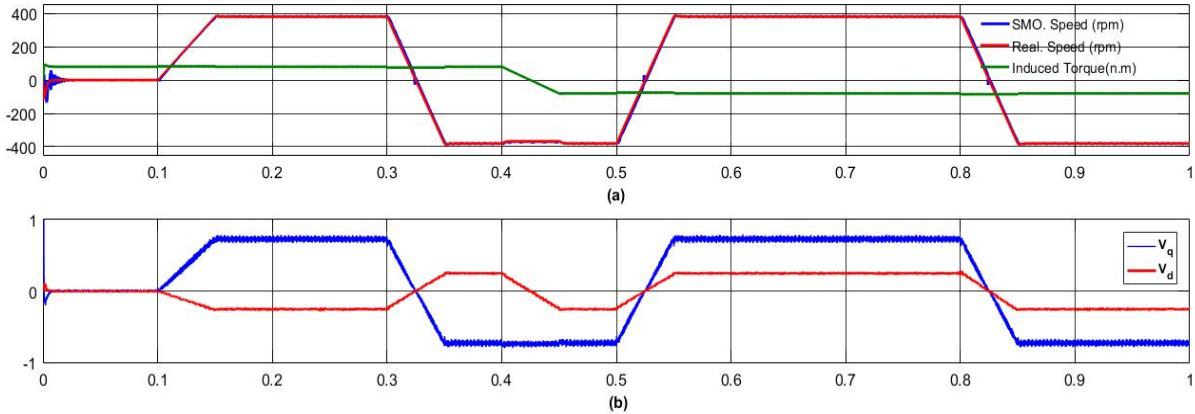


Fig. 4-17. (a): The SMO Estimated Mechanical Speed for Variable Reference Speed and Reference Torque (b): The Rotational Components of the Controlled Voltage

Fig. 4-17 shows how the estimated rotation reference frame components of the controller output d-q voltages describe the operated speed-torque regions. These components are used to determine the direction of the motor rotation even during the reversed torque, by using the multiplication of both of the voltage components and using a logical sign comparator to detect the direction. On the other hand, these components could be used to define the region of operation to accurately calibrate the estimated position and speed compensators in all operating conditions of torque and speed.

### 4.1.3 SMO Conclusion and Contributions

It can be concluded from the previous subsections that; the improved SMO estimates the rotor PM electrical position accurately with negligible error compared to the conventional and other estimators even at very low speeds. The proposed estimator could start the controller from a standstill to any dedicated speed without holding the zero speed during the standstill (DC-Injection), making it robust and the best choice for sensorless vector control.

The estimator has been simulated and tested during the four operation regions of the motor's motoring-breaking modes, at low and high speed and different loads.

On the other hand, the proposed estimator fails to estimates the rotor position during standstill operation and zero speed (DC-Injection) process, because the Back Electromotive Force depends on the rotation of the motor, as the motor does not have a significant Back EMF during zero speed, which fails the estimator during this condition.



## 4.2 Direct Extraction Method

This method studies the PMSM stator currents in its stationary  $\alpha\beta$  reference frame, which can be used to extract the rotor's position for the loaded motor in a simple process. On the other hand, it can find the initial rotor's position for the unloaded motor, which can predict the polarity of the PM in its rotation cycle for the other unipolar estimation methods.

Fig. 4-18 shows the reference speed of the motor, the measured abc electrical reference frame currents, the  $\alpha\beta$  stationary reference frame currents, and the extracted rotor's PM electrical position of the fully-loaded motor in all its speed ranges and standstill.

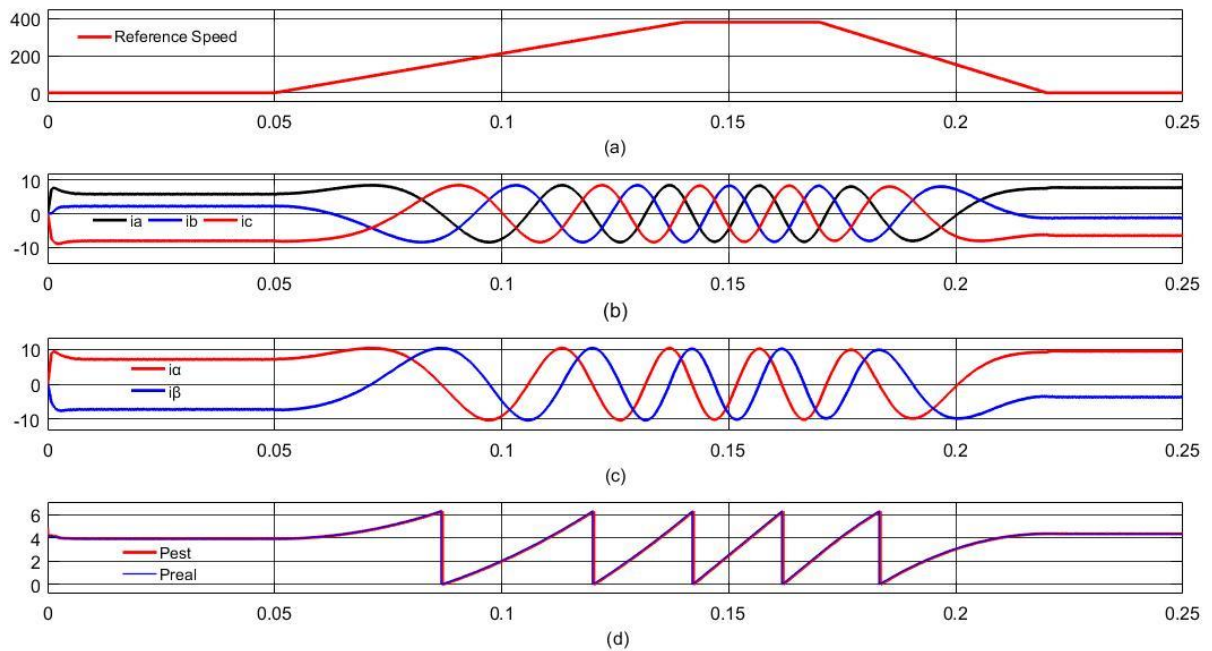


Fig. 4-18. (a): The Controller Reference Speed (b): The Stator Electrical Reference Frame Currents (c): The Stator Stationery Reference Frame Currents (d): The Estimated Position Using the Direct Extracted Method

Fig. 4-18(b) and (c) show that the measured stator currents rotate according to the rotating speed of the motor, which represents the variable position of the rotor. While during zero speed, the DC current components of the three-phases abc currents and the two-phase  $\alpha\beta$  stationary components vary according to the stopping position of the rotor. Fig. 4-18(d) compares the extracted position to the Matlab real position and shows that the direct extraction method is

able to estimate the rotor's position during zero, low and high speed precisely in a fully-loaded motor condition.

According to the torque constant theorem [45], the stator current represents the applied torque, making the direct extracting method affected by the load torque, and the external environment of the motor. Fig. 4-19 shows the load torque effect on the directed extraction estimated position during zero and medium speeds. The method estimation error is inversely proportional to the motor's load according to the load-current dependent, while it fails to estimate the rotor's position in the case of the unloaded motor, and during the speed and load transient response.

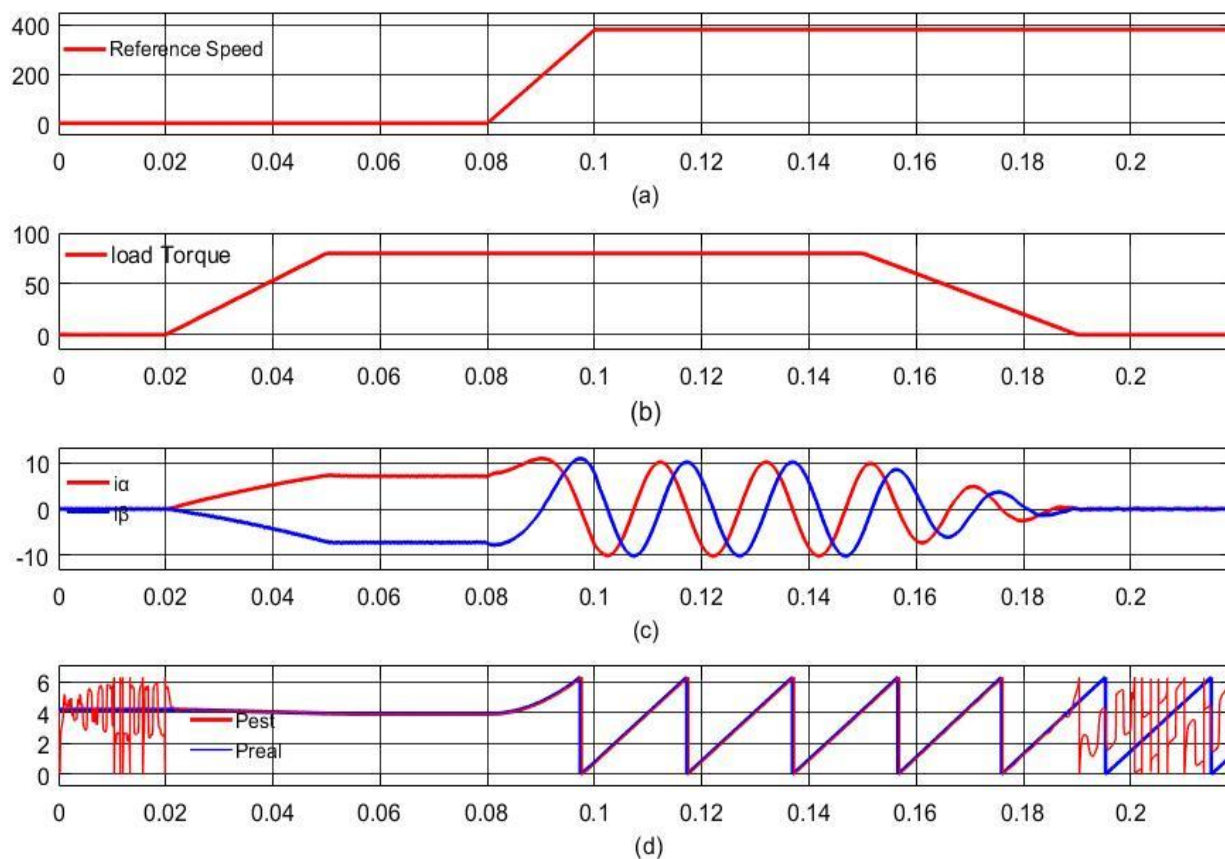


Fig. 4-19. (a): The Controller Reference Speed (b): The Tested Load Torque (c): The Stator Stationary Reference Frame Currents (d): The Estimated and the Real Position Using the Direct Extracted Method

The direct extraction method contributes the rotor's position estimation in the simplest filterless estimation method for the PMSM, which is suitable for the loaded motors that works

in constant torque applications. On the other hand, it fails in estimating the unloaded motor, which could be faced in some cases of the motor's variable load applications such as electric vehicles and hoists. Therefore, the direct extraction method fails to estimate the position of the rotor in all load conditions and needs to be combined with other estimators for the no load condition by using a torque meter to complete the estimation process in all load conditions.

Fig. 4-20 studies the direct extraction method on the unloaded motor during the starting. The method can use the starting current of the motor to determine the initial position of the rotor, which could be compared to the constant  $\pi$  to decide if the north pole of the PM is located in the first half, or located in the second half of the rotation cycle.

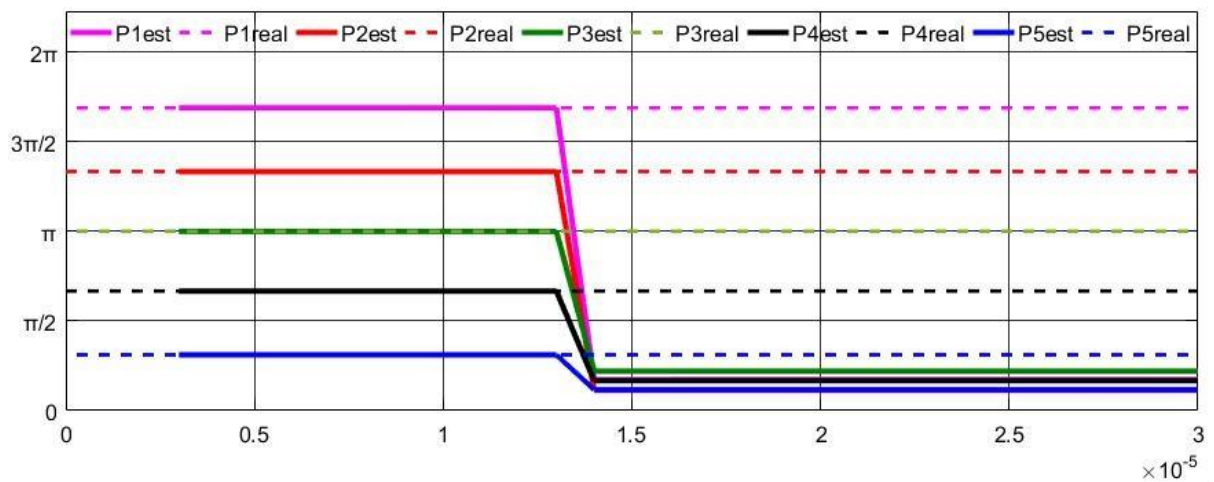


Fig. 4-20: The Initial Values of the Estimated and the Real Position While Standing at Different Positions

It has been shown that the initial value of the rotor position can be determined even if there is no induced torque. The initial position was determined using the stationary components of the motor starting current, and the direct method estimates the rotor position for the first  $10\mu\text{s}$ . Which is enough time for the controller to detect and holds the PM location polarity for the other position estimators in the combined hybrid estimation system. To measure the current components and to calculate the position, two sampling cycles have been used. Therefore, an initial null result appears in the estimation. This initial information about the PM polarity will be used in the following sections to complete the estimation process for the following unipolar position estimation method.

### 4.3 High-Frequency Injection

The system is controlled by implementing Field-Oriented Control (FOC) with a current controller, by using the rotating frame transform, which determines the rotor position and speed, using High-Frequency Injection (HFI). Fig. 4-21 shows the Simulink model of the simulated system.

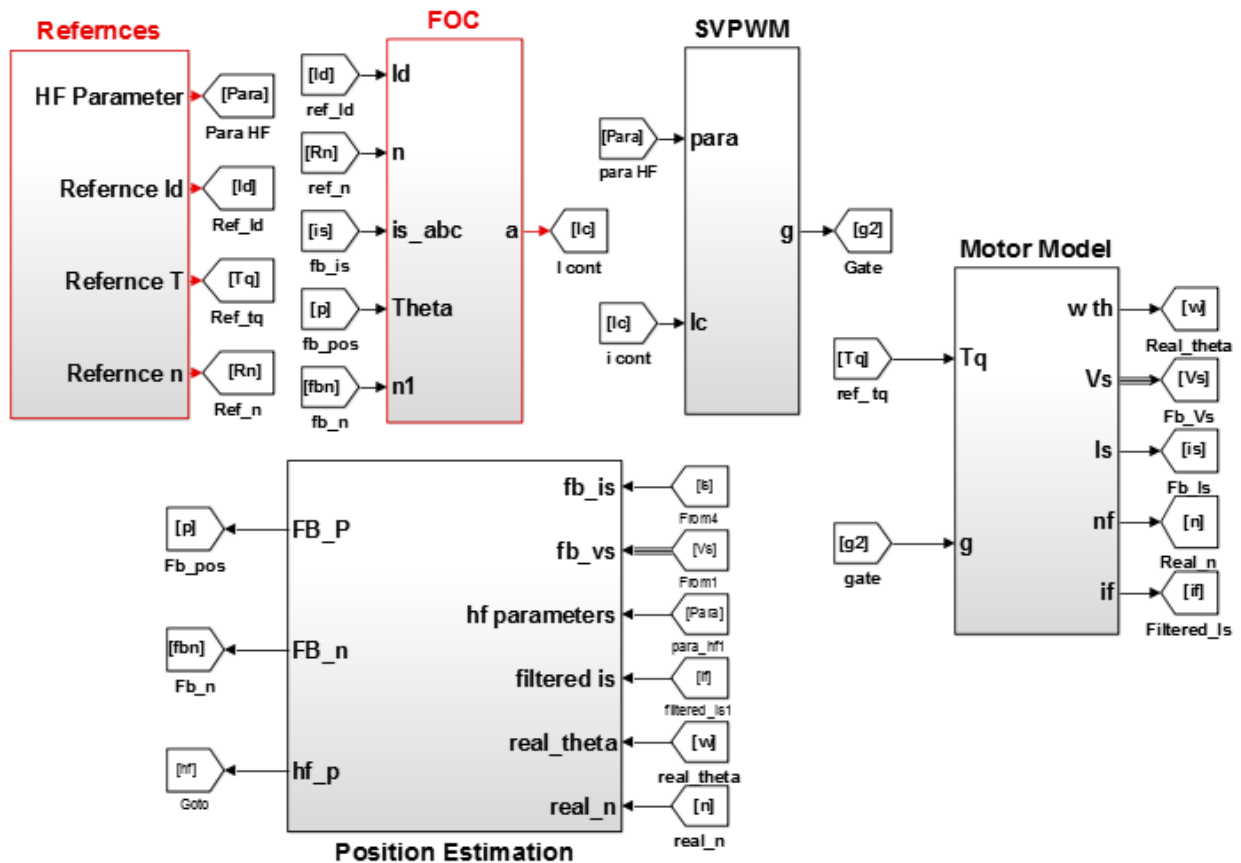


Fig. 4-21: Simulink Model of the Simulated HFI System

#### 4.3.1 Blocks Description

The reference block in Fig. 4-18 contains the references of speed, torque, and the direct component of the reference current. The reference speed expresses the speed order in rads per second, the reference torque contains the motor applied torque in Newton’s meter, while the direct component of the reference current is set to zero forcing the controller to produce the maximum motor torque per Ampere, such as which presented in the previous section.

However, the system contains the injection process parameters, such as the reference frequency and the reference voltage. The reference frequency expresses the injected voltage frequency in rads, while the reference amplitude contains the injected voltage amplitude.

The controller block contains the Field Oriented Control, Park and Clark transformation, speed and currents regulators, and the current controller. Fig. 4-3 in the previous section shows the design of the controller block.

The Space Vector Pulse Width Modulation (SVPWM) block transforms the controlled currents of the controller block into  $(\alpha, \beta)$  stationary reference frame, to establish the inverter gate signal, by using Matlab's library SVPWM block with a carrier frequency of 8kHz.

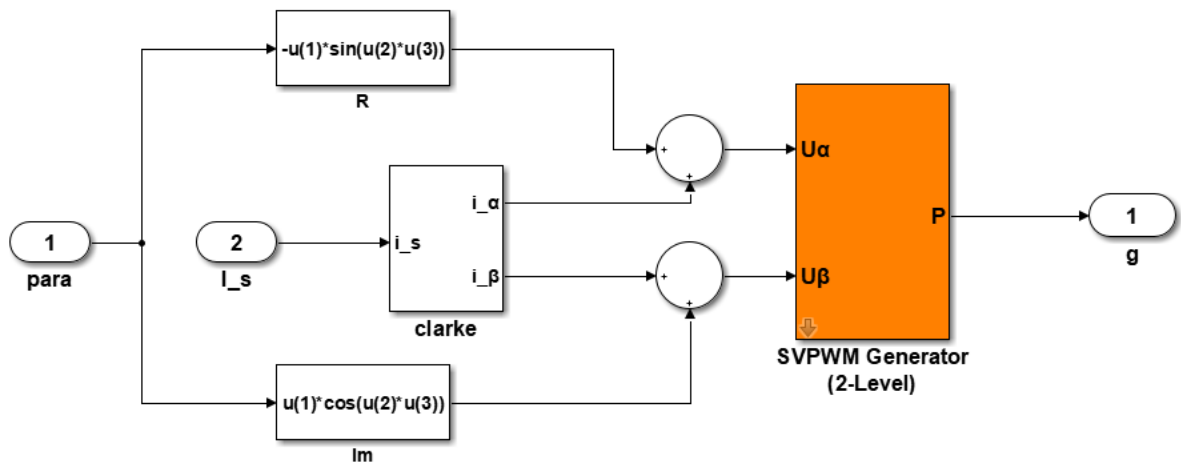


Fig. 4-22: Space Vector Pulse Width Modulation (SVPWM) Block

It has been shown in Fig. 4-22 that, the modulated  $(\alpha, \beta)$  injected signals are added to the controlled  $(\alpha, \beta)$  signals to feed the Space Vector Pulse Width Modulation (SVPWM) block, which generates the gate signals to drive a two-level voltage source inverter driving the motor.

The voltage source inverter and the Inner Rotor Permanent Magnet Synchronous Motor (IRPMSM) are contained in the motor model block which was shown in Fig. 4-4.

The position estimation block uses the measured currents from the motor model to estimate the rotor position and speed, described in Fig. 4-21.

Fig. 4-23 shows the position and speed estimation model, five cascaded processes are introduced; 4 cascaded filtering stages, and a speed-position calculation. The four filtering stages are performed according to eqs. (3.14) to (3.17), while the position calculation is

performed according to eq. (3.18). The bandpass filter emulates the fundamental component of the measured ( $\alpha, \beta$ ) components of the motor stator currents, the synchronous filter removes the positive sequence of the measured high-frequency stator current depending on the injection reference parameters, while the high pass filter emulates the DC component, which appeared from removing the positive sequence. The second synchronous filter breaks down the negative sequence, which contains the position information.

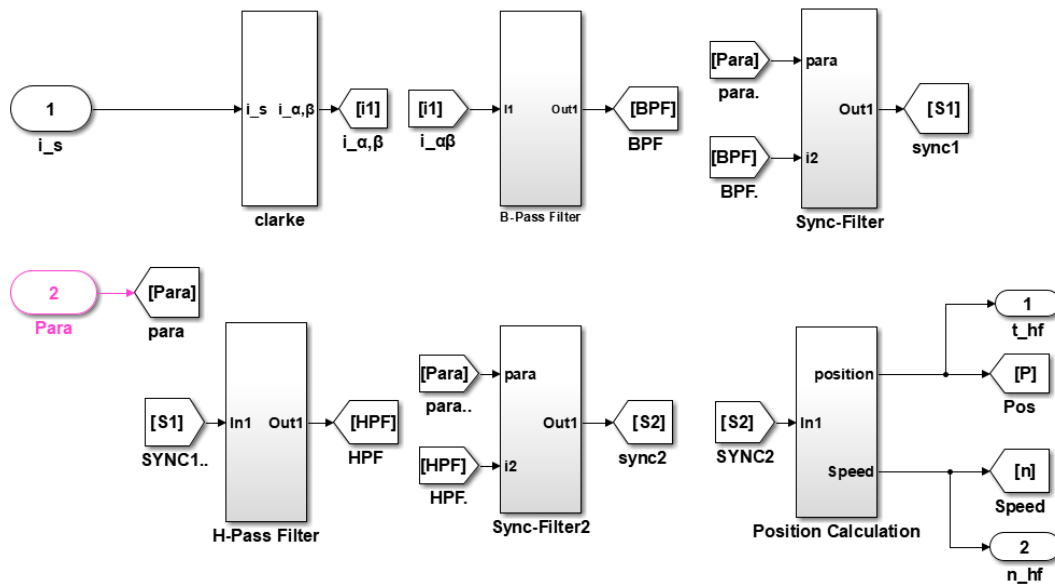


Fig. 4-23: The HFI Estimation Stages Blocks

### 4.3.2 Estimator Design and Simulation

The estimator's filters are designed according to the selected injection frequency, while the injection frequency should be 10 times higher than the maximum fundamental frequency and 10 times less than the inverter's switching frequency. The injected voltage amplitude should be considered to be effective to generate the appropriate current establishing the saliency property and extracting the rotor position information, it should be considered not to be large avoiding torque ripples. A sinusoidal vector with 5 Volts amplitude rotating at 15000 rad/s is generated and injected into the space-vector PWM in the alpha-beta stationary reference frame.

The motor model draws in its stator winding the fundamental component of the control current and the injected signal. Fig. 4-24 shows the measured alpha-beta stator currents.

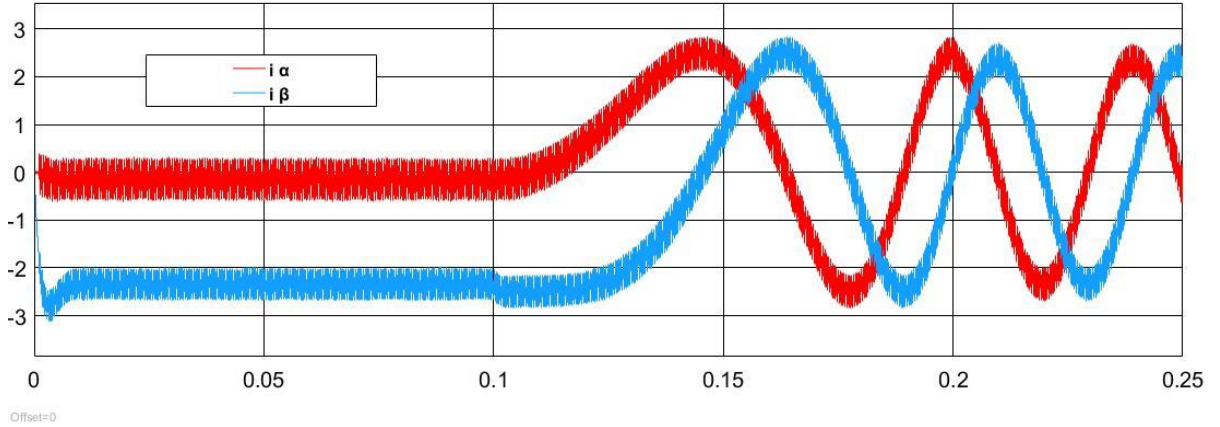


Fig. 4-24: The Stationary Drawn Currents During Injection

According to the previous design and the injected power, the rotor position information is filtered and processed to estimate the rotor position in radians. The band-pass filter has been used to remove the fundamental component of the stator currents, drawn in the motor stator windings during the operation of the motor, the filter has a center frequency of 15000 rad and a quality factor of 1, while the other stages are used to extract the rotor position from the measured high-frequency injected currents in the stator windings, as shown in Fig. 4-22 and the stages of extraction described as follow.

Fig. 4-25. (a) shows that, the filtered stationary components of the stator currents, which contain the summation of the positive and negative sequences of the injected frequency according to the (3.14), which implies the saliency property of the studied (IRPMSM). The negative sequence contains the rotor position information. To exploit the sequences, the synchronous filter is developed and designed using the injected frequency, which uses the cross-product calculations between the current's components and the sinusoidal vector as in eq. (3.15) to eliminate the positive sequence.

Fig. 4.25. (b) shows that, the positive sequence is broken down into offset modulated signals. On the other hand, Fig. 4-25. (c) shows that, the high-pass filtering process, which removes the offset signal caused by eliminating the positive sequence, and passes the doubled frequency negative sequence which contains the position information.

The passed high frequency signal could be broken down into orthogonal sinusoidal signals, which rotate with a frequency at twice the rotor speed in radians per second. The sinusoidal position information signals are extracted using an inverse synchronous filter rotating at twice the injected frequency. The extracted position information is shown in Fig. 4-25. (d).

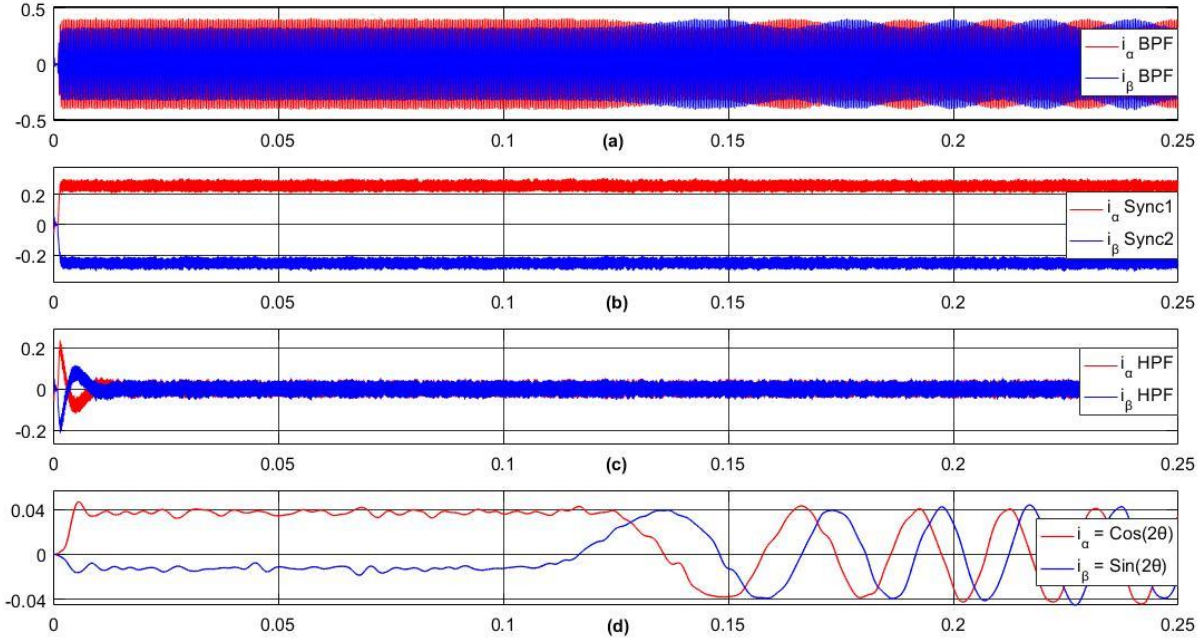


Fig. 4-25: The Four Stages of Position Sinusoidal Information Extraction.

Fig. 4.26 shows the first synchronous filter effect on the stator current, using simple cross-product operation with the vector  $[e^{-j\omega_i t}] = [\cos(-\omega_i t) \quad \sin(-\omega_i t)]^T$ , while this operation does not have any effect on the signal phase shift.

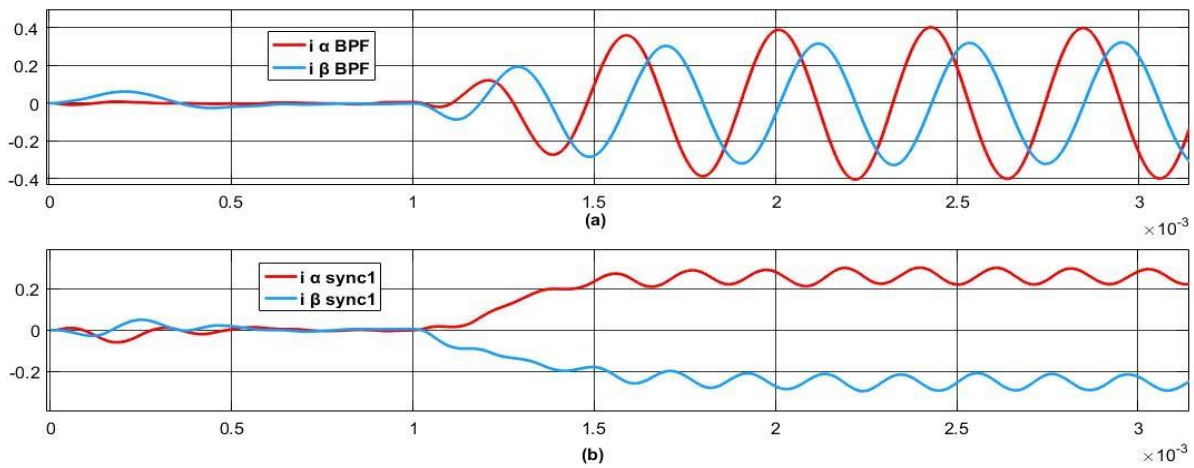


Fig. 4-26: The First Synchronous Filter Frequency Effect

The synchronous filtering process removes the unwanted positive sequence. On the other hand, it doubles the negative sequence frequency to be twice the injected frequency and produces a DC component in the filtered signal, as shown in Fig. 4-26. (b). To remove the DC



component, a high-pass filter has to be designed with a cutoff frequency ten times less than twice the injected frequency and quality factor of 1 to avoid the phase shift problem.

### 4.3.3 All-Speed Ranges Simulation

The designed estimator predicts the low-speed rotor position with some noise and phase delay. The estimation noise is produced due to the existence of the fundamental component during the low speed, while the voltage source inverter (VSI) produces harmonics at the sidebands of the injection frequency, which affects the filtered alpha-beta estimation signals.

On the other hand, the phase delay caused by the band-pass and the high-pass filters could be minimized by controlling the quality factors of the filters and the operating frequency during filtering. Fig. 4-27. (a) shows the HFI estimated position during standstill, low, medium, and high speeds, which represented in factor of rated speed as one-tenth, half, and full rated speed respectively. The system could extract the rotor position at all speed ranges, even at high speeds, but it differs in its phase delay effect and the position estimation error. While Fig 4-27. (b) shows the HFI position estimation error, which describes these previous effects and their relations during all speed ranges. It also shows that the electrical position estimation error increases by increasing the operating speed due to the filter's delay, which increases the output delay by moving the filter's input frequency away from its center frequency.

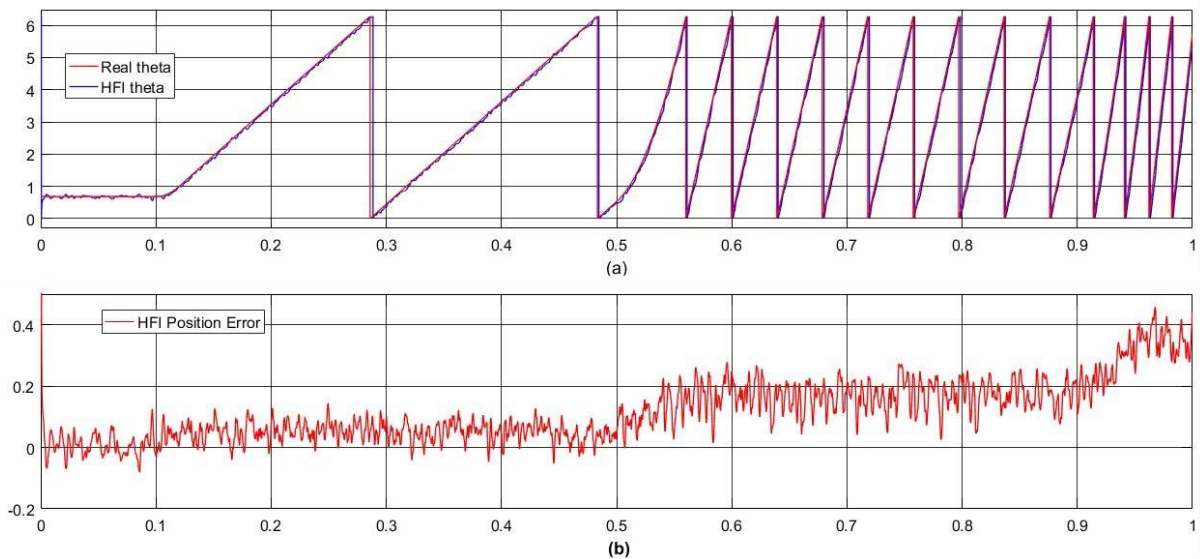


Fig. 4-27. (a): The HFI Estimated Position During Deferent Ranges of Speed, (b): The HFI Estimated Electrical Position Error from Low to High Speed

Fig. 4-28 shows the phase delay of the estimated position during the motor rotation at the full rated speed. It shows also the fluctuation in the estimation result, which is caused by the non-ideality of the filtration process and the high injected frequency effect on the position modulated information.

The filter bandwidths, cutoff frequencies, and quality factors are designed according to the range of the operating speed. To increase the quality of the estimator, the bandwidth is minimized to overcome the noise around the dedicated frequency. On the other hand, minimizing the bandwidth of the filter will decrease the range of the operating speed and will cause a variable phase delay at the filter's output.

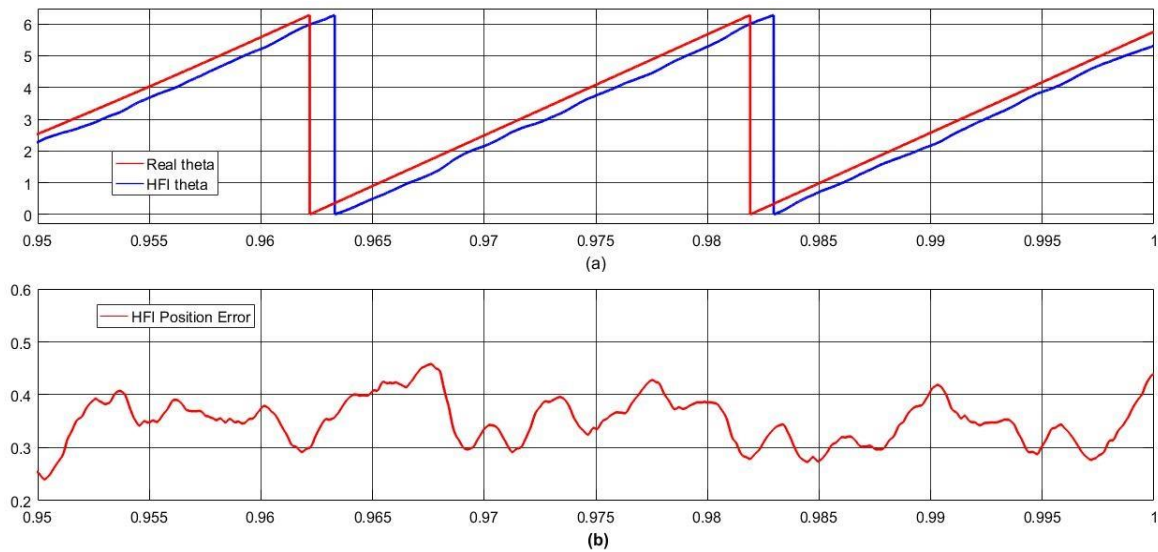


Fig. 4-28: The Estimation Delay Shown in the Estimated Position and Error

#### 4.3.4 Polarity Detection and Zero-Speed Simulation

The HFI estimation system can extract the rotor's position by measuring the stator drawn currents using high-frequency injection during standstill (DC-Injection). However, it extracts the position information in half the electrical cycle of rotation according to eq. (3.18), and the system should determine the polarity of the permanent magnet to pre-determine in which cycle the estimated electrical position is located before the high-frequency injection is started for standstill electrical position estimation.

According to the presented polarity detection procedure, which has been shown in the previous chapter and simulated in the previous section, the permanent magnet direct stationery conversion extraction process will extract the position in different accuracies depending on the motor's applied torque, which affects the significant motor's drawn currents. On the other hand, the motor at starting draws a significant current for a small period depending on the settling time even at zero loads. This starting extraction can be used to calculate the position of the PM at any polarity, which could be used to detect the polarity only at starting, which can be used to compensate the HFI estimation process during the zero and low speeds.

The system has been tested and simulated for a zero-reference speed with different locations of rotor positions at the stall, the drawn stator currents are filtered and processed to extract the rotor position using the same procedure of the low-speed estimation. The usage of the first band-pass filter depends on the existence of the applied torque, which causing drawing a DC current in the stator winding, which implies the usage of the filtering process. On the other hand, modulating the zero speed DC-injection with a constant value of rotor position has no phase shift on the modulated HFI, making the measured stator currents centered exactly with the center frequency of the second-order BP Filter which does not cause filtering time delay.

Fig. 4-26 shows the zero-speed estimated position at different stopping electrical positions of the magnetic poles. It shows that, if the permanent magnets are located at the first cycle of its electrical rotation at the beginning of the estimation, as depicted in Fig. 4-29 (a), the system can complete the estimation without determining the polarity of the permanent magnets even if the motor stops at the Permanent Magnet (PM) second electrical rotation cycle according to the used  $2\pi$  rapping procedure. While Fig. 4-29 (b) shows that the system has a  $\pi$  offset in its estimation when starts the estimation while the PM's located at the second polarity rotation cycle, and completes the estimation with the estimation error offset even if it stops permanently at the first polarity rotation cycle of the PMs.

On the other hand, the system can estimate the rotor position at a zero speed without any delay by selecting the filter's center frequency according to the injection frequency with zero modulated position variation at any starting or stopping position location. In other words, designing the bandpass filter center frequency exactly at the same frequency which rotates the dedicated passing signal, avoid the filter delay problem, and the need of the compensation mechanism

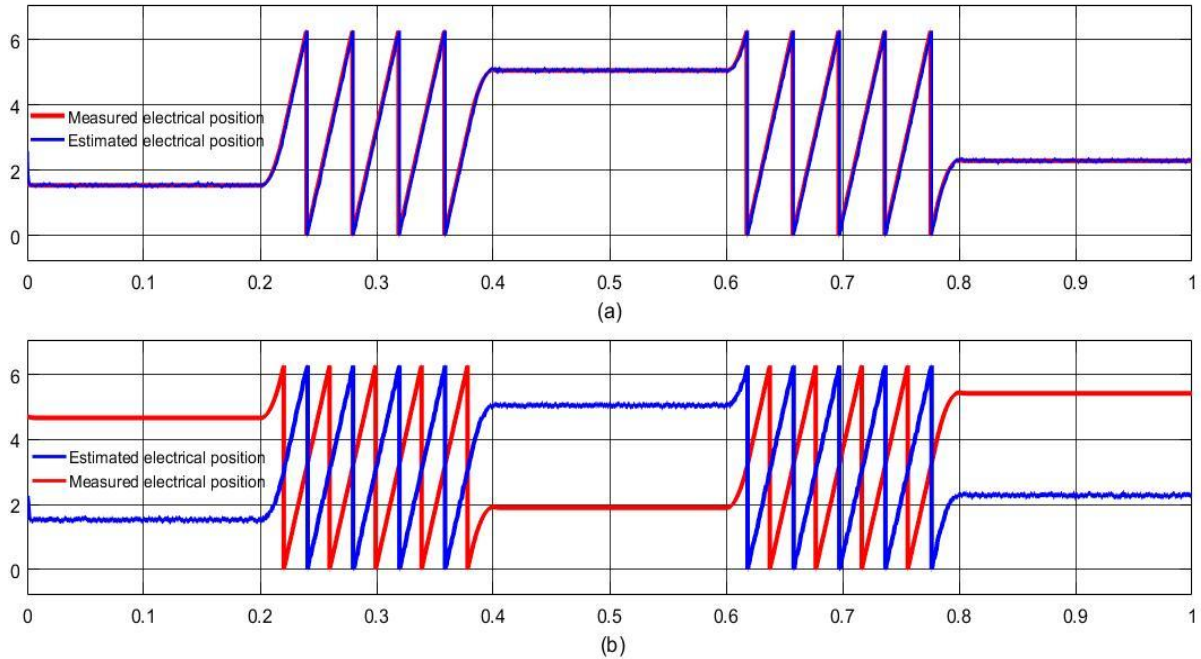


Fig. 4-29: The Uncompensated Polarity Estimated Position When the Permanent Magnets Located: (a) At the First Polarity Cycle at Starting, (b): At the Second Polarity Cycle at Starting.

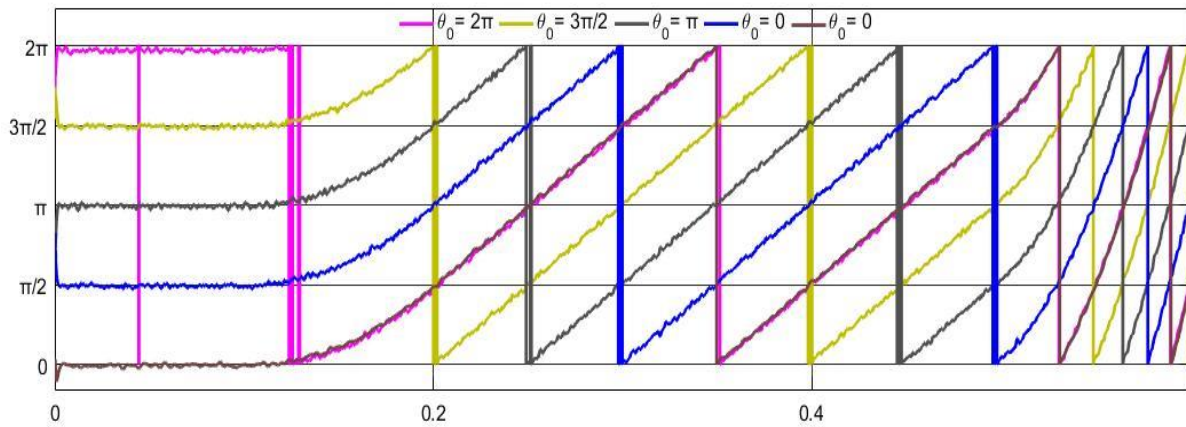


Fig. 4-30: Polarity Compensated SMO Estimated Position for Different Polarity Locations

Fig. 4-30 shows the estimated position after using the proposed polarity compensation procedure by starting the estimation at different starting electrical positions of the magnetic poles in both PM polarity cycles, where the compensator detects the polarity and then compensates the position avoiding the polarity offset.

### 4.3.5 Injection Voltage Magnitude and Frequency Effect

The following simulation studies the effect of the injection voltage magnitude on the estimation process and the overall system. The injection frequency is maximized to ten times larger than the maximum possible operating frequency of the motor during the HFI estimation, and is also minimized to ten times less than the Space Vector Modulation (SVM) switching frequency. In order to increase the estimation accuracy, the voltage magnitude needs to be maximized, while increasing the injection voltage affects the fundamental operation of the system.

Fig. 4-31 shows the effect of increasing the injected voltage magnitude on the estimated position error ( $P_{real} - P_{est}$ ) in rad, the motor's induced torque error ( $T_{ref} - T_{ind}$ ) in N.M, and the rotor's speed error ( $n_{ref} - n_{out}$ ) in rpm. This study has been conducted while increasing the speed from zero to the rated speed, in three different parallel simulations for the same system with different injection voltage amplitude, (7.5, 15, and 30 V) rotating at 15krad/s. It shows that, increasing the injection voltage magnitude makes the measured stationary currents more significant to be processed for position's extraction, which decreases the position estimation error and reduces the estimation delay. On the other hand, the injected voltage became more significant on the stator windings, which in case increases the torque pulsating and vibration during all speed ranges. The torque vibration affects the motor's speed and increases the speed pulsation.

Increasing the injection voltage in a constant not controlled amplitude reduces the maximum controlled fundamental rotated voltage which produced from the Voltage Source Inverter (VSI) at high speeds, and will reduce the maximum effective fundamental rotated voltages supplied to the motor windings, reaching the rated motor voltage and the maximum VSI output voltage before reaching the motor rated speed. Therefore, increasing the injection voltage amplitude reduces the maximum effective operated speed due to the VSI output voltage protection limit.

In order to reduce the estimation error, the voltage amplitude need to be increased, but not more than 15 volts to avoided increasing the winding losses, and gaining the maximum operation speed before reaching the inverter and the motor voltage ratings.

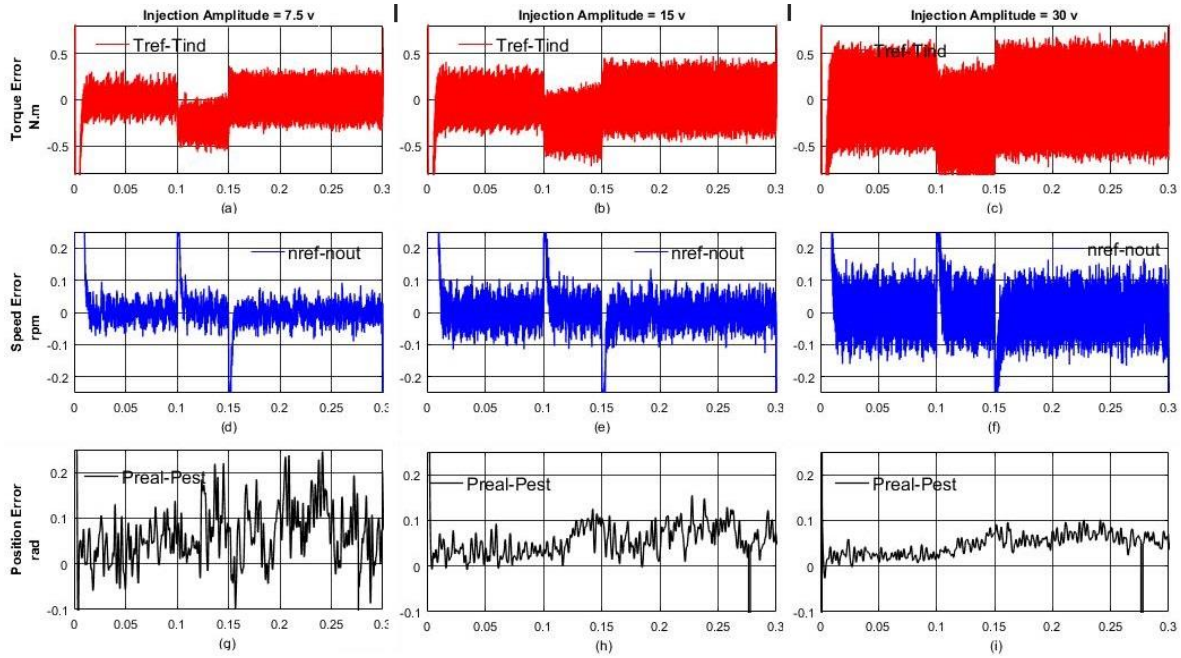


Fig. 4-31: Injection Voltage Amplitude Effect on Torque, Speed and Estimated Position

#### 4.3.6 Loading Effect

In estimating the rotor position and as an electric vehicle, this section studies the ability to estimate the rotor's position during applying different load torques. Fig. 4-32 shows the estimated rotor electrical position while applying zero, half, full, and overload to the studied motor during standstill condition. It is clear that, the load does not affect the estimation accuracy during the zero speed according to the dependency of the estimator on the filtered high-frequency currents components, which have their position information centered, located and modulated with zero rotating frequency at the point of the injected frequency without any frequency shift on the modulated position information during the zero speed without any phase shift effect from the BPF. The load torque during standstill causes the motor to draw the DC-injection currents, while increasing the applied load increases the drawn DC currents values, which are far away from the modulation frequency and do not have harmonics near the modulation frequency according to Fourier's theorem.

To study all the motor operation regions, the system needs to be simulated and studied during both directions of the motor rotation while rotating at zero, low and high speeds, on the loaded motor while applying different load torque amounts in both directions.

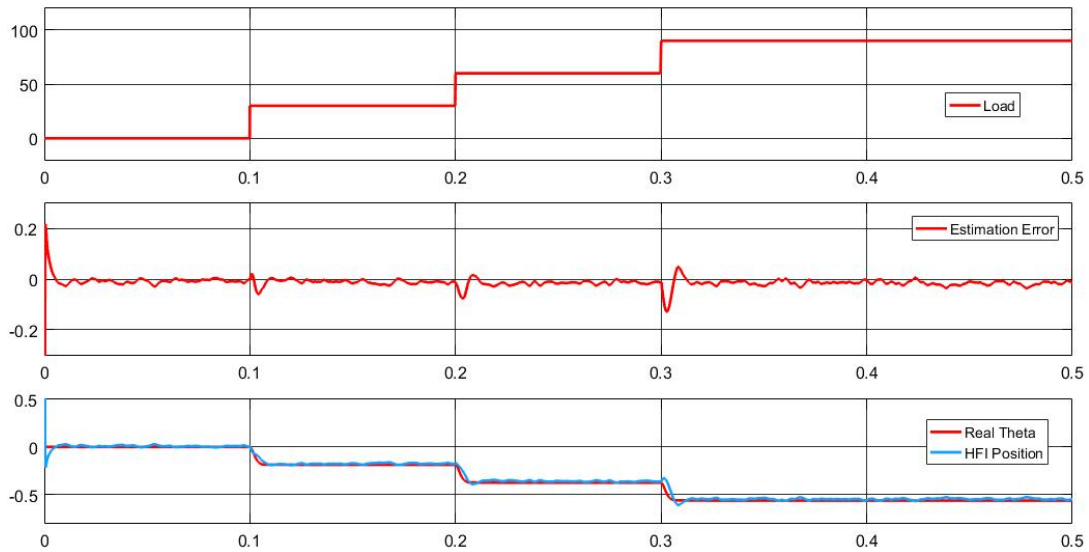


Fig. 4-32: The Load Effect on the Estimated Position During Standstill

Fig. 4-33 shows the estimation ability of the presented HFI estimator and the estimation error during motoring and braking modes when the motor is rotating at low and high speeds fully loaded with both directions of torque load. The HFI process estimates the rotor position with minimum estimation error during zero and low speeds, while the estimation error increases by increasing the rotor speed in both directions due to the delay of the designed filter. On the other hand, the HFI process uses load-independent high-frequency signals to extract the rotor position, and this is independently achieved by injecting the dedicated injection signal directly to the SVPWM block. While a negligible load effect appears inside the controller, which appears in the increasing in estimation error during medium speed as depicted in Fig. 4-33 (g) at the region  $0.4s < t < 0.5s$ , this effect is due to reversing the applied torque from positive to negative.

It has been shown in Fig. 4-33 (c) and (d) that, the injection process affects the speed estimation direction during transient starting of the motor at zero speed while the fully-loaded motor rolls back. Minimizing the controller q-axis proportional gain during the HFI process increases the settling time, causes a significant delay to reach the steady-state of the quadrature component of the controlled voltage, which causes the speed direction estimation problem at the controller transient region of the loaded motor.

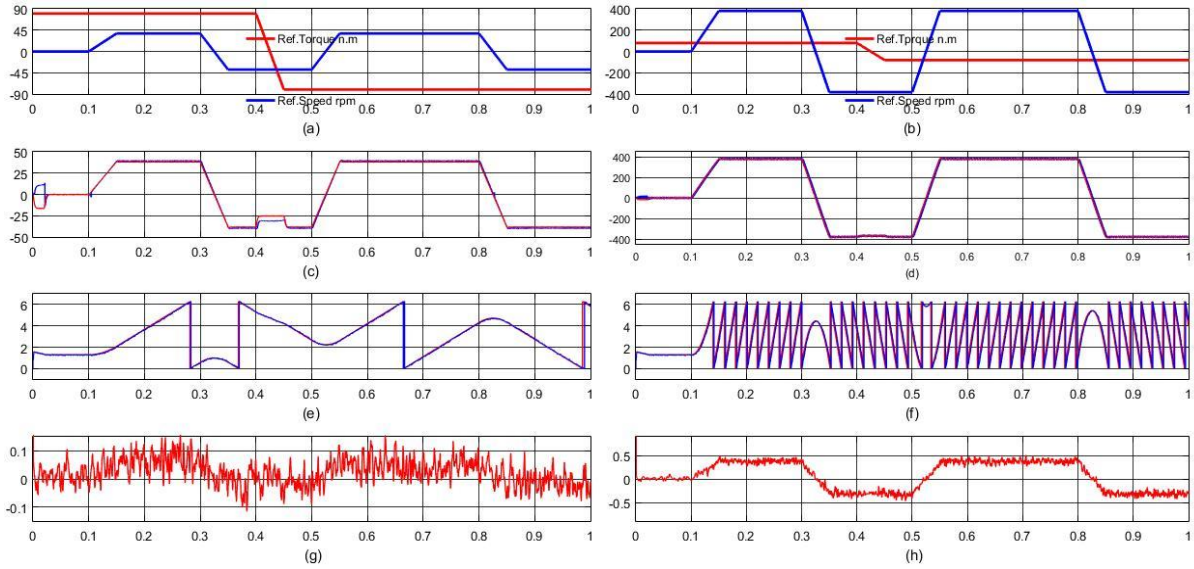


Fig. 4-33: The General Simulation of the Proposed HFI Estimator under Full load in both Directions and at Low and High Speeds in both Directions.

#### 4.3.7 HFI Conclusion and Contributions

It has been shown in this section that, the HFI estimation process can estimate the rotor electrical position during all speed ranges, which makes it a robust estimation technique to be used in sensorless applications. On the other hand, the injection process added additional power loss in the motor windings, and this effect become more significant by increasing the injected signal amplitude, which could be minimized by selecting an acceptable power loss and a dedicated accuracy of the estimation. While injecting a significant high-frequency voltage into the motor winding during the operation of the motor produces high-frequency currents into the current controller which affects the overall torque control process.

Applying high-frequency signals to the motor winding produces an audible noise, related to the selected frequency of injection. Increasing the speed of the motor increases the phase shift of the modulated frequency away from the center frequency of the designed filters, which in turn increases the estimation delay. On the other hand, it increases the amplitude of the measured stator currents significantly, which in turn reduces the pulsation and the fluctuation in the estimation process.



## 4.4 Hybrid System

It has been shown from the previous two sections of the simulation part, that the presented estimators differ in their speed ranges of estimation ability; the observer one can estimate the rotor electrical position during the speed ranges, where the motor produces a significant electromotive force, by using a filterless observer and smooth switch for the sliding process, which makes it a robust estimator for the medium and high speeds during all regions of motor operation. On the other hand, the HFI estimator can estimate the rotor position during all speed ranges with minimum filtering effect during the zero and low-speed ranges, and with some drawbacks on the estimator accuracy during the high-speed ranges. The HFI estimation process affects the operation of the motor, by producing audible noise as an effect of supplying a high-frequency signal into the motor stator windings, and increases the power loss during the injection, due to applying a significant amplitude of the injected signal. To overcome these drawbacks, the HFI procedure implementation needs to be minimized by tightening the speed ranges of the HFI estimation process. Therefore, an intelligent hybrid system has been designed to combine it with the third stage of the high-speed estimation process at its edge with the lowest possible error.

The overall system needs to be combined in its three stages, zero-start, zero–low speeds, and high speeds of operation. The first two stages use the HFI procedure in its estimation and polarity detection, while the SMO procedure has been used in the third stage of the medium and high speeds. Fig. 4-34 shows the estimated speed during all speed ranges using the hybrid estimation technique, which estimates the rotors electrical position at starting with standstill speed using the HFI and compensates the estimated position for the polarity issue by adding  $\pi$  to the estimated position, while continuing the estimation until reaching 5 rpm to switch the FOC position feedback to the SMO estimated position and turning off the injection process at all to reduce its effect on the control system. The SMO estimation estimates the electrical position as in Fig. 4-34 (b) in the speed ranges above 5 rpm for increasing speed and before 8 rpm for decreasing and constant speed to ensure the Schmitt-trigger switching mechanism avoids sliding around the switching point during speed oscillations and ensuring the stability of the hybrid estimator.

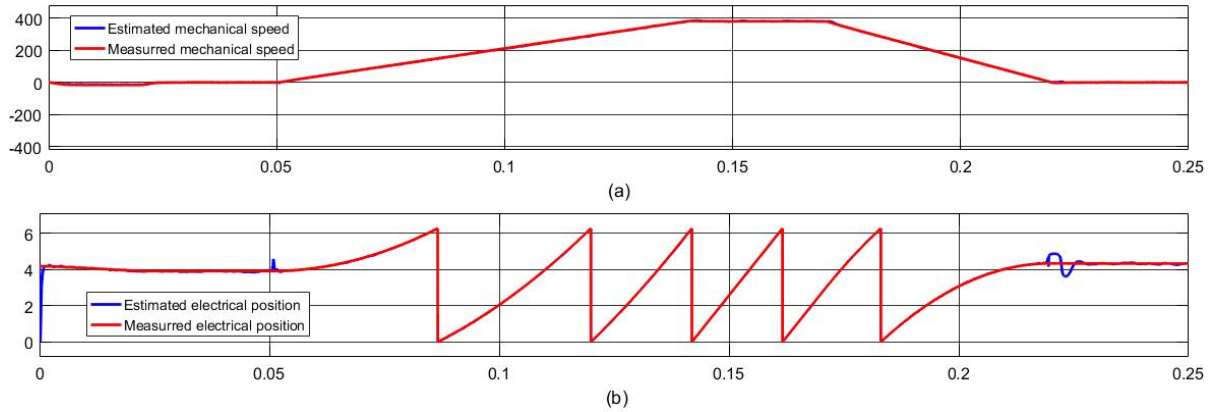


Fig. 4-34: Full Speed Hybrid Estimated Mechanical Speed and Electrical Position

Fig. 4-34 (b) shows the estimation process of the presented hybrid technique, which estimates the electrical rotor position with minimum estimation error, as it uses the advantages of both of the estimators when combined.

Fig. 4-34 (a) shows the estimated speed according to the SMO estimated back electromotive force, which can be estimated during all speed ranges using the modified PI controlled SMO. The SMO PI controller decreases the estimation error, increasing the estimation stability response time, and reduces the estimation oscillations by adding two degrees of freedom to the SMO calibrations parameters.

During the low-speed estimation region, the hybrid switch guarantees turning the injection process off for the increased speed to enhance the observer estimation process, which uses the filterless measured stator currents. This point comes after the point of changing the feedback from low speed to high-speed estimation position data. According to the injection effect on the operated SMO, and the response time of the observer, the hybrid feedback affected by turning the injection “off”. The transient response of the SMO shown it the time 0.05s in Fig. 4-34. (b). The presented PI controller can reduce the injected power effect on the observer by increasing the response speed, which can be achieved by increasing the controller gain. On the other hand, the estimation accuracy and estimation noise can be reduced by controlling the SMO soft switch gain in the observer stability region.

On the other hand, the HFI filters response time affects the estimation response time and the beginning of the injection process, which appears at the point of changing the hybrid estimation process from SMO into HFI estimated data, which appears at 0.22s in Fig. 4-34 (b). While to

reduce the response time and the HFI transient effect at the beginning of the estimation, the hybrid system should turn the injection process “on” early before reaching the point of changing the feedback from SMO to HFI estimated position signal, which is shown in Fig. 4-35 (d).

The general simulation in Fig. 4-35 shows the estimation process and its effect on the estimated speed and the motor induced torque during all the operating regions of the studied motor, at motoring and braking, in both directions of speed and load; ranging from zero to full speed and load. It is shown in Fig. 4-35 (a) that, the presented PI-directional SMO estimator estimates the rotor mechanical speed in both directions and all speed ranges with estimation error varying between  $\mp 1 \text{ rpm}$ , which contributes to the SMO speed estimation process. Thanks to the PI controller, which inserts two additional parameters to reduce the switching chattering effect, the oscillations appear in the salient pole SMO estimation technique and reduce also the overall estimation error. The PI controller also decreases the estimation response time, which reduces the estimation error during all the fast changes in motor speed and the load variation applied on the motor in all directions and any operating region of the motor, even at reversing the applied load from the full positive load into the full negative load at the same speed direction in 0.01 seconds, such as presented in Fig. 4-32 (a) and (b).

Fig. 4-35 (c) shows the estimated electrical position in all speed ranges in both directions and during standstill by stopping the motor at different positions in both polarity regions of the permanent magnets by turning the HFI process and injection on before reaching the estimator operating speed range, which ensures the polarity detection ability of the estimator in all rotation directions during stopping. The position estimation is affected by the mutual effect between both of the estimators, as was shown in the same figure at 0.39s at starting of forward rotation after the HFI standstill estimation.

The HFI transient problem, which is shown in Fig. 4-35 (c) at 0.422s occurs at the HFI switching point during deceleration to low speed. This problem could be reduced by turning the injection “on” early, offering enough time to the HFI to reach its stability before reaching the point of the Hybrid low-speed switching as was shown in Fig. 4-35 (d). This method offers extra time to the HFI to reach the steady-state estimation region. The previous method can be achieved by starting the injection at higher speeds, or by decreasing the deceleration value, where the time could be increased during decaying to the zero-speed turning on and stabilize

the injection process before using it in the hybrid estimation feedback. On the other hand, both of the previous cases increase the consumed injection power and the noise produced due to the high-frequency injection.

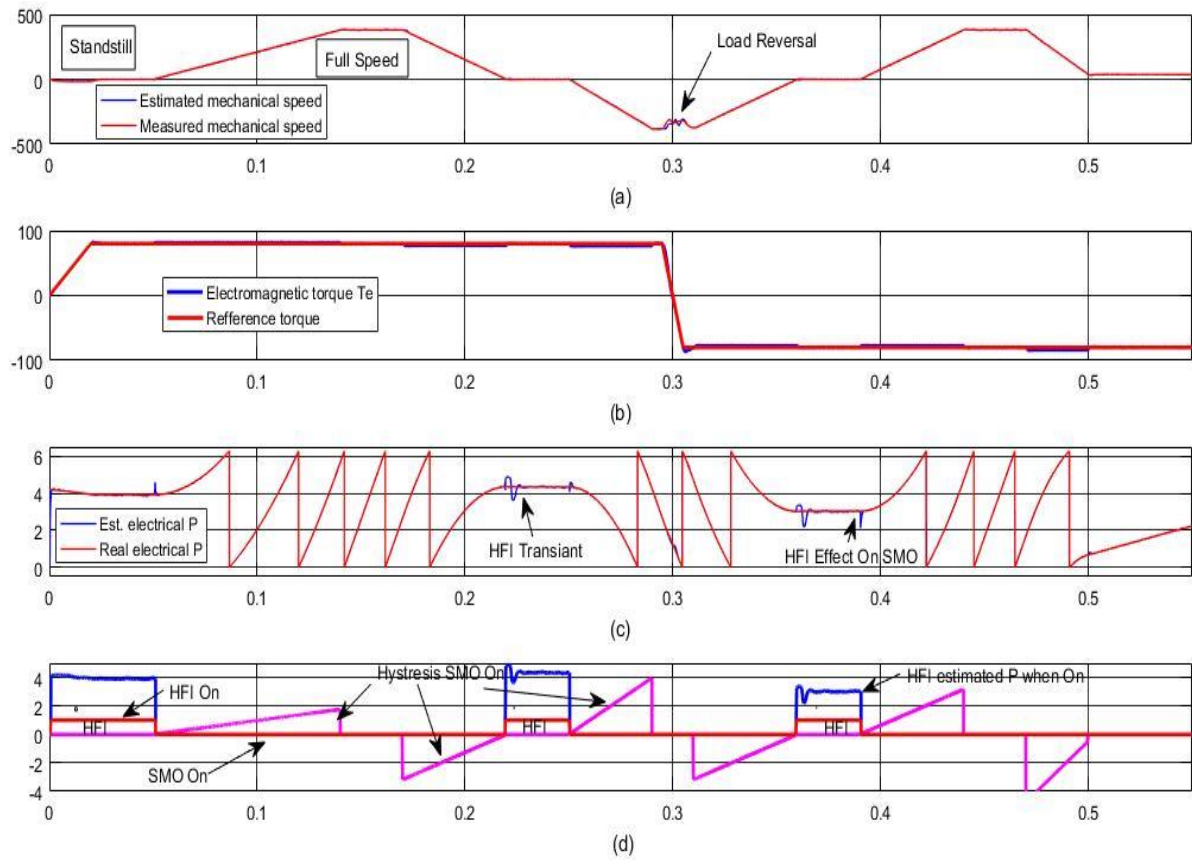


Fig. 4-35: General Simulation of Electrical Position and Mechanical Speed Hybrid Estimation During all Operation Regions of the Studied Motor

Fig. 4-35 simulates the presented hybrid estimation of the electrical rotor position and speed with minimum mutual effect, minimum HFI noise and losses, and maximum acceptable error at the point of switching the feedback between the estimator's outputs.

# Chapter 5

## Conclusions and Future Work

---

### 5.1 Conclusions

In this Thesis, the IRPMSM has been studied as an application of electric vehicle traction machine, the motor has been controlled using FOC with sensorless position and speed feedback, decreasing the cost of the controller, and enhancing the reliability of the system, using different contributions in the presented position estimators such as Sliding Mode Observer (SMO) and High-Frequency Injection (HFI).

It has been concluded and validated that, the improved PI-controlled Salient Poles SMO estimates the rotor position accurately during all speed ranges with some estimation error at low speeds and fails to estimate the rotor position accurately during standstill for the salient pole PMSM. It also eliminates the usage of the filtering process and the chattering phenomenon, which reduce the complexity of the observer and avoids the time delay caused by the filtering process, while it decreases the speed ripple compared to the conventional SMO. The estimator shows the ability to estimates the rotor position and speed during all the operating regions of the motor in all speed-load ranges and directions, which generalize the estimator in all conditions. The estimation error and the estimated position noise have been minimized using the proposed SMO PI controller, which added two degrees of freedom to the calibration.

The HFI estimator has been studied, simulated, and validated. It estimates the rotor position during standstill accurately and all speed ranges with speed-related estimation error according to the filtering phase shift delay effect. The filter effect can be overcome by designing an appropriate compensator. The system has been studied in all speed-load ranges and directions to generalize the estimator in all operating regions. The estimator polarity detection has been

made without any extra injection procedure, nor the need of an independent polarity detection system. The injection amplitude and modulation frequency affect the estimation accuracy, power loss, and the produced noise, while the noise and power loss are the main disadvantages of this estimator.

The direct extraction of the rotor position from the stationary components can be used to estimate and complete the rotating reference frame transformation achieving the stability of the control process during zero speed operation, but fails to complete the control process during medium and high speeds according to the position delay and the current controller dependency. The direct extraction during zero speeds can be achieved accurately for medium and heavy loads, but is acceptable at very light loads, and fails to extract it for zero loads. This method replaces the HFI process for the loaded motor even if the load was low.

The System has been studied under the proposed hybrid estimation procedure, which consists of the advantages of both of the estimators. The switching process has been designed to minimize the position estimation error. The hybrid system is designed to decrease the produced noise and the power loss by avoiding the injection process. The system estimates the rotor position during zero and low speeds by using the direct extraction procedure in the cases where the applied load is greater than 5% of the rated load. The load decision has been made and calculated using the estimated direct current value during the starting of the motor without any extra sensors. The polarity has been detected using injection-less built-in methods for every zero-speed operation, which reduces the complexity of the HFI or using an independent injection system as in the conventional injection estimators.

This thesis contributes to the estimation process for the sensorless vector control system of IRPMSM in an intelligent hybrid system, by modifying an SMO for the non-equivalent inductance component's salient rotor PMSM with minimum estimation error, and designing a reduced delay, reduced noise HFI estimator with an accurate zero speed estimation, non-complex polarity detection, and minimum range of operation in its hybrid estimation system. It also generalizes the estimation process in all speed-load conditions making it an effectively applicable choice for sensorless controlled traction machines and electric vehicles applications.

## 5.2 Future Work

Reference to the results and conclusions, the following recommendations are pointed out as future work for the research needs.

- Validating the proposed method experimentally on a prototype system
- Reducing the operation times of the standstill HFI estimator by using the last position data and memory usage
- Studying the effect of parameter variation and noise injection on both estimators
- Designing an online stator resistor estimator, to overcome the temperature effect on the stator winding and the motor parameters
- Designing and simulating an Artificial Intelligent Error Reduction system to overcome the speed estimation with a minimum error of the hybrid system
- Using the direct stator starting estimator and the observed SMO speed to estimate the position during all speed ranges and standstill condition in an injection-free estimator





# References

---

- [1] M. A. Rahman and A. M. Osheiba, "LITERATURE SURVEY OF PERMANENT MAGNET AC MOTORS AND DRIVES," in *IEEE Transactions on Energy Conversion*, vol. 5, no. 1, pp. 211–217, 1990, doi: 10.1109/60.50833.
- [2] S. Singh and A. Anvari-Moghaddam, "Sensor-based and Sensorless Vector Control of PM Synchronous Motor Drives: A Comparative Study," *Recent Advances in Electrical & Electronic Engineering*, vol. 13, no. 2, pp. 276–284, 2020.
- [3] S. Goyal and M. Dubey, "Comparison of Sensor-Based and Sensor Less Technique Position Estimation," *International Journal of Industrial Electronics and Electrical Engineering*, vol. 2, no. 3, pp. 1–4, 2014.
- [4] L. K. Jisha and A. A. Powly Thomas, "A comparative study on scalar and vector control of Induction motor drives," *Proceedings of the International Conference on Circuits, Controls and Communications, (CCUBE)*, Bengaluru, India, Dec. 27-28, 2013, doi: 10.1109/CCUBE.2013.6718554.
- [5] V. M. Bida, D. V. Samokhvalov, and F. S. Al-Mahturi, "PMSM vector control techniques - A survey," *Proceedings of the IEEE Conference of Russian Young Researchers in Electrical and Electronic Engineering*, pp. 577–581, St. Petersburg and Moscow, Russia, Jan. 29, 2018, doi: 10.1109/EIConRus.2018.8317164.
- [6] H. Celik and T. Yigit, "Field-Oriented Control of the PMSM with 2-DOF PI Controller Tuned by Using PSO," *International Conference on Artificial Intelligence and Data Processing*, Malatya, Turkey, Sep. 28-30, 2018, doi: 10.1109/IDAP.2018.8620902.
- [7] S. Sakunthala, R. Kiranmayi, and P. N. Mandadi, "Investigation of PI and Fuzzy Controllers for Speed Control of PMSM Motor Drive," *Proceedings of the IEEE*

- International Conference on Recent Trends in Electrical, Control and Communication*, pp. 133–136, Malaysia, Mar. 20-22, 2018, doi: 10.1109/RTECC.2018.8625636.
- [8] F. M. Zaihidee, S. Mekhilef, and M. Mubin, “Fractional Order SMC for Speed Control of PMSM,” *6th International Electrical Engineering Congress, (iEECON)*, pp. 1–4, Krabi, Thailand, Mar. 7-9, 2018, doi: 10.1109/IEECON.2018.8712281.
- [9] Y. Chen and J. Chen, “The Simulation Research of PMSM Control Based on MPC,” *Proceedings - International Conference on Industrial Informatics - Computing Technology, Intelligent Technology, Industrial Information Integration*, no. 2, pp. 250–253, Wuhan, China, Dec. 2-3, 2018, doi: 10.1109/ICIICII.2017.43.
- [10] S. Hussain and M. A. Bazaz, “Comparative analysis of speed control strategies for vector controlled PMSM drive,” *Proceeding - IEEE International Conference on Computing, Communication and Automation*, pp. 1314–1319, Greater Noida, India, April. 29-30, 2017, doi: 10.1109/CCAA.2016.7813950.
- [11] G. S. Buja and M. P. Kazmierkowski, “Direct torque control of PWM inverter-fed AC motors - A survey,” *IEEE Transactions on Industrial Electronics*, vol. 51, no. 4, pp. 744–757, Aug. 2, 2004, doi: 10.1109/TIE.2004.831717.
- [12] Y. Liu, J. Wan, H. Shen, G. Li, and C. Yuan, “PMSM speed sensorless direct torque control based on EKF,” *4th IEEE Conference on Industrial Electronics and Applications, (ICIEA)*, pp. 3581–3584, Xian, China, May. 25-27, 2009, doi: 10.1109/ICIEA.2009.5138873.
- [13] S. Bolognani, L. Tubiana, and M. Zigliotto, “Extended Kalman filter tuning in sensorless PMSM drives,” *Proceedings of the Power Conversion Conference-Osaka, (Osaka)*, vol. 1, no. 6, pp. 276–281, 2002, doi: 10.1109/PCC.2002.998560.

- [14] J. S. Jang, B. G. Park, T. S. Kim, D. M. Lee, and D. S. Hyun, "Parallel reduced-order extended Kalman Filter for PMSM sensorless drives," *Proceedings Industrial Electronics Conference (IECON)*, no. 2, pp. 1326–1331, Florida, USA, Nov. 10-13, 2008, doi: 10.1109/IECON.2008.4758146.
- [15] R. Li and G. Zhao, "Position sensorless control for PMSM using sliding mode observer and phase-locked loop," *IEEE 6th International Power Electronics and Motion Control Conference (IPEMC '09)*, pp. 1867–1870, Wuhan, China, May. 17-20. 2009, doi: 10.1109/IPEMC.2009.5157699.
- [16] G. el Murr, D. Giaouris, and J. W. Finch, "Universal PLL strategy for sensorless speed and position estimation of PMSM," *IEEE Region 10 Colloquium and 3rd International Conference on Industrial and Information Systems (ICIIS)*, pp. 6–11, Kharagpur, India, Dec. 8-10, 2008, doi: 10.1109/ICIINFS.2008.4798473.
- [17] Z. Yan and V. Utkin, "Sliding mode observers for electric machines - An overview," *Industrial Electronics Conference Proceedings (IECON)*, vol. 3, pp. 1842–1847, Sevilla, Spain, Nov. 5-8, 2002, doi: 10.1109/iecon.2002.1185251.
- [18] C. Li and M. Elbuluk, "A sliding mode observer for sensorless control of permanent magnet synchronous motors," *Conference Record - IAS Annual Meeting (IEEE Industry Applications Society)*, vol. 2, no. C, pp. 1273–1278, Chicago, USA, Sep. 30-Oct. 4, 2001, doi: 10.1109/ias.2001.955672.
- [19] V. Srikanth and A. A. Dutt, "A comparative study on the effect of switching functions in SMO for PMSM drives," *IEEE International Conference on Power Electronics, Drives and Energy Systems*, no. 2, pp. 1–6, Karnataka, India, Dec. 16-19, 2012, doi: 10.1109/PEDES.2012.6484351.

- [20] L. Qi, T. Jia, and H. Shi, "A novel sliding mode observer for PMSM sensorless vector control," *IEEE International Conference on Mechatronics and Automation*, pp. 1646–1650, Beijing, China, Aug. 7-10, 2011, doi: 10.1109/ICMA.2011.5985961.
- [21] D. Wu, D. Yang, and J. Chen, "Vector Control of PMSM Based on Sliding Mode Observer," *Journal of System Simulation*, vol. 30, no. 11, pp. 4256–4267, 2018, doi: 10.16182/j.issn1004731x.joss.201811026.
- [22] S. Mode, C. For, and M. C. Applications, "A Generalized Approach for Lyapunov Design of Sliding Mode Controllers for Motion Control Applications," *Proceedings of 4th IEEE International Workshop on Advanced Motion Control*, vol. 1, pp. 407–4012, Mie, Japan, Mar. 18-21, 1996.
- [23] J. Chu, Y. Hu, W. Huang, M. Wang, J. Yang, and Y. Shi, "An improved sliding mode observer for position sensorless vector control drive of PMSM," *Proceedings IEEE 6th International Power Electronics and Motion Control Conference*, no. 2, pp. 1898–1902, Wuhan, China, May. 17-20, 2009, doi: 10.1109/IPEMC.2009.5157706.
- [24] D. H. von Seggern, "Transcendental Functions," in *CRC Standard Curves and Surfaces with Mathematica*, 2nd ed. (Chapman & Hall/Crc Applied Mathematics and Nonlinear Science), ch. 3, 2007.
- [25] C. Zhou, Z. Zhou, W. Tang, Z. Yu, and X. Sun, "Improved Sliding-Mode Observer for Position Sensorless Control of PMSM," *Proceedings Chinese Automation Congress*, no. 3, pp. 2374–2378, Hangzhou, China, Nov. 22-24, 2019, doi: 10.1109/CAC.2018.8623482.
- [26] C. Zhou, X. Huang, Y. Fang, and L. Wu, "Comparison of PMSMs with Different Rotor Structures for EV Application," *Proceedings - 2018 23rd International Conference on Electrical Machines, ICEM 2018*, no. i, pp. 609–614, Alexandroupoli, Greece, Sep. 3-6, 2018, doi: 10.1109/ICELMACH.2018.8507258.

- [27] H. Ahn, H. Park, C. Kim, and H. Lee, "A Review of State-of-the-art Techniques for PMSM Parameter Identification," *Journal of Electrical Engineering & Technology*, vol. 15, no. 3, pp. 1177–1187, Mar. 2020, doi: 10.1007/s42835-020-00398-6.
- [28] H. Mirahki and M. Moallem, "Torque calculation in interior permanent magnet synchronous machine using improved lumped parameter models," *Progress in Electromagnetics Research M*, vol. 39, no. October, pp. 131–139, Isfahan, Iran, Oct. 27-30, 2014, doi: 10.2528/PIERM14093004.
- [29] C.-H. Choi and J.-K. Seok, "Pulsating Signal Injection-Based Axis Switching Sensorless Control of Surface-Mounted Permanent-Magnet Motors for Minimal Zero-Current Clamping Effects," *IEEE Transactions on Industry Applications*, vol. 44, pp. 1741–1748, Jan/Feb, 2009, doi: 10.1109/TIA.2008.2006350.
- [30] S. Nakashima, Y. Inagaki, and I. Miki, "Sensorless initial rotor position estimation of surface permanent magnet synchronous motor," *IEEE Transactions on Industry Applications*, vol. 36, no. 6, pp. 525–527, Jan/Feb, 2000, doi: 10.1109/IEMDC.1999.769165.
- [31] H. Jiang, "Audible noise reduction in the high frequency injection based sensorless torque control for EPS applications," Ph.D. thesis, Dept. Elect. Eng., Univ. Nottingham, UK, 2012. [Online]. Available: [www.eprints.nottingham.ac.uk/29091](http://www.eprints.nottingham.ac.uk/29091)
- [32] J. Agrawal and S. Bodkhe, "Low speed sensorless control of PMSM drive using high frequency signal injection," *12th IEEE International Conference Electronics, Energy, Environment, Communication, Computer, Control: E3-C3 (INDICON 2015)*, pp. 4–9, New Delhi, India, Dec. 17-20, 2016, doi: 10.1109/INDICON.2015.7443383.
- [33] G. Wang, R. Yang, Y. Wang, Y. Yu, and D. Xu, "Initial rotor position estimation for sensorless interior PMSM with signal injection," in *Proceedings International Power*

*Electronics Conference (IPEC)*, pp. 2748–2752, Sapporo, Japan, Jun. 21-24, 2010, doi: 10.1109/IPEC.2010.5543182.

- [34] S. Medjmadj, D. Diallo, C. Delpha, and G. Yao, “A salient-pole PMSM position and speed estimation at standstill and low speed by a simplified HF injection method,” *in Proceedings 43rd Annual Conference of the IEEE Industrial Electronics Society*, no. 1, pp. 8317–8322, Beijing, China, Oct, 2017 doi: 10.1109/IECON.2017.8217460.
- [35] M. J. Corley and R. D. Lorenz, “Rotor position and velocity estimation for a permanent magnet synchronous machine at standstill and high speeds,” *IEEE Transactions on Industry Applications*, vol. 34, no. 4, pp. 784–789, Jul/Aug, 1998, doi: 10.1109/ias.1996.556994.
- [36] S. Damkhi, M. S. N. Said, and N. N. Said, “Slotting effects and high frequency signal injection for induction machine rotor speed estimation,” *Proceedings of the International Conference and Exposition on Electrical and Power Engineering (EPE 2012)*, pp. 401–408, Iasi, Romania, Oct. 25-27, 2012, doi: 10.1109/ICEPE.2012.6463863.
- [37] R. Leidhold, “Position sensorless control of PM synchronous motors based on zero-sequence carrier injection,” *IEEE Transactions on Industrial Electronics*, vol. 58, no. 12, pp. 5371–5379, 2011, doi: 10.1109/TIE.2011.2112323.
- [38] Y. Jeong, R. D. Lorenz, T. M. Jahns, and S. Sul, “Initial rotor position estimation of an interior permanent magnet synchronous machine using carrier-frequency injection methods,” *IEEE Transactions on Industry Applications*, vol. 41, no. 1, pp. 38–45, 2005, doi: 10.1109/IEMDC.2003.1210395.
- [39] P. Kumar, O. Bottesi, S. Calligaro, L. Alberti, and R. Petrella, “Self-adaptive high-frequency injection based sensorless control for interior permanent magnet synchronous motor drives,” *Energies*, vol. 12, no. 19, 2019, doi: 10.3390/en12193645.

- [40] Y. Yan, J. Zhu, and Y. Guo, "Multiphase induction motor drives-a technology status review," *IET Electric Power Applications*, vol. 1, no. 5, pp. 42–48, 2008, doi: 10.1049/iet-epa.
- [41] Y. gu Kang, D. D. Reigosa, and R. D. Lorenz, "SPMSMs HFI Based Self-Sensing Using Intentional Magnetic Saturation," *IEEE Access*, vol. 8, pp. 228731–228739, 2020, doi: 10.1109/ACCESS.2020.3045275.
- [42] J. Hu, L. Xu, and J. Liu, "Magnetic pole identification for PMSM at zero speed based on space vector PWM," in *Proceedings CES/IEEE 5th International Power Electronics and Motion Control Conference (IPEMC)*, vol. 1, pp. 704–708, Shanghai, China, Aug. 13-16, 2007, doi: 10.1109/IPEMC.2006.297118.
- [43] W. ZINE, "HF signal injection and Machine Learning for the sensorless control of IPMSM-based EV drives," Ph.D. thesis, Dept. Elec. Eng, Univ. CERGY-PONTOISE, France, Oct, 2017. [Online]. Available: <https://www.theses.fr/2017CERG0914.pdf>
- [44] N. Mohan," Sinusoidal Permanent Magnet AC (PMAC) Drives, LCI-Synchronous Motor Drives, and Synchronous Generators," in *Electric Machines and Drives: A First Course*, 1<sup>st</sup> ed, Don Fowley, Hoboken, NJ, USA: Wiley, ch. 10, sec. 3, 2012.
- [45] N. Mohan," Vector Control of Permanent-Magnet Synchronous Motor Drives," in *Advanced Electric Drives*, 1<sup>st</sup> ed, John Wiley & Sons, Hoboken, NJ, USA: Wiley, ch. 10, 2014.